室蘭工業大学
学術資源アーカイブ
Muroran Institute of Technology Academic Resources Archive

部分充填スクッテルダイト化合物 YbxRh4Sb12 の高圧合成と熱電特性

メタデータ	言語: eng 出版者: 公開日: 2020-06-08 キーワード (Ja): キーワード (En): 作成者: シリマート, ジラッタガン メールアドレス: 所属:
URL	https://doi.org/10.15118/00010185

令和元年度

博士学位論文

題目

High-pressure synthesis and thermoelectric properties of partially filled skutterudite compounds $Yb_xRh_4Sb_{12}$

（部分充填スクッテルダイト化合物 $Yb_xRh_4Sb_{12}$ の高圧合成と熱電特性）

提出者　室蘭工業大学大学院

工学研究科 博士後期課程

工学専攻

強相関電子物性研究室

平成28年度入学

学籍番号 16096503

Jirattagan Sirimart

提出日　令和２年２月３日

Abstract

The “phonon-glass electron-crystal” model is an ideal thermoelectric materials and the imagining of the extra framework cation rattling with in a cage to yield very low thermal conductivities and produce excellent thermoelectric properties. The thermoelectric performance of a material is characterized by the figure of merit, ZT = $(S^2/\rho\kappa)T$, where S is Seebeck coefficient, ρ is electrical resistivity, κ is thermal conductivity and T is temperature. To enhance performance of ZT, though, doping heavy atom into skutterudite structure. Skutterudite structure have strong in thermoelectric properties. In skutterudite structure contain of transition metal and pnictogen atom, in structure consist of a square ring of pnictogen atoms that sharing bonding and form with transition metal then created empty cages. Yb has been filled in CoSb3-base skutterudite, It provide effect on low-vibration frequency according to reduce thermal conductivities. Yb-filled skutterudite. Whereas, heavy mass and small radius have affected on strong interaction in structure

A new candidate thermoelectric material is $Yb_xRh_4Sb_{12}$, because $RhSb_3$-base structure have large void than $CoSb_3$-base skutterudite. This work reported new information of $Yb_xRh_4Sb_{12}$. Yb content was filled from 0 – 0.8. This compounds were prepared under high pressure and high temperature method at 2 GPa, 750°C for 2 min with heating rate at 50°C/min and after decrease temperature to 450-550°C. The maximum actual filling fraction of Yb was found at 0.4. This compound is in body-centered cubic structure (Im3). From this condition, the temperature dependence of electrical resistivity decrease and seebeck coefficient decrease (that mean show in n-type behaviors) at the same time, thermal conductivity also decrease from 8.11 W/mK (Rh_4Sb_{12}) to 2.43 W/mK ($Yb_{0.8}Rh_4Sb_{12}$) the ZT value increase to 0.042 at 300K for $Yb_{0.8}Rh_4Sb_{12}$. Maxmimum actual Yb doped Rh_4Sb_{12} was improved thermoelectric performance by spark plasma sintering method. The maximum ZT was found 0.1 at 420K

CONTENTS

Chapter 1 Introduction

1.1 Thermoelectric effect 1
1.2 Skutterudite 7
1.3 Thermoelectric properties of skutterudite 10
1.4 High pressure synthesis 11
1.5 Motivation 15

Chapter 2 Experimental method

2.1 Preparation of material 16
2.2 Synthesis 16
2.3 Characterization 18
2.4 Measurements electrical and thermal properties 19

Chapter 3 Results and discussion of $Yb_xRh_4Sb_{12}$ (2 GPa)

3.1 Experimental details and characterization 48
3.2 Electrical properties 59
3.3 Thermal conductivity 65
3.4 Dimensionless figure of merit 70
3.5 Specific heat 71
3.6 Magnetic properties 74

Chapter 4 Results and discussion of $Yb_xRh_4Sb_{12}$ (SPS)

4.1 Experimental details and characterization 79
4.2 Electrical properties 82
4.3 Thermal properties 85
4.4 Figure of merit 87

Chapter 5 Summary

5.1 Summary 88

Reference

Acknowledgement

CHAPTER 1

INTRODUCTION

In the present energy is an important factor in human life, in all of manufacturing which use energy, always have an energy lost, most 60% of energy lost are in form of heat. It is better if we can recovery heat lost back to electrical energy. Thermoelectric (TE) is technology that can directly and reversibly convert heat to electrical energy or transform electrical energy into thermal power for cooling by using the temperature different. The advantages of TE is small size, high reliability, no pollution and friendly with environment. Now thermoelectric technology can apply to use in many manufacturing. For example in power generation such as (automobiles, industrial processes) hand watch and radioisotope and for cooling side they are also use in refrigerator system and CPU

Thermoelectric module consist of two semiconductor we call n type and p type. The semiconductor is mean thermoelectric material that has electrical conductivity greater than insulator but less than metal.

1.1 Thermoelectric effect

Thermoelectric effect is direct conversion of temperature difference can created voltage. When heat applied at one side, electron at hot end are more energetic and faster than electron at cold end. Therefore, electron at hot end are move towards cold end and leave positive ion at hot end. So, cold end is present negative charge and hot end is present positive charge. If electron diffuse from hot to cold end, then the cold end is negative with respect to the hot side and seebeck coefficient is negative (P-type). Holes would diffuse from the hot to cold end. The cold end is positive which would make seebeck coefficient positive.

Thermoelectric efficiency can be quantified by the dimensionless figure of merit (ZT), which is derived from eq. 1.1.1

$$ZT = S^2T/\rho\kappa \qquad 1.1.1$$

when S = Seebeck coefficient

ρ= electrical resistivity

κ = thermal conductivity ($\kappa = \kappa_e + \kappa_L$)

κ_e = electrical thermal conductivity

κ_L = lattice thermal conductivity

- Seebeck coefficient

Seebeck coefficient is a temperature difference between two points in a conductor or semiconductor results in a voltage difference between these two point

- Thermal conductivity

Thermal conductivity is kinetic energy of atomic motion and potential energy of distortion of interatomic bond, which is consist of electrons and holes transporting heat (κ_e) and phonon traveling through the lattice (κ_L).

When temperature increase, the large is the mean atomic velocity and the amplitude of atomic vibration lead to larger thermal energy. The vibration of individual atoms in solids are not independent from each other. The coupling of atomic vibration of adjacent atoms results in waves of atomic displacement. Each wave is characterized by its wavelength and frequency for a wave of a given frequency, there is the smallest quantum of vibrational energy that call phonon. Therefore, thermal energy is the energy is energy of all phonon (all vibration waves) present in the crystal at a given temperature.

In thermoelectric materials, free electron stabilized with lattice vibrations in hot end, migrate to cold end and transfer a part of their thermal energy back to lattice by phonon scattering. So, heat is transferred by phonon (lattice vibration) and electron.

Since free electron are responsible for both electrical and thermal conduction. The two conductivities are related to the Wiedemann-Franz law

$$L = \frac{\kappa_e \rho}{T} \quad 1.1.2$$

The decreasing of electrical resistivity not only produces an increase in the electronic thermal conductivity but also decrease thermopower. While the power factor can be increased by varying the concentration of charge carrier in materials. The power factor (PF) is given as

$$PF = \frac{S^2}{\rho} \quad 1.1.3$$

In generally, the power factor is difficult to manner the numerical to improvement of ZT [1]. The optimization of PF can be raised performance of ZT.

In the part of lattice thermal conductivity (κ_L) is determined by structure, rigidity, atomic masses and other characteristic of lattice.

The enhance ZT by reduce lattice thermal conductivity depend on factor as

1. Use of compound with complex crystal structure
2. Insert heavy atoms with weakly bonded to the structure.
3. The existence of inclusion or impurities
4. The formation of solid solution
5. The existence of a large number of grain boundaries.

- Electrical resistivity

The value of electrical resistivity at room temperature is indicative of whether a material. If the lattice is perfect, the electron would travel infinitely through it and the material would only exhibit finite conductivity because of the thermal motion of the lattice and impurity.

A variation of electrical resistivity depend on changes in the carrier concentration and the mean free path of the charge carriers.

The rattling atom

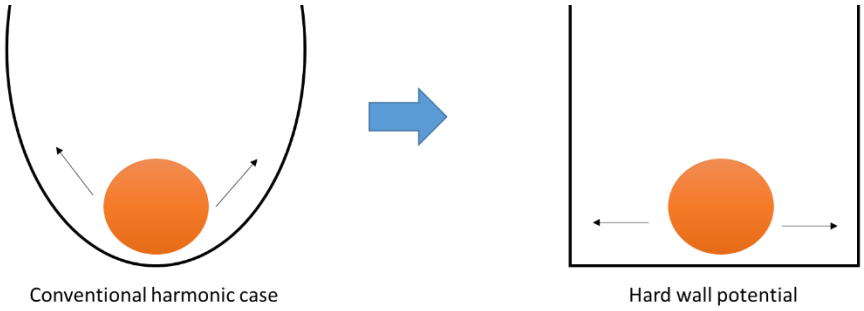

Fig 1.1.1 rattling harmonic of atom

There is a number of metallic materials in which atom can make very extended oscillations around their equilibrium position. Such a situation occurs in particular in materials in which certain atoms are surrounded by an oversized “cage structure” of other atoms.

In these case the atomic vibrations are highly anharmonic and one speaks of a “rattling” motion. In the fig 1.1.1, the effective potential for an atom is illustrated for a conventional harmonic case (left) and a strongly rattling type case with a hard wall potential (right). Such materials are promising as high efficiency, thermoelectric materials because they have high electrical conductivity but low thermal conductivity due to the rattling.

The anharmonic motion strongly influences the nuclear spin-lattice relaxation rate and the electrical resistivity of such materials.

Thermoelectric are solid-state devices that consist of two or more elements of n-type doped semiconductor and p-type doped semiconductor material connected together with conductive metal. Their electrical interconnected are mounted between two ceramic substrates and connected electrically in series and thermally in parallel.

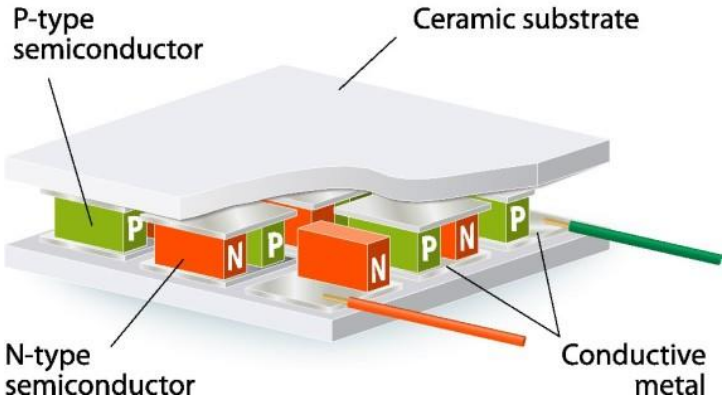

Fig 1.1.2 Thermoelectric device module[2]

Thermoelectric efficiency (η) is defined by combining the Carnot efficiency and the figure of merit (ZT), as following eq 1.1.4.

$$\eta = \frac{\Delta T}{T_{hot}} \frac{(\sqrt{1+ZT_{avg}}-1)}{\sqrt{1+ZT_{avg}}+\frac{T_{cold}}{T_{hot}}} \qquad 1.1.4$$

Where T_{hot} = temperature of the hot end

T_{cold} = temperature of the cold end

ΔT = temperature difference between hot end and cold end.

To enhance thermoelectric efficiency, both type of thermoelectric materials should be high in ZT values and large temperature difference across the thermoelectric materials. Now a day, thermoelectric materials performance was improve to ZT>1, especially p-type materials as show in fig 1.1.3.

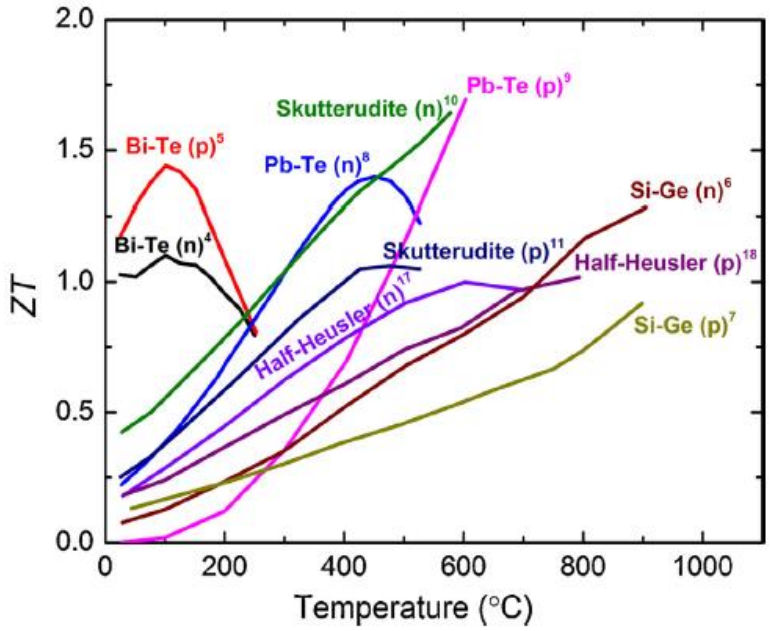

Fig 1.1.3 Temperature dependence of ZT of difference thermoelectric materials[3]

1.2 Skutterudite

Skutterudite structure have strong in thermoelectric properties because of this structure is one of the class in Zintl compounds. The Zintl compounds is the product between alkali metal, alkaline earth, post-transition metal or metalloid, those element made up of electropositive cations which donate their electrons to electronegative anions, which in turn use them to form bonds in order to satisfy valence. In skutterudite structure contain of transition metal and pnictogen atom, in structure consist of a square ring of pnictogen atoms that sharing bonding and form with transition metal then created empty cages. So that, In Fig 1.2.1 represent six pnictogen such pnictogen ring in a large square divided into eight smaller square. It suggest that there are two small square, one at the upper right front and another at the lower left back, which do not contain a ring of pnictogen atom. In the other words, skutterudite contain two structural voids often called “cage”. This instead of MX_3, this structure in the cubic space group Im3.

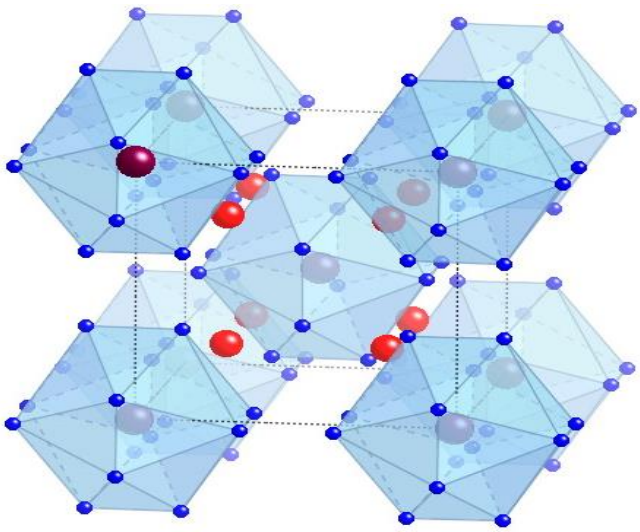

Fig 1.2.1 skutterudite crystal structure

Binary skutterudite compounds AB_3 can form with various elements. That was predicted as fig 1.2.2. Transition element is 8c position and pnictogen atom is in 24h. the octahedras create large voids in structure, that are able to accommodate electropositive element such as rare earth, alkali metal etc. Filler element are just loosely bound in the cages giving rise to low energy optical modes.

The skutterudite form by substantial overlap and minor electronegativity differences between cation and anion to produce a highly covalent structure with exceptional

carrier mobility that relatively high intrinsic electrical conductivity. The concept of introducing guest atoms into these voids without structure distortion because unfilled skutterudite can maintain the cage structure without guest ions. A marked rattling effect is expected owning to large vibration of small guest ions located inside the cage. When M is transition metal and X is pnictogen This formula (MX_3) is equivalently $\square_2M_8X_{24} = 2\square M_4[X_4]_3$ when $\square$ symbol represent the void and $[X_4]$ represent four-member pnictogen rings. If take only one-half of the unit cell including a single void and designate the skutterudite structure as $\square M_4X_{12}$

Rattling effects is not only decreased in lattice thermal conductivity but also increases in electrical conductivity because fillers generally are electro positive elements even though having a negligible effect on the band structure.

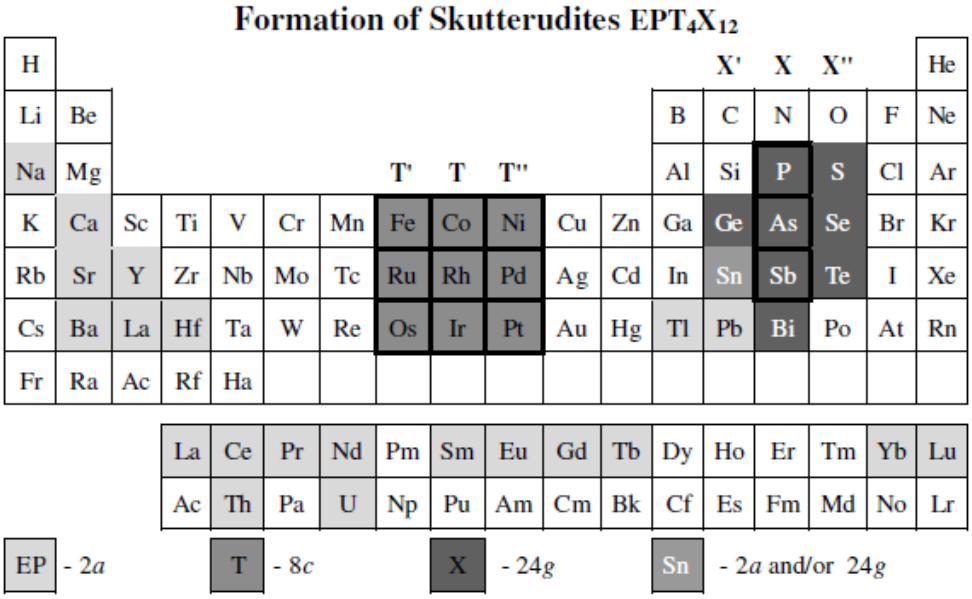

Fig 1.2.2 Formation of binary skutterudite[3]

Filled skutterudite

$$R^{4+}[M_4X_{12}]^{4-}$$

Where R = electronegative ion (the balance of charge)

$[M_4X_{12}]^{4-}$ = a tetravalent negative charge

$[M_4X_{12}]$ = appears as a neutral.

The filled skutterudite consist of 2 groups

1. Compounds are formed by a simple filling of the 2a site of the framework built by 8c and 24h atom
2. Electronically promoted formation of filled skutterudites.

Alkaline earths, rare earths can be considered the main skutterudite because the filler must have a size consistent with the host void and the difference of electronegativity (χ), $\chi_x - \chi_{filler} > 0.8$.

The filler weak bonds with x, their delocatization is responsible for the decrease of thermal conductivity.

Electronegativity of Yb, Rh and Sb

Yb = 1.1

Rh = 2.28

Sb = 2.05

The filled skutterudite consider that the lattice parameter and the size of voids consistently increase passing from skutterudite. The lattice parameter increase with the increase of the mass of metal within a given family of skutterudites.

The role of filler was associated with additional and independent resonant scattering introduced by the weak interaction between the filler and the host structure.

When filled guest atom into structure, a lattice parameter of structure are increase. These is the effect of the increasing of atomic mass in structure.

The limit of the filling fractions depends on

- Radius of the void in the structure
- Radius of the ionic
- The valence state of the guest ion
- Moreover, partially filled skutterudites are very sensitive to difference of electronegativity between the antimony and the guest atom.

1.3 Thermoelectric properties of skutterudite.

As we know, thermoelectric performance can calculated from figure of merit or ZT equation. To enhance thermoelectric performance, the figure of merit should be develop. It have many way to increase figure of merit such as nanostructure techniques or the doping of transition metal or pnictogen-atom. The other method is filled atom into empty cages leading to the formula $A_yM_4X_{12}$ $y \leq 1$ Because of large size between filler atom and empty cage. The filler atom act as independent oscillation then reduce in thermal conductivity. Moreover, Filled skuterudite voids has effect on electrical conductivity, although smaller than the decreasing of total thermal conductivity.

Many studies have investigated reduce lattice thermal conductivity of rare earth filled skutterudite[4]. The filling rare-earth element is not only reduced lattice thermal conductivity but also enhance carrier concentration in compounds, especially, Yb-filled skutterudite. Whereas, heavy mass and small radius have affected on strong interaction in structure[5]. From previously, $Yb_xCo_4Sb_{12}$ had been studied[6], have succeeded in synthesis heavier rare earths filled skutterudite compounds such as $Yb_xCo_4Sb_{12}$ by using high pressure and high temperature (HPHT) synthesis technique. This compound shows high filling ratio, nearly theoretical investigation[8,9]. Accordingly, higher ZT values may be accomplished if the lattice thermal conductivity can be further reduce towards minimum thermal conductivity by increasing Yb filling fraction while maintaining the high power factors observed in Yb-filled compounds.

Therefore, the control of Yb filling fraction is an important issue in optimizing the thermoelectric properties of filling skutterudite compounds. The limit of Yb filling fraction is known to be only 0.2 in $Yb_xCo_4Sb_{12}$. To achieve high filling fraction, it is necessary to compensate for the charge of Yb ions by substitution on either the Co site or the Sb site[10]

Moreover, it shows various interesting physical properties, indicate that high pressure can introduce heavier rare earths into voids skutterudite. High pressure has many advantages, such as decrease impurity phase in preparation method or prevent the disorder[11,12]

1.4 High Pressure Synthesis

The cubic-anvil type high pressure apparatus was used to synthesis thermoelectric materaisl of skutterudite structure. In this work, DIA-type (UHP-500) was used for synthesis, as show in fig 1.4.1. High pressure technique has ability to restrain of disorder phase. Moreover, High pressure method is not complicated and faster than convention method. Accordingly, HPHT method allow heavier rare earth atom easily to entrance into skutterudite structure. A cubic anvil high pressure apparatus was used in this work.

UHP-500 (DIA-type)

A cubic anvil high pressure apparatus type apparatus also known as the equipment can deform materials under high pressure and high temperature. This apparatus consists of six anvils, two of the anvils are fixed opposite to each other on the upper and lower guide blocks, which are driven by uniaxial hydraulic ram. The inner surfaces of the guide blocks from a tetragonal pyramid. The anvil size is 12 mm suitable for a 16 mm pyrophyllite cube. The upper and lower anvil bases are fixed to the upper and lower guide blocks respectively, and the four anvil bases on the side are set slide ably on the 45 ° inclined surface machined into the upper and lower guide blocks. When the upper and lower guide blocks thus configured are advanced relative to each other in the vertical axial direction, the six anvils can uniformly compress six surfaces of the sample to form a hydrostatic pressure field. Regarding the hydraulic pressure, the cylinder first adopts a push-up method in which the guide block attached to the lower part of the frame is pushed up and pressurized. The maximum working pressure is 70MPa. As a system, pressurization, holding pressure and pressure reduction control are set in advance as a pattern for the ultrahigh

pressure generating hydraulic cylinder, and pressure control of the cylinder is performed based on the pattern. With regard to the sample section, the sample chamber is formed in a cubic pressure medium as shown in Figure 1.4.2, and this is placed in line with the anvil surface. An alternating current source is used to generate high temperature, and two opposing anvils are used as electrodes to make the graphite heater in the sample part flow current and raise the temperature. The other two opposing anvils were electrodes for thermocouples for temperature measurement.

Although this size changes depending on the size of the anvil with respect to the generated pressure, the UHP-500 used in this research uses a 12 mm anvil, and as a pressure medium for high temperature and high pressure synthesis, 16 mm square pyrophyllite (habitite: $Al_2O_3 \cdot 4SiO_2 \cdot H_2O$) was used.

Fig 1.4.1 a cubic anvil apparatuses of UHP-500

A cubic anvil high pressure apparatus can be work three step. Firstly, after the sample was being placed in the apparatus at the center of the anvil. The pressure was applied to anvil by the control of hydrostatic compression. Secondly, after the pressure reached a set up pressure, the temperature would increase to the set up temperature. The pressure and temperature were held constant for a period time and detect by using thermocouple and sent to controller (computer). Finally, the sample was quenched to the room temperature and then the sample was characterized composition and thermoelectric properties.

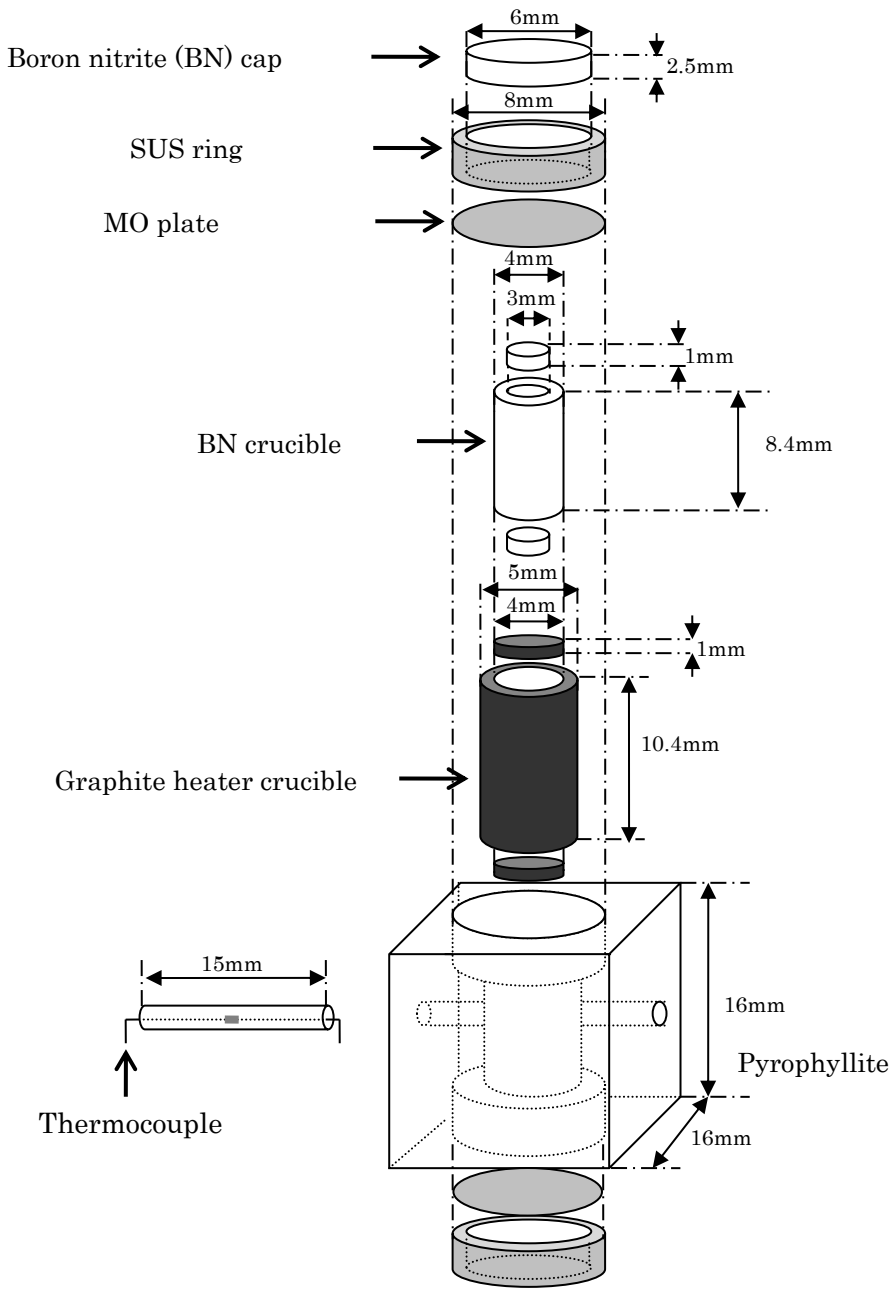

Fig 1.4.2 Assembly of parts for UHP-500

1.5 Motivation

To enhancement thermoelectric performance, the lattice thermal conductivity should be reduce. Skutterudite structure is one of candidates because this compound has large voids inside structure. Guest ion could be filled inside the void. The guest atom act as rattler interact with phonon modes in structure. From previously report, $Yb_xCo_4Sb_{12}$ has been fill in void site with nearly theoretical by synthesis under high pressure and high temperature technique. Beside, lattice thermal conductivity can reduce by insert Yb-atom in Co_4Sb_{12} about 30%. Nevertheless however, Rh_4Sb_{12} system have larger void radius from 7%. Because of Rh4Sb12 is hole dominated semiconductor with strongly covalent Rh-Sb bonds. The strong covalency create high charge carrier mobility and high lattice thermal conductivity. Moreover, Yb is small and heavy. It is believe that if can insert Yb-atom in void cage with highest percentage. It can reduce lattice thermal conductivity then enhance with high thermoelectric performance.

CHAPTER 2

Experimental method

2.1 Preparation of materials

Before synthesis by using a cubic anvil high-pressure apparatus. We need to prepared materials as following,

- Pyrophyllite cube (16x16x16 mm)
- Pyrophyllite lid (Diameter, Ø 2.5 mm)
- Graphite container (inner Ø = 4 mm, outer Ø = 5 mm, length = 10.4)
- Graphite lid (Ø = 4 mm, thickness = 1 mm)
- Boron nitrate (BN) container (inner Ø = 3 mm, outer Ø = 4 mm, length = 8.4)
- Boron nitrate (BN) lid (Ø = 4 mm, thickness = 1 mm)
- Molybdemun (Mo) plate
- Thermocouple

2.2 Synthesis

In this study, a cubic anvil high-pressure apparatus (Sumitomo Heavy Industries UHP-500) was used for synthesis. The cubic-anvil apparatus is shown in fig 2.2.1 The powder of starting materials, Ytterbium (Yb- 99.9%), rhodium (Rh-99.9%) and antimony (Sb- 99.9999%), were mixed by stoichiometric ratio. Those compounds were mashed and mixed in agate mortar and then loaded to boron nitrite (BN) container and graphite to become a pellet. The pellet was insert to pyrophyllite cube. After that, the cube was cover with molybdenum plate and stainless-ring (SUS-ring) for conduct current pass thought SUS-ring and molybdenum plat into sample. An assembly of sample for high pressure apparatus UHP-500 shows in fig 2.2.2. After assemble, the cubic was place in apparatus. The upper stage was rise up and pressure to setting pressure. The compress pressure was control by hydrostatic compression. After press sample to setting pressure, AC current was entering to system. The current is pass through anvil to initial sample. The temperature inside the sample was detect by using K-type thermocouple. In this work, the synthesis condition of $Yb_xRh_4Sb_{12}$ is below,

Synthesis condition.

Pressure: 2 GPa

Temperature: 750°C

450-550°C (Keeping)

The heating rate: 50°C/min, 25 W/min

Time: 2 min (over shoot)

120 min (Keeping)

Fig 2.2.1 A cubic anvil high-pressure apparatus (Sumitomo Heavy Industries UHP-500), Muroran Institute of technology.

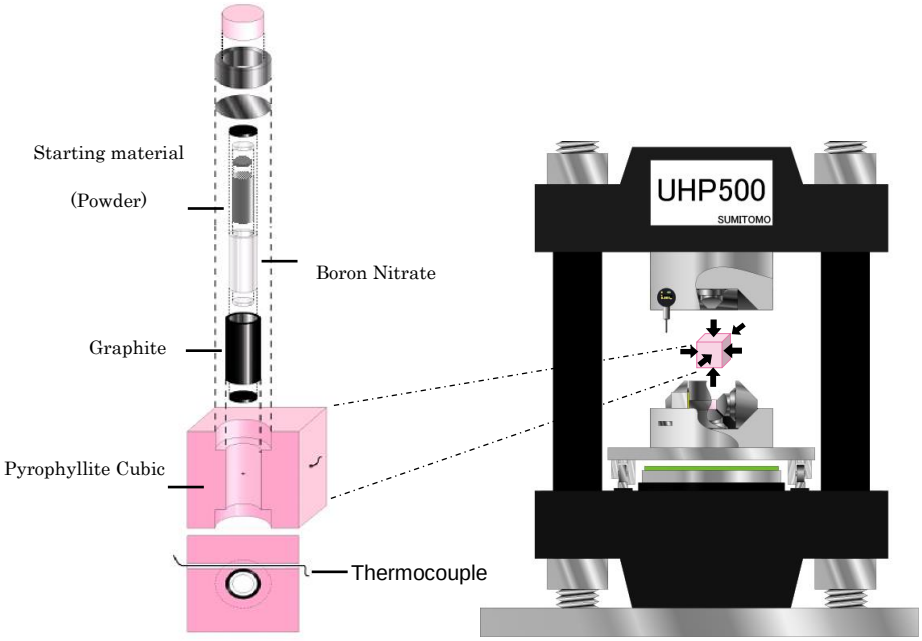

Fig 2.2.2 A assemble of cubic-anvil apparatus (UHP-500)

2.3 Characterization

After finish the synthesis, the sample was cut by diamond cutter and clean by using sand paper number #1500, #5000 and #8000, respectively. Then sample was analyzed phase purity and element composition by using X-ray diffraction instrument (XRD) and Scanning electron microscope (SEM)

- X-ray diffraction (XRD) instrument

In this work, Phase composition and actual element distribution in all sample were investigated by using Rigaku RINT-RAPID-II with with Co Kα radiation and Si powder as a standard. The XRD instrument is shown in Fig 2.3.1

Fig 2.3.1 X-ray diffraction (Rigaku RINT-RAPID-II) instrument, Muroran institute of technology, Hokkaido, Japan

- Scanning electron microscope (SEM)

Scanning electron microscope (SEM) is one of electron microscope that using electron beam to interact sample surface and create an images. The scanning electron microscope (SEM) with energy dispersive X-ray Spectroscopy (EDS),JEOL JSM-6510 Series, was used for measurement chemical electron composition, as show in fig 2.3.2. The EDS using for detects x-rays emitting of element composition to analyse actual element composition. In this work, we use back scattered electron image (BEIW) with magnification 3000 for measure actual composition and select 8-9 point for reduce error.

Fig 2.3.2 a scanning electron microscope and EDS (JEOL JSM-6510 Series Scanning Electron Microscope), Muroran institute of technology, Hokkaido, Japan

2.4 Measurements electrical and thermal properties.

The high quality sample, which is lowest impurity, was chosen for measurement electrical and thermal properties. Those sample were shape to rectangle with wide x length x height about 1.0 x 2.0 x 0.5 mm, as show in fig 2.4.1. The sample should be small in wide and height size but large in length in order to reduce resistivity of materials, as following equation 2.4.1.

$$R = \frac{\rho l}{A} \qquad (2.4.1)$$

where, R= Electrical resistance of a uniform specimen of the material (Ω)

ρ = Resistivity of the material ($\Omega.m$ *or* $\Omega.cm$)

A = Cross-sectional area of the specimen (m^2 *or* cm^2)

L = Length of the piece of material (*m or cm*)

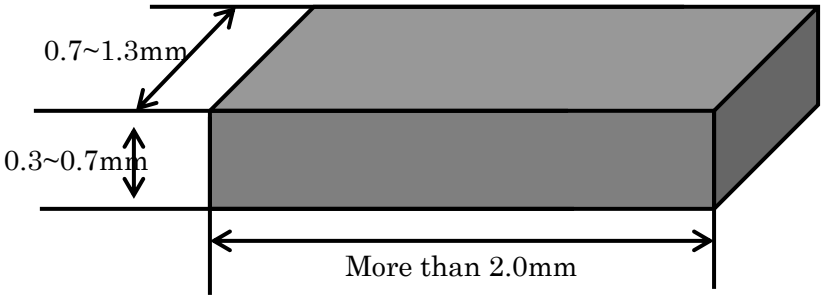

Fig 2.4.1 Sample standard size for measurement thermoelectric properties.

- Cryostat and vacuum system (Thermal block company, Saitama Japan).

This machine was used for measurement electrical resistivity with standards four-probe method. We use the gold wires as a probe, and contact with silver paste. An amount of silver paste is taken out with a toothpick on a glass plate and diluted with α-butyl (the ethylene glycol mono-n-butyl ether acetate) to attach on gold wires and sample same as fig 3.4.2. A current is pass through two outer probe while a voltage is measured through two inner probe. The gold wires and silver paste couldn't touch on each other for prevent short circuit of system. A cryostat and vacuum system (Thermal block company, Saitama Japan) is shown in fig 2.4.3

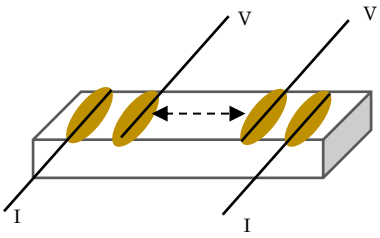

Fig 2.4.2 four – probe measurement for electrical resistivity.

Fig 2.4.3. A cryostat and vacuum system (Thermal block company, Saitama Japan), Muroran Institute of technology, Hokkaido, Japan

- Physical property measurement system (Quantum Design: PPMS)
  The quantum design PPMS can measure various physical properties such as thermal conductivity and Seebeck coefficient as well as electric resistivity and specific heat can be performed. Moreover, this machine can operate over 24 hours per day and 7 days per week. In this experiment, we use PPMS to execute thermal transport option and heat capacity option. A Quantum design PPMS is shown in fig 2.4.4

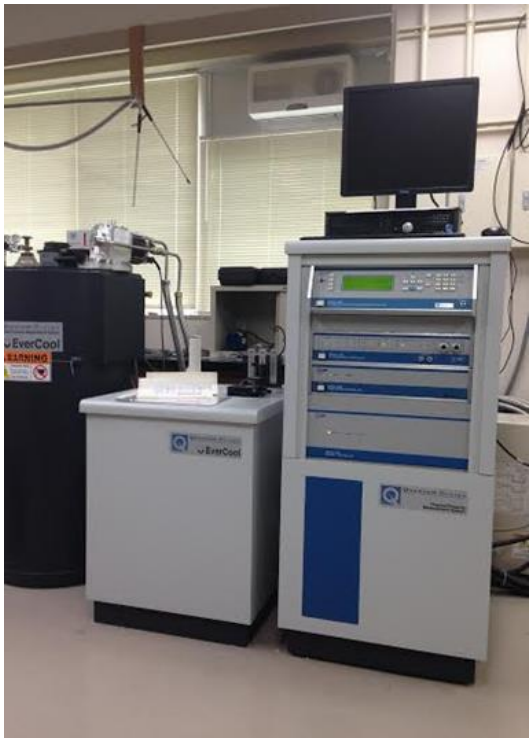

Fig 2.4.4 Physical property measurement system (PPMS; Quantum Design), Muroran Institute of technology, Hokkaido, Japan

- Thermal transport option (TTO)

Thermal transport option (TTO) can measure thermal conductivity (κ), Seebeck coefficient (S) for determined thermoelectric figure of merit (ZT). For TTO measurement, copper lead was use for probe. Prepare two copper lead in length about 1.5 cm and bend as in fig 3.4.5, then mount copper lead and sample by using epoxy(Silver-filled epoxy A part and B part) on the heat plate. After that connect sample with wires shoe in the position as following fig 2.4.6 (The wires shoe is very easy to damage, so we should touch it softly.)

In order to measure thermal conductivity, heat is apply from heater shoe to create a temperature differential between two thermometer shoe and detect on each side of sample.

Thermal conductivity was measured by PPMS Model 7100. The thermal was pass though the sample and then detect by each side of sample. In the parts of measure Seebeck coefficient, while create temperature differential, the voltage drop is also created and detect seebect coefficient.

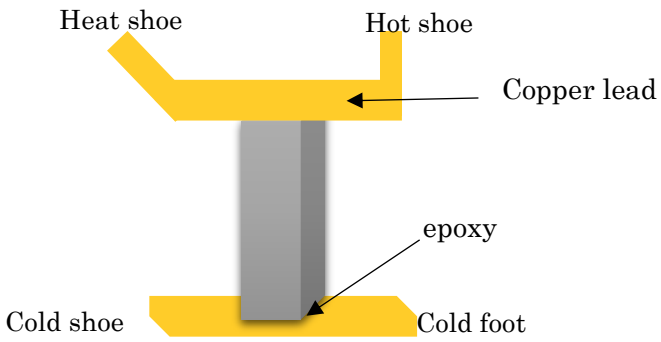

Fig 2.4.5 Sample connection for TTO

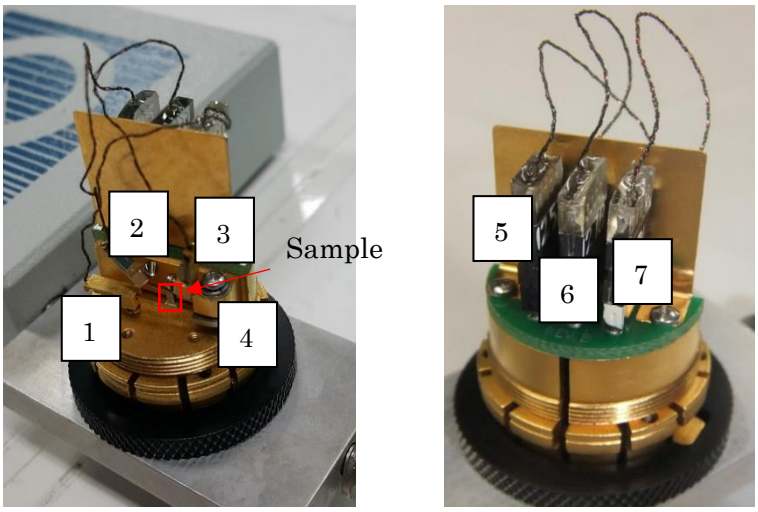

Fig 2.4.6 Illustration sample of TTO puck. (1. Cold shoe, 2. Heat shoe, 3. Hot shoe, 4. Cold foot, 5. Cold shoe, 6. Hot shoe and 7. Heat shoe)

- Hall effect measurement

Hall effect measurement is determine the carrier concentration and carrier mobility under magnetic field. In this experiment, the magnetic was set at 5T. The assemble sample with gold wires method as show in fig 2.4.7. The measurement method can see as following.

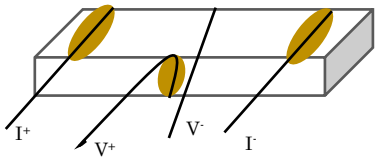

Fig 2.4.7 Sample assembly for Hall effect measurement

(1) PPMS can measure various physical properties function. It can be chose the function by control in option manager mode, as show in fig 2.4.8. Various operations can be performed on the Multivu screen shown in fig 2.4.9. If Option Manager is not displayed, it can be select the **Utilities-Activate** Option menu command in PPMS MultiVu, select on option that we need to be activated in Available Option panel, and then select **Connection Diagram**

* Only one measurement option can be active at a time. If another option is activated. Select Deactivate before select option that we need to measurement.

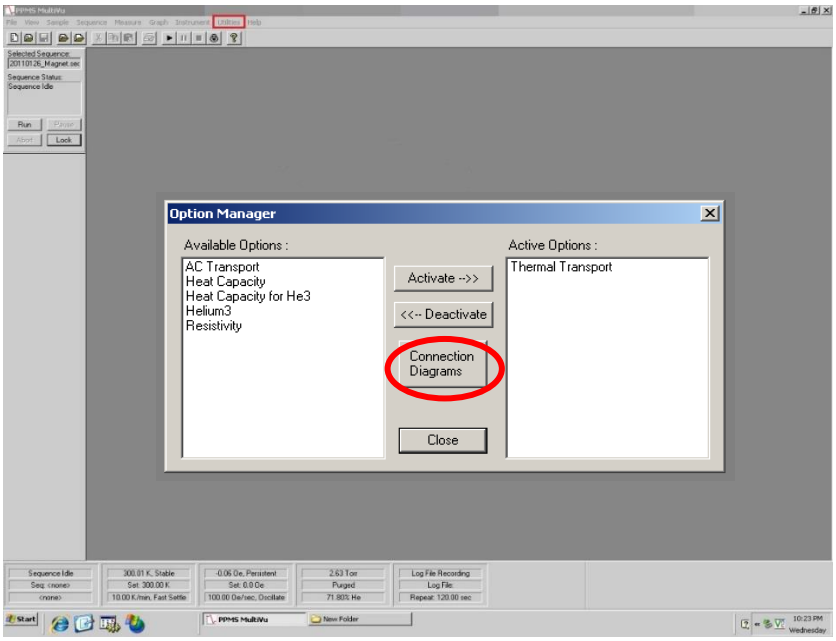

Fig. 2.4.8 PPMS Option manager

(2) Change cable according to the Connection Diagram

(3) Before insert sample. It is necessary to set the inside of the chamber to 1 atm. To

control the pressure in the chamber, select the **Vent Cont.** at the Chamber state panel as shown in Fig 2.4.9. Waiting until state become flooding, then insert the sample pack into the chamber using the sample insertion tool shown in Figure 2.4.10 (a).

(4) Insert the radiation shielding cap tool (as shown in Fig 2.4.10 (b)) into the chamber

(5) Select **Purge / Seal** at the Chamber state panel, wait until the state become purged. (It cannot use High-Vac)

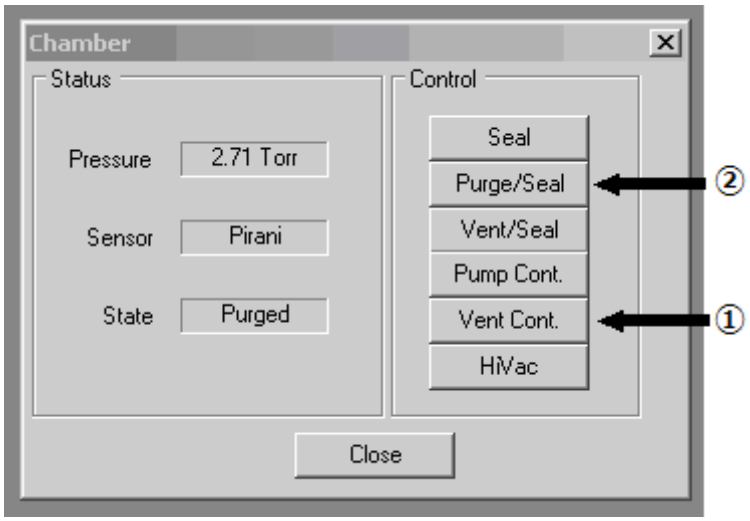

Fig 2.4.9 Chamber Control

Fig 2.4.10 (a) Sample insert tool.

Fig 2.4.10 (b) Radiation shielding cap tool

4.1 Active Resistivity Option (Hall effect).

(1) Select **Resistivity** in the Available Options panel, as shown in Figure 2.4.8. And then select **Activate**. As soon as when resistivity option is activated, the resistivity control, the screen in Figure 2.4.9, appear in to PPMS MultiVu interface.

(2) Create a data file. Press **Browse** button in the resistivity control center in Figure 2.4.11. Select the drive and directory. (Do not use special characters in file names.)

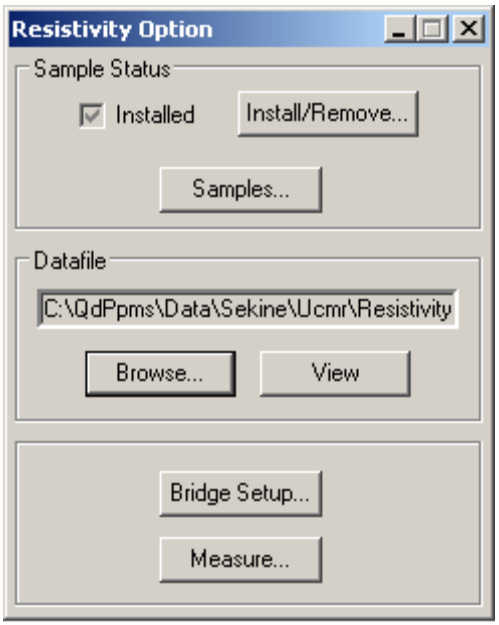

Fig 2.4.11 Resistivity Option

(3) Enter sample description to the File and Sample Properties dialog box open (Figure 2.4.12). After creating the data file, press Samples in Figure 2.4.13 The Sample description represent the user bridge channel that installed sample, the following information:

(a) The name of each sample

(b) The area in mm^2 of each sample. Use "1" when set Units information to Ohm.

(c) The Length in mm of each sample. Use "1" when set Units information to Ohm.

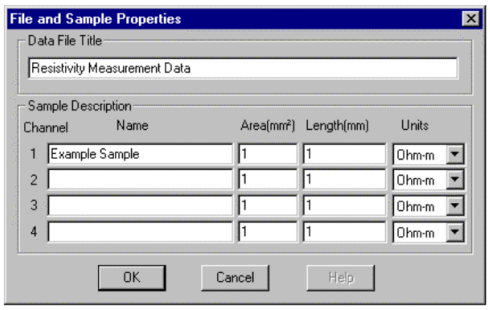

Fig 2.4.12 File and Sample Properties dialog box

(4) Select **Bridge Setup** in Figure 2.4.13 to make various settings. Basically, we can set from 5000,3000,2000,1000,… in current limit (μA) for check resistivity in AC and DC mode in Drive mode, set power limit to1000 μV and Voltage limit to 95 mV in Figure 2.4.13. When setting, Resistance is calculated to the right, so confirm that it is not an abnormal numerical value (Resistance of all value should be constant).

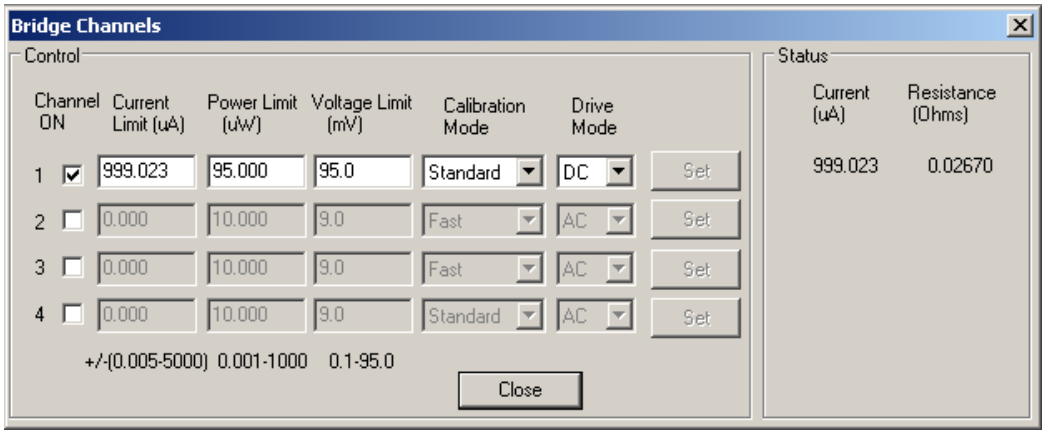

Fig 2.4.13 Bridge Channels

(5) Write Sequence. And then Run sequence

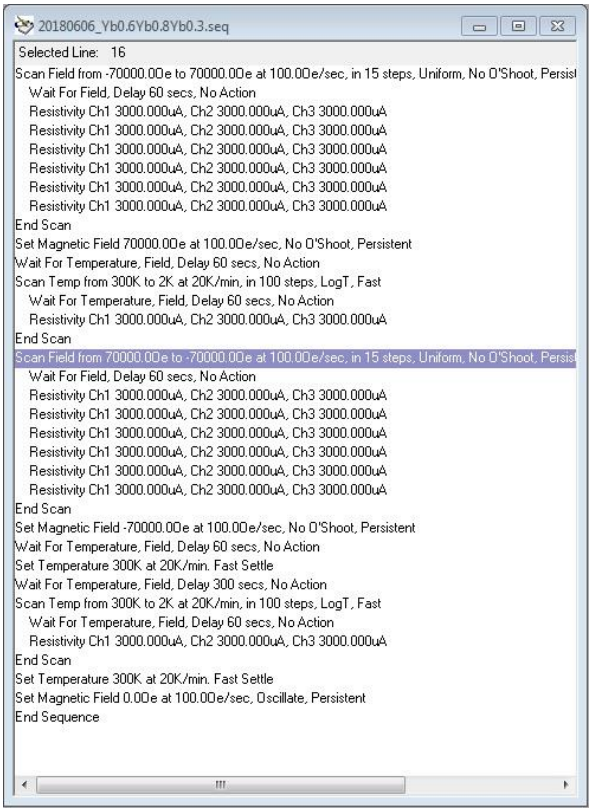

Figure 2.4.14 Sequence data

(6) Log. Open **Utilities-Log PPMS Data**. Since Log Data in Figure 3.4.15 opens, select **Stop** and then select **Browse** on the General tab, and create a new folder named Log

in the folder. Within the created new folder, set the File name as the date of the measurement date and make a file. Select **Start**.

(7) Select **View Data** and Press Select **All** on all tabs, including the Standard Item tab, and take Log of all items.

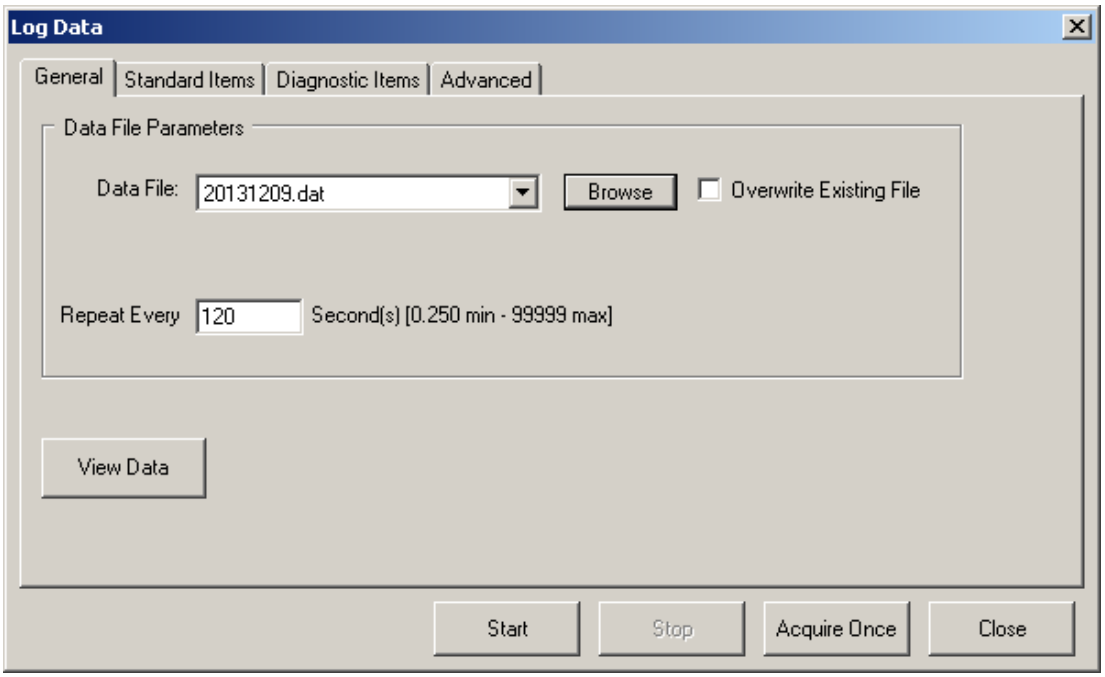

Fig 2.4.15 Log Data

(8) Display the state of measurement a graph. When select **View** in Figure 2.4.11, the graph on the left of Figure 2.4.16 is displayed. **Right click** on the graph - **Data Selection** will display the screen on the right. Select the item you want to display on this screen. In Figure 2.4.16, x-axis select temperature.

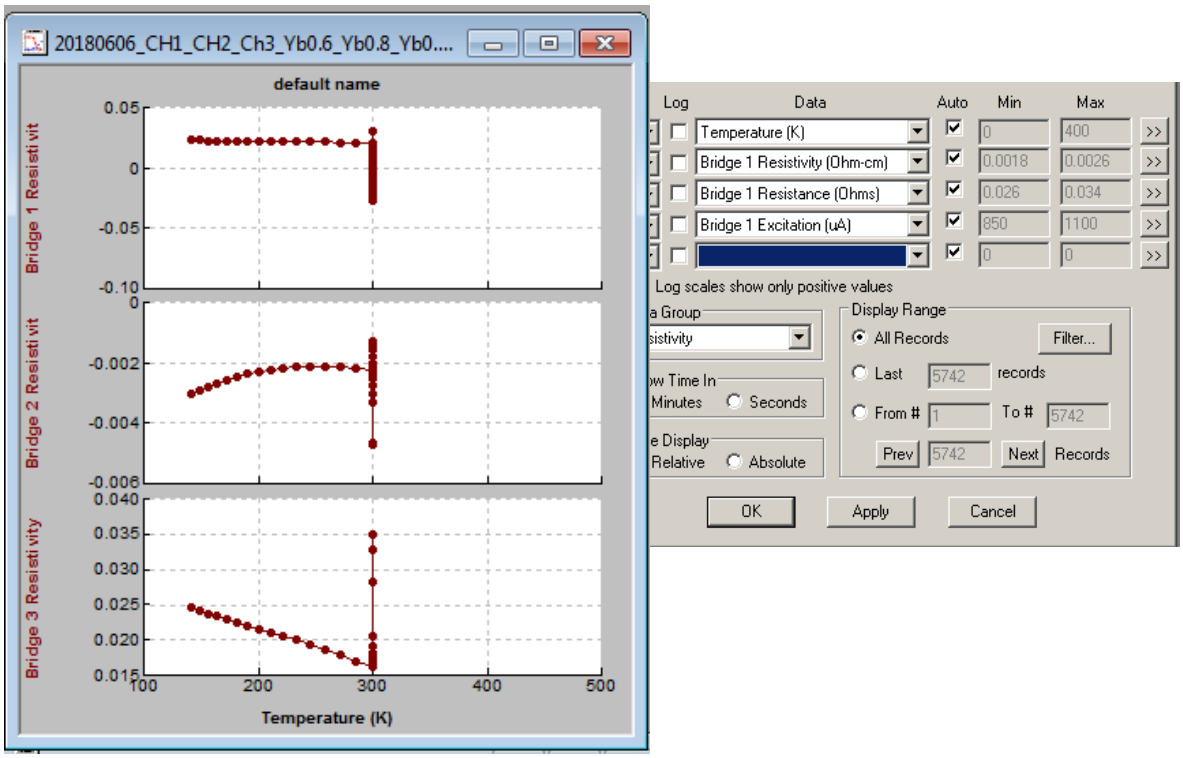

Fig 2.4.16 measurement graph and Data Selection

(9) When it is finished, press View Data to display a graph of temperature change. All necessary screens with reference to Figure 2.4.17.

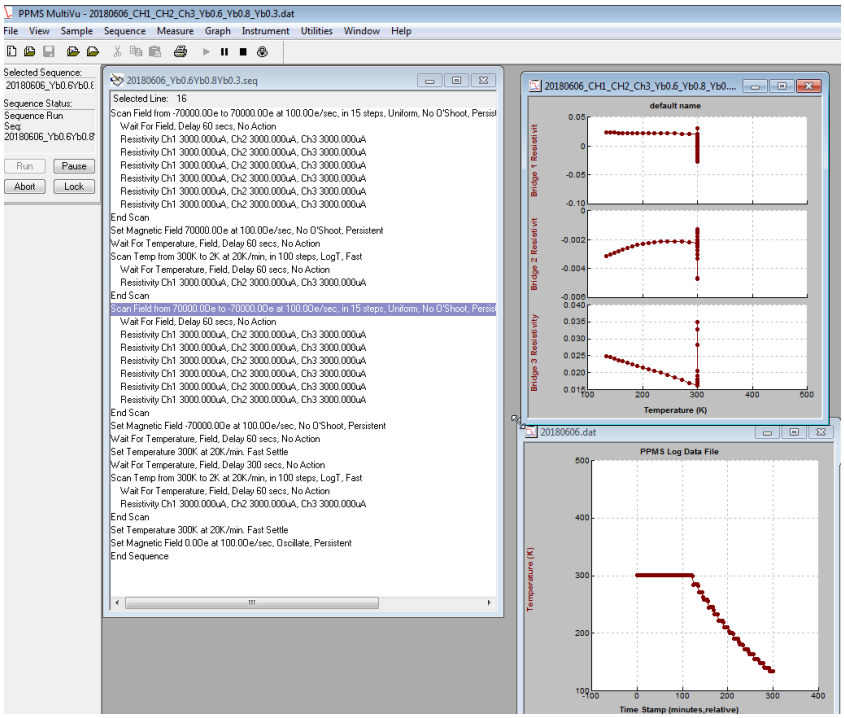

Fig 2.4.17 Measurement screen

- Heat capacity

Heat capacity (HC) measurement, the sample should smaller than 3.0mm×3.0mm. The one side of surface should be parallel with puck. Before measurement of HC the size and the mass sample should be measured. The mounting sequence proceed as below.

(1) Install vacuum pump (Fig 2.4.18) and sample-mounting station (Fig 2.4.19). Turn on vacuum pump and connect puck (adjust to the center of platform holder) and lock puck interlock arm ***be careful do not break platform holder!**

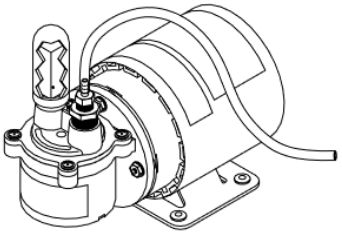

Fig 2.4.18 Vacuum Pump for Sample-Mounting station

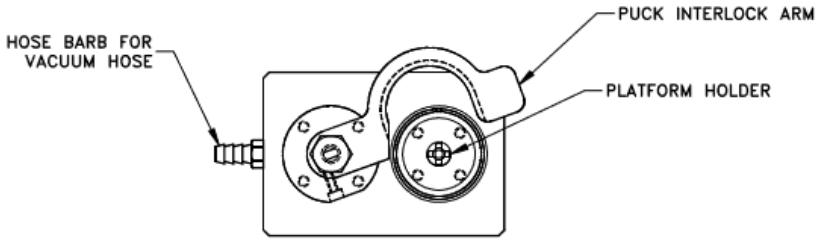

Fig 2.4.19 Sample-Mounting station (top-view)

(2) Clean platform holder by using cotton bud and an apply N grease to platform holder by using toothpick. (Should use N grease as least as possible)

(3) Place the shield on the puck (Fig 2.4.20)

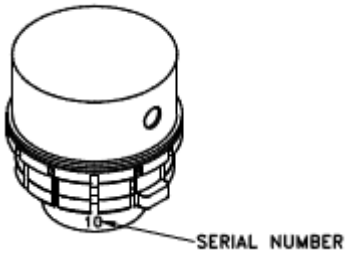

Fig. 2.4.20 Sample holder with the shield.

After assembled sample on the parts, the measurement sequence needs to be prepared as following.

(4) Change cable according to the Connection Diagram

(5) Connect cable, labeled "Heat Cap" (Fig 2.4.21) to P1-Option3, port on model 6500 and connect P2-system Bridge to P2-system Bridge on port model 6000.

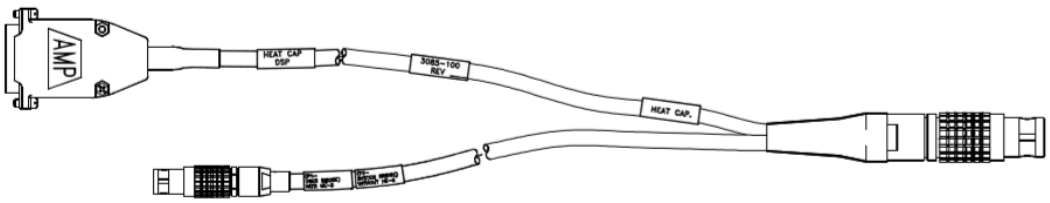

Fig 2.4.21 Heat Cap cable assembly

(6) Check the Power. TTO measurement use the MODEL6000, MODEL6500. (Fig 2.4.22)

Fig 2.4.22. MODEL6000, MODEL6500, and MODEL7100.

(7) Ensure Temperature at 300 K. Before open the chamber, first ensure the temperature is 300 K and field is 0 Oe.

(8) Insert sample into the chamber. Do the following: click **Vent Cont.** button at the **Chamber** windows (Fig 2.4.23); After the state became Flooding at the bottom of the status bar. Insert the sample puck inside the chamber using the sample insert tool as shown in the Fig. 3.4.24

(9) Assembled Charcoal (4038-010) in the bottom of the Contact Baffle (as illustrated in Fig. 2.4.25) and insert it inside the chamber and then close the chamber. The Charcoal will prevent helium from adsorbing on the sample platform when temperature below 10K.

(10) Click **Purge/Seal** button to vacuum the chamber. Wait until the status become purge, then click the **HiVac** button. The status will show At HiVac when the chamber became high vacuum.

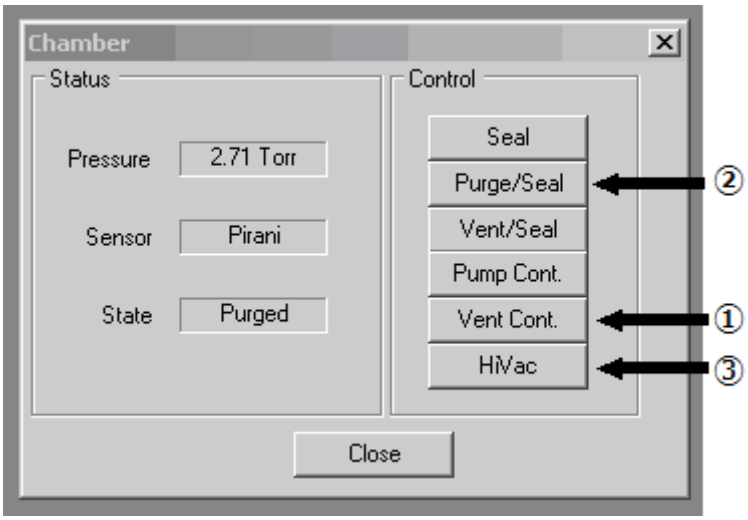

Fig.2.4.23 Chamber control window

Fig.2.4.24 Sample insert tool.

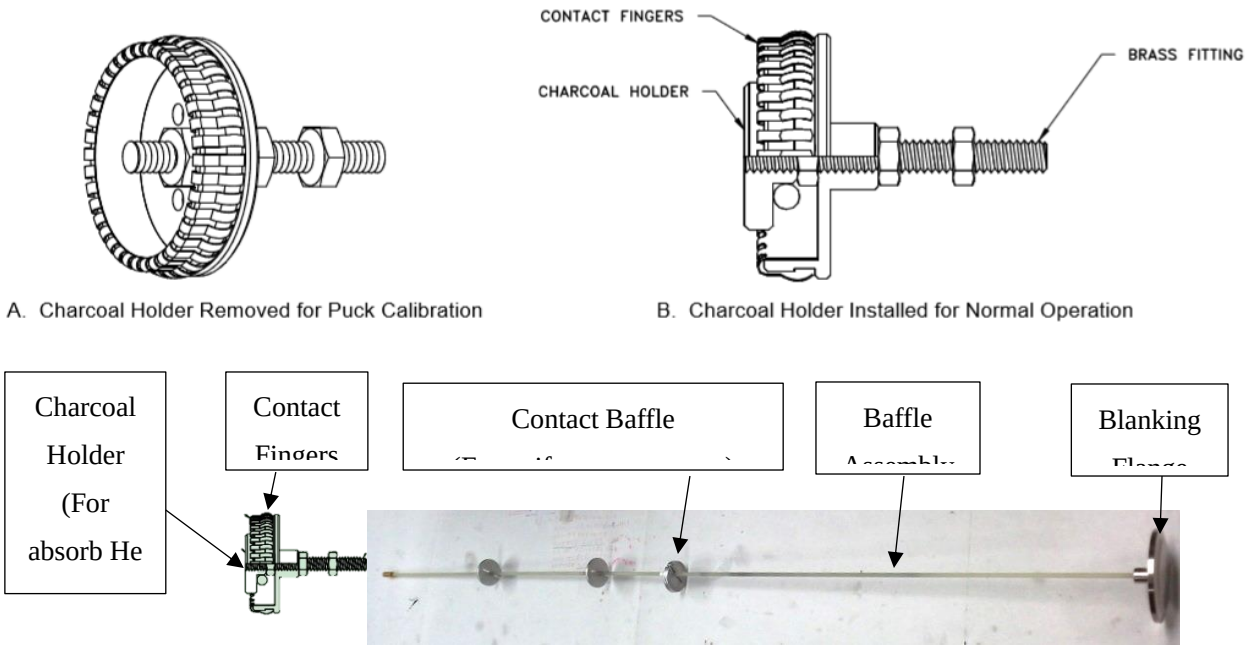

Fig. 2.4.25 Charcoal and Contact Baffle Assembly.

(11) Do the following at the PPMS Multivu window: select **Utilities – Activate Option**, click on **Heat capacity** under the Available Options heading, and then

select **Activate.** (Fig 2.4.26)

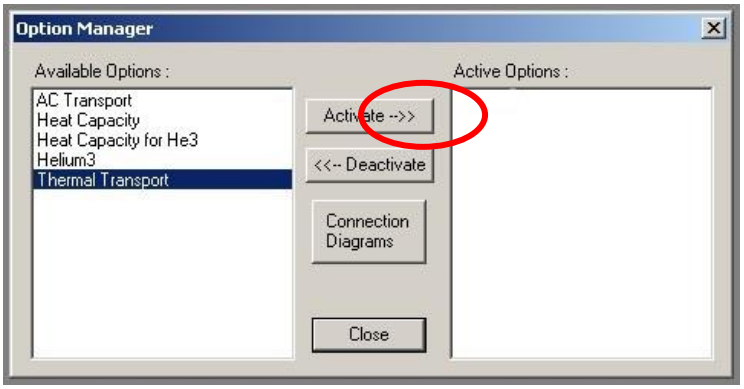

Fig. 2.4.26 Option manager

1. Measurement addenda

(12) Do the following: Click Prepare **Addenda Measurement** (Fig 2.4.27) and check puck serial number and confirm puck (Fig2.4.28) and click **Next** button. Create New file and click **Finish** (Fig 2.4.29)

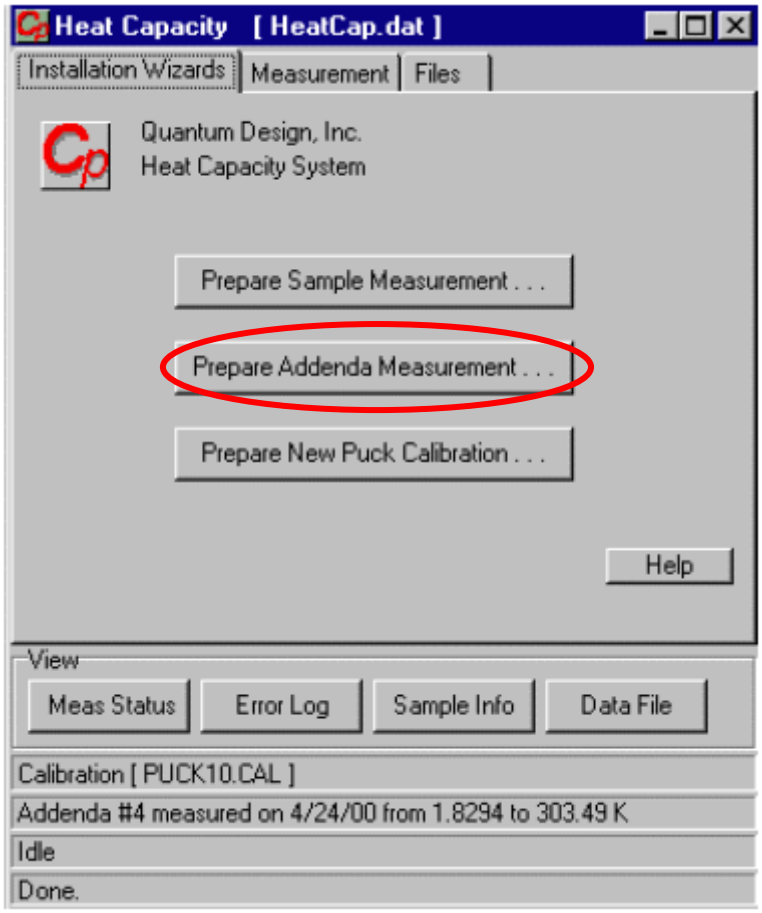

Fig 2.4.27. Windows after activate for Heat capacity

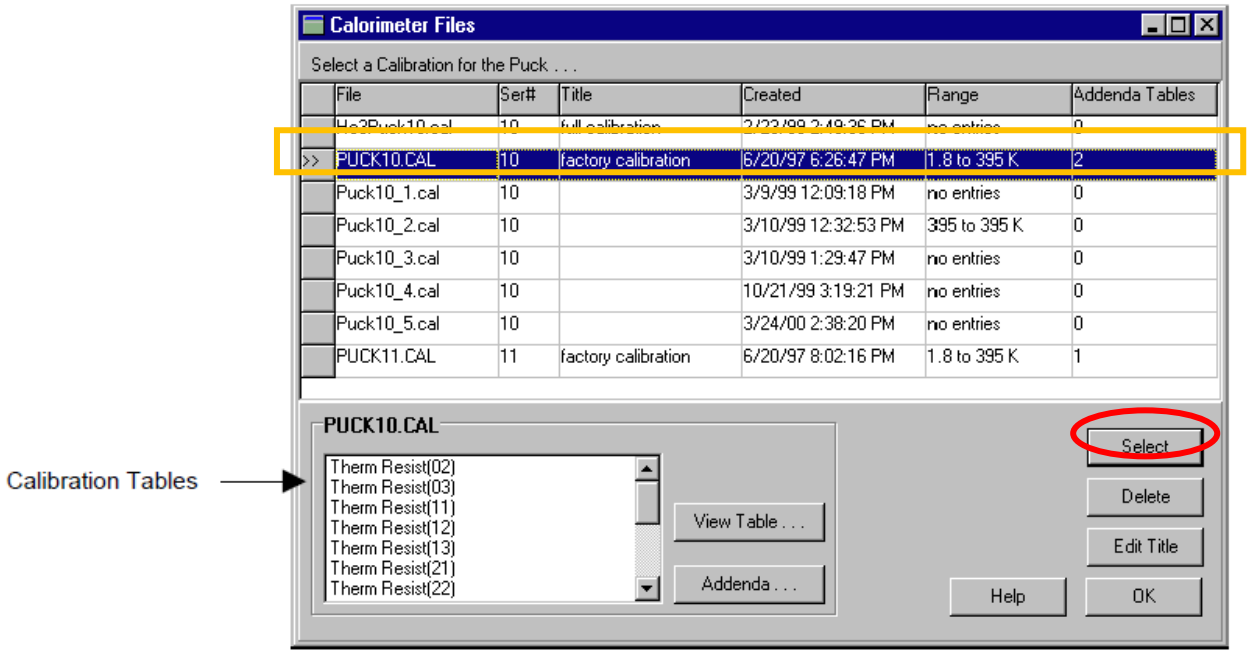

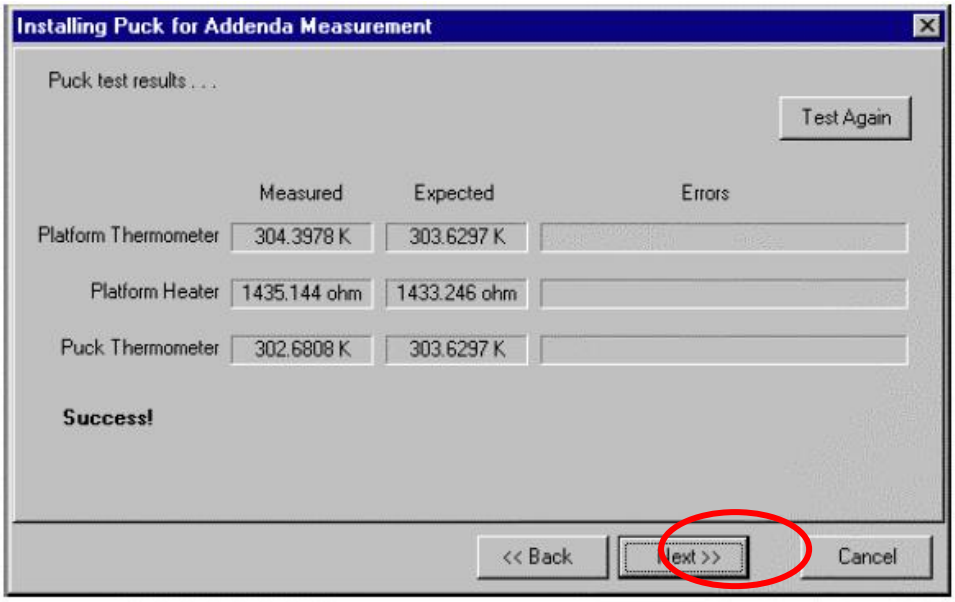

Fig 2.4.28. Puck Calibration

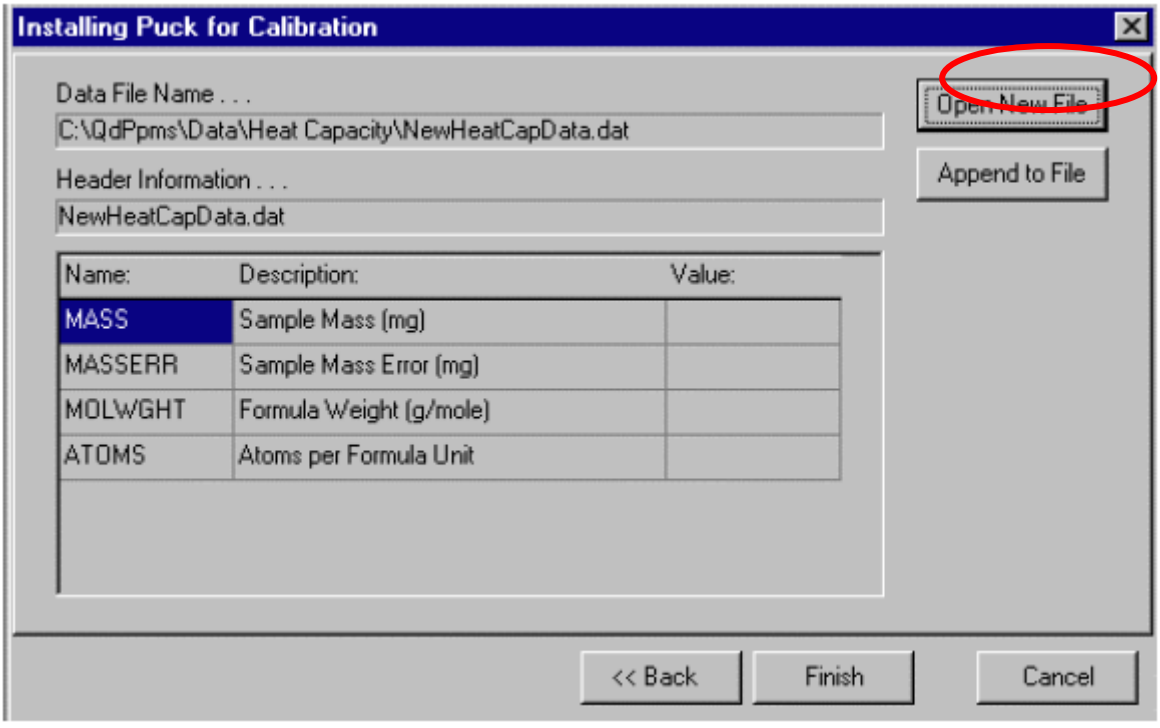

Fig 2.4.29 Data file

(13) Write Sequence. As shown in Fig 2.4.30

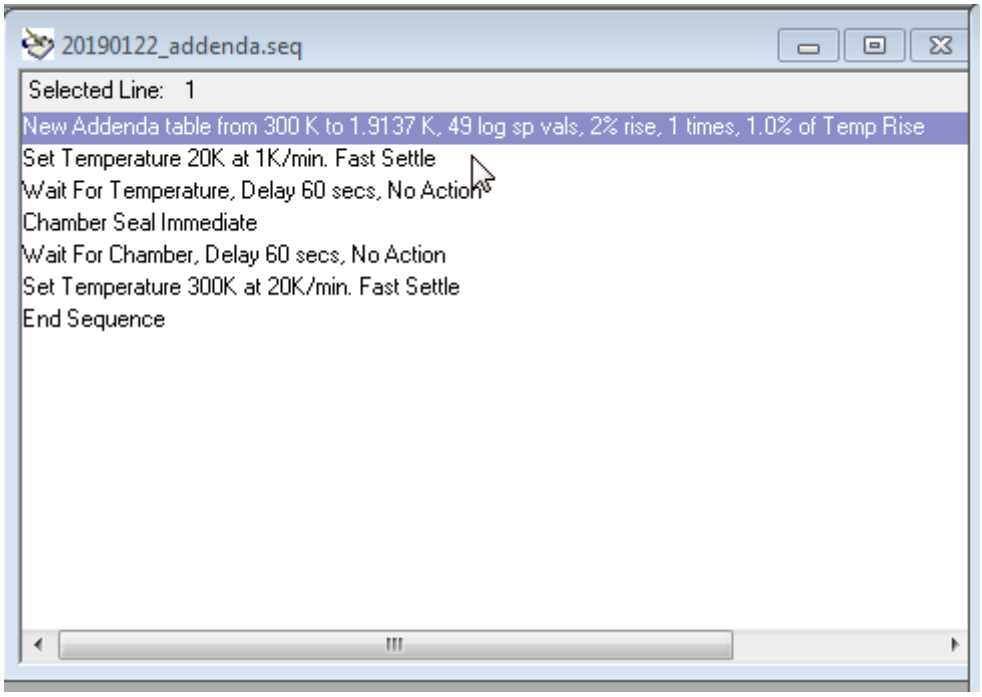

Fig 2.4.30. Example for addenda Sequence.

(14) **Run** sequence and click the **Graph** in file Manu bar and select save name file for view graph (Fig2.4.31). In data selection, select log scale in x and y axis. In y axis should show addenda HC (μJ/K)

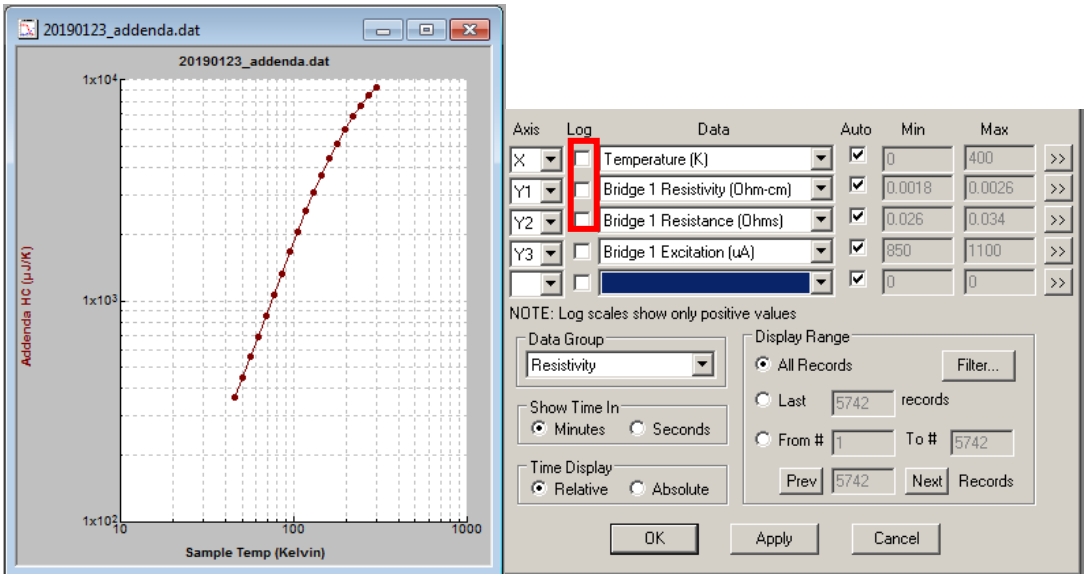

Fig 2.4.31 Measurement graph and Data Selection

(15) In addition, the Log need to be taken for any measurement. Do the following: **Utilities/Log PPMS Data/General-Browse**, make a new folder and click open, **Select all** the Standard Item and Diagnostic Items/Click **Start** button to take the Log data/Click the **View Data** to show the Log Data. (Fig 2.4.32)

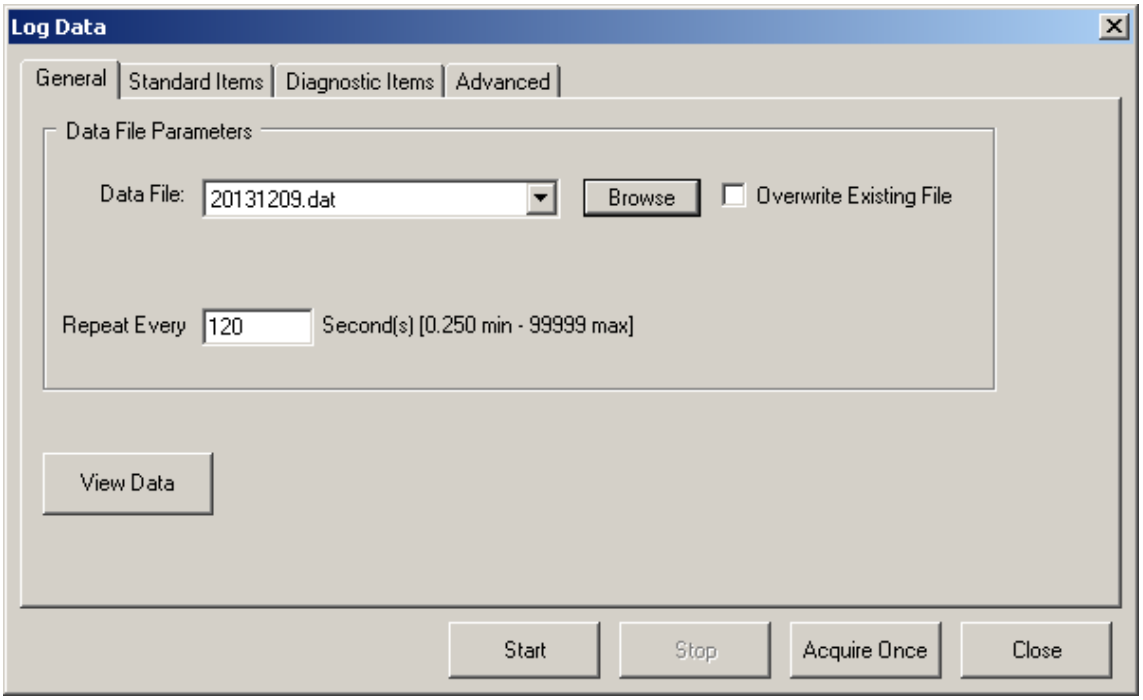

Fig. 2.4.32 Log Data.

(16) Display the state of measurement graph. When select View in Fig 2.4.32 and measurement status viewer (Fig 2.4.33)

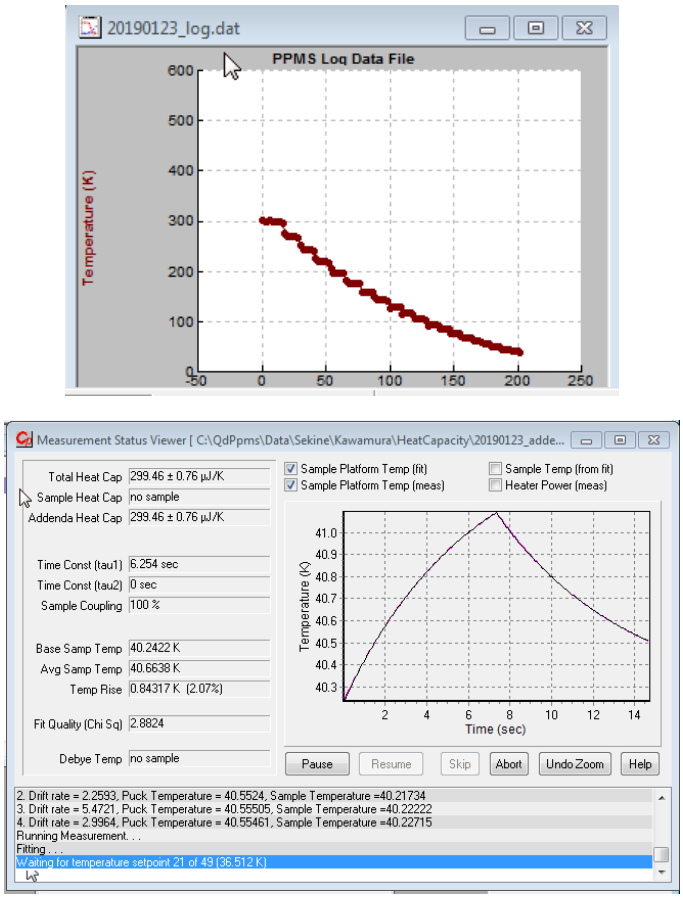

Fig 2.4.33 Log data view and Measurement status viewer

2. Measurement sample

(17) Do the following (7). Adhere sample and platform holder (Fig 2.4.34) and insert sample and do the following (7) to (10). Click Prepare sample measurement (Fig 2.4.27 – Fig 2.4.29). Input sample mass information and select sample heat capacity unit in µJ/K (Fig2.4.35)

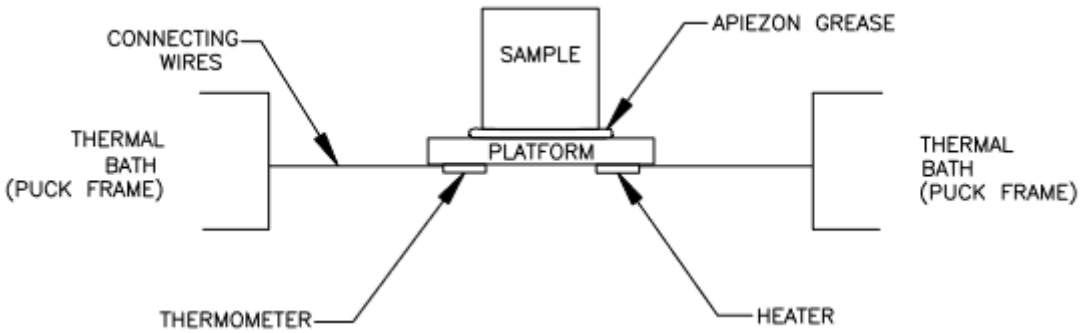

Fig 2.4.34. Connection between sample and sample platform for Heat Capacity

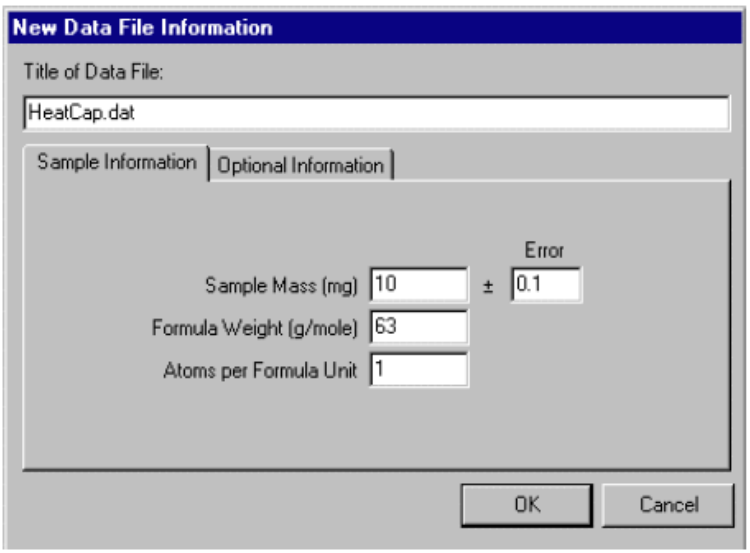

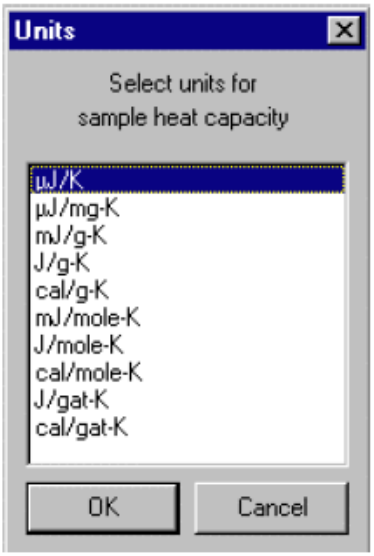

Fig 2.4.35 Input sample information.

(18) Write and Run Sequence (following (12)-(15))

(19) After the measurement finish, the status in left will became **Sequence Idle**. Ensure the chamber temperature is 300K. Then, open the chamber by click **Vent Cont.** Button. Then open the Dewar and take off the sample. Close the Dewar and click **Purge/Seal** button to seal the chamber.

- Magnetic property measurement system (MPMS)

Attach the sample

The weight of sample should be measured before measurement. In the prepared sample section, we use a clear plastic drinking straw to attach a sample because the straw has minimal magnetic susceptibility. The step of attach the sample as following

1. Cut off a clear plastic drinking straw to 12 cm
2. Place the straw segment inside the drinking straw, and insert the sample into the side of straw segment as show in Fig3.4.36. Then move the straw segment and sample until the middle of the length of the drinking segment. The sample should parallel to straw

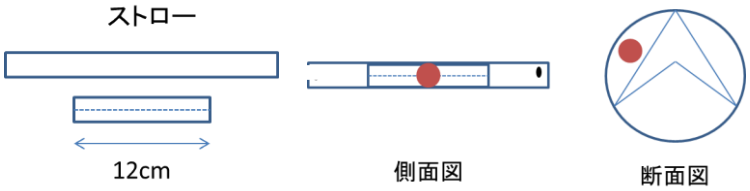

Fig 2.4.36. Correctly positioned sample

3. Punch one side of drinking straw on top and bottom
4. Wrap a tape around the brass-coloured end of the drinking straw.
5. Measure the length between sample and the sample rod, and adjust to 122.7±0.5 cm as show in fig 2.4.37 (* the sample should in the middle of straw segment and drinking straw)

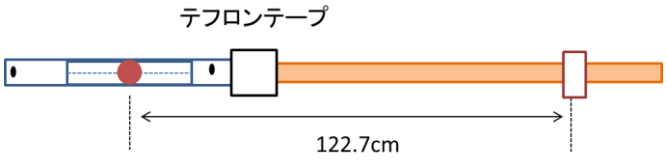

Fig 2.4.37. Sample assemble

■ Insert the sample

Turn the airlock lever to **Closed** position (Fig 3.4.38), the airlock level is closes for protect the lower portion from the air flowing into the top of the chamber. Select **Instrument** on the menu bar, and select **Chamber** and **Vent Sample space**. Verify the O-rings are properly seated and lubricated

1. Insert the sample and sample rod, and push the two slide seal clamps on the socket block assembly.
2. Select **Purge sample space** around 3 time (Waiting for green "**Ready**" LED for insert sample)
3. Turn the airlock lever to **Opened** position, and slowly to insert the sample rod and slowly until the black slide clamp on the rod engages the actuator shoe. If the rod does not move easily, apply a small amount of Grease (Fig 2.4.39) to the rod. Run your fingers along the length of the rod even coating of grease. The knurled nut and two clip screws on top of the actuator shoe should be tight.

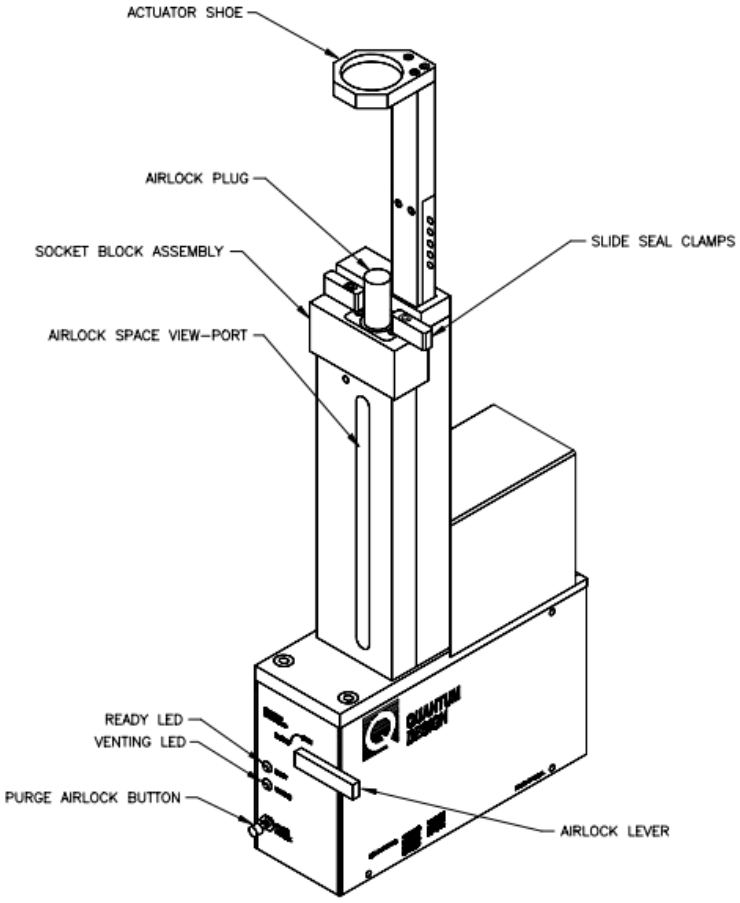

Fig 2.4.38 Sample Transport and Electronic Control Assembly

Fig 2.4.39. Grease

■ Measurment

1. Select **Actual field** in status bar. For example, Set field to 10000 Oe, Approach to oscillate and Mode Hi-Res enabled. (at 10000 Oe with Oscillating with Hi-res enable, if higher than 50000 Oe with on over shot with Hi-res enable)

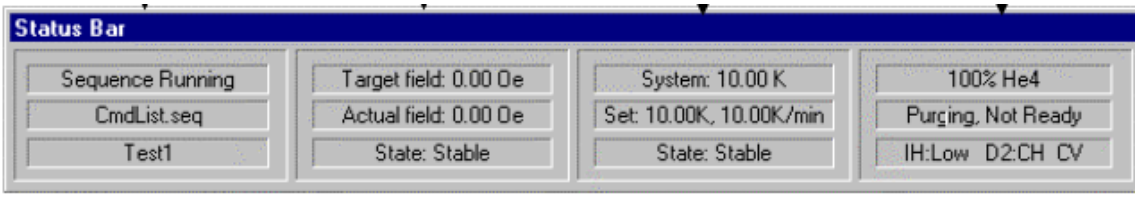

Fig 2.4.40 Status bar

2. Select **Center** and **DC**. The DC Centering dialog box show in fig 2.4.41. Select Initialize Transport for calibrate the sample transport.

3. Select **Parameters**. Set scan length 4 cm and Data points 24 (fig 2.4.42)

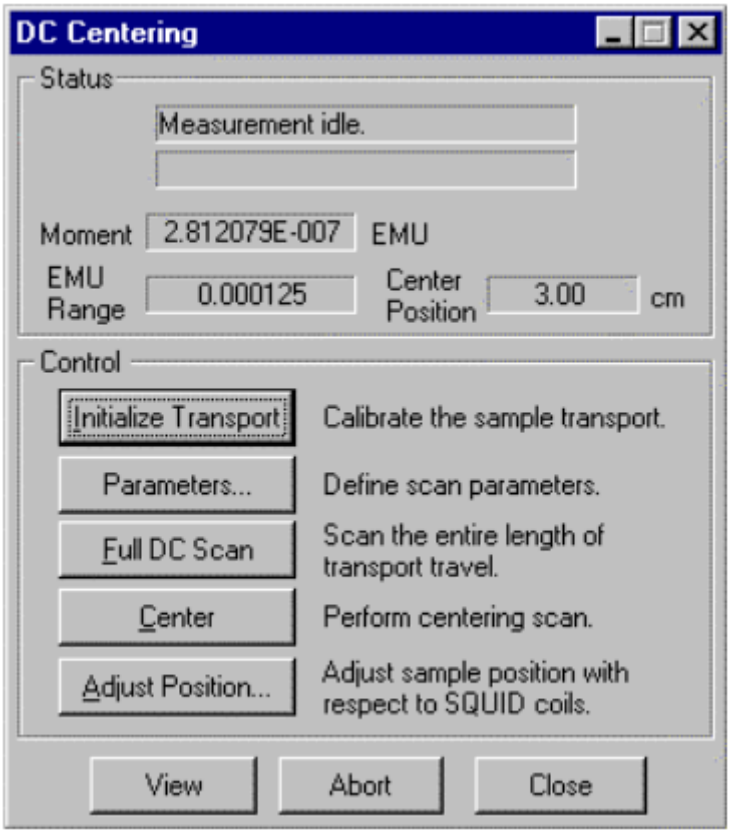

Fig 2.4.41. DC Centering dialog box

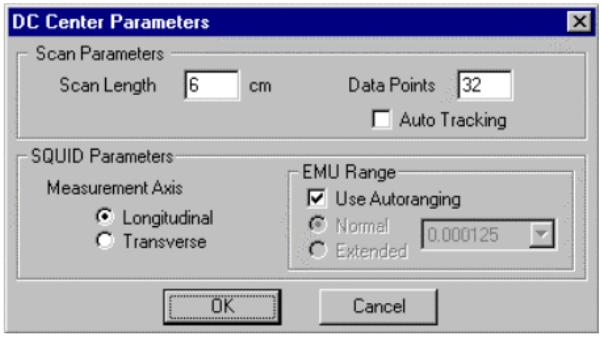

Fig 2.4.42 Parameter dialog box

4. Select **Full DC Scan** for scan full centering measurement, which cover length of the sample transport`s travel path.

5. Select **Center,** scan the location of sample only a partial centering measurement. Check the center of position box, the different position should around 1.5 ±0.5 cm (fig 2.4.43). If different position select **Adjust Position** in DC Centering dialog box, and Select **Adjust manually** (fig. 2.4.44) (If still different select adjust manually again). The sample location should show 2.0 cm. Select **Adjust Automatically**.

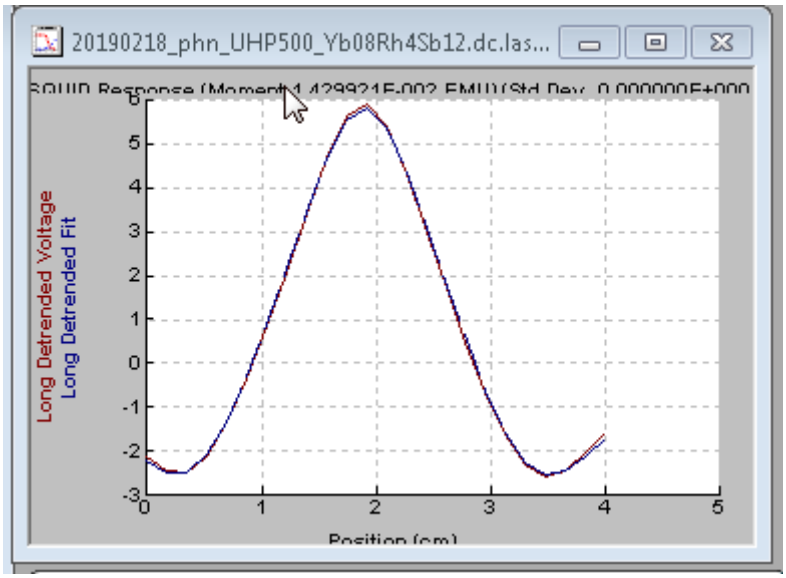

Fig 2.4.43 Center position

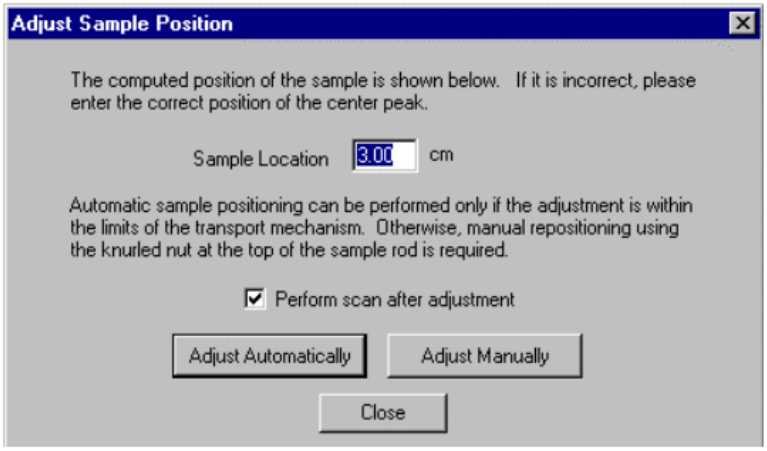

Fig 2.4.44. Adjust sample position dialog box

6. Before run sequence, check He at status bar.

7. **Write sequence**, Save as sequence. Select **Change** sample name in control center, Select **Change** Sequence base data file name (fig 2.4.45).

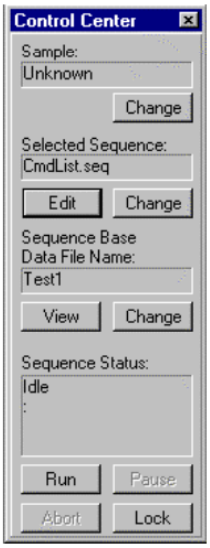

Fig 2.4.45. Control center

8. Select **Utilities and log data**. Select **Stop** and then select **Browse** on the general tab and create files name. Select **Start and View Data** and Press Select **All** on all tabs.

9. Display the state of measurement a graph as show in fig 2.4.46.

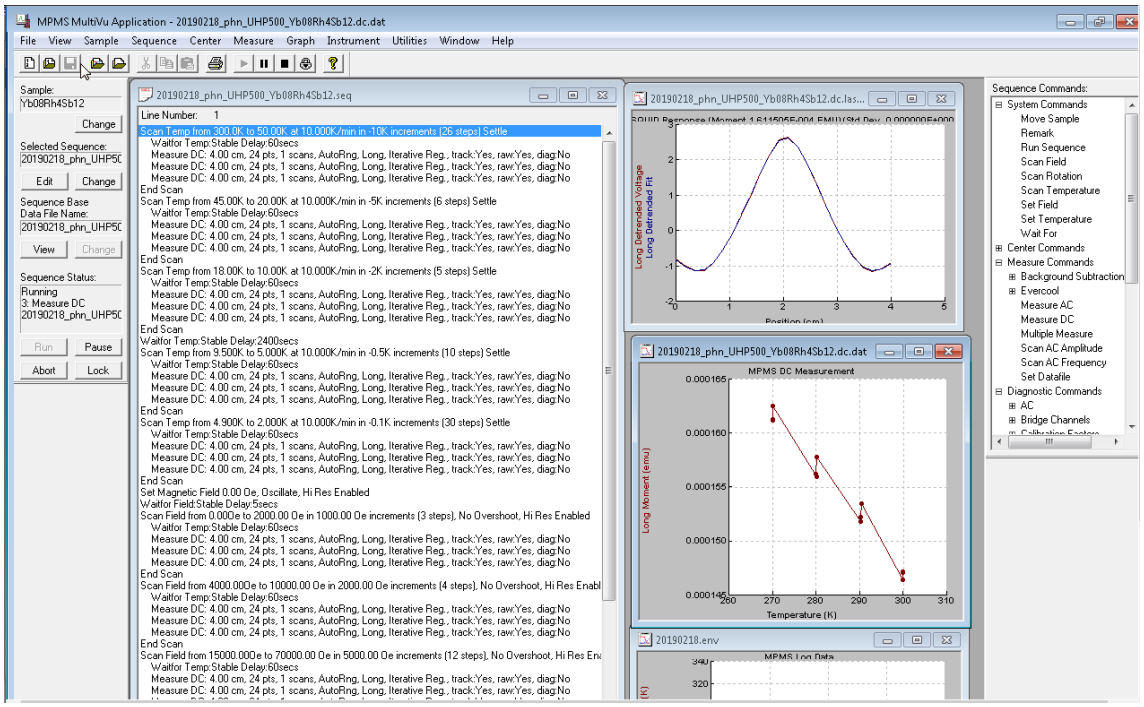

Fig 2.4.46. Measurement screen.

■ Remove sample

1. Ensure Temperature at 300 K. Before open the chamber, first ensure the temperature is 300 K and field is 0 Oe. (Sequence indle)

2. loose two clip screws, Pull sample rod, and turn the airlock lever to **closed** position

3. Set lower chamber to 1 atm. by select **Instrument**, **Chamber** and **Vent Sample space.**

4. Remove sample rod and drinking strew.

5. Install the airlock puck (blue color).

6. Set vacuum the bottom chamber by select **Instrument**, **Chamber** and **Purge Sample space.**

3.5 High temperature range measurement.

Before measurement at high temperate range, sample was prepared by using spark plasma sintering (SPS), at the national institute of advanced industrial science and technology (AIST), Tsukuba, Ibaraki, Japan

High actual Yb filling fraction of $Yb_xRh_4Sb_{12}$ was synthesized using a high-pressure apparatus (UHP-500, Sumitomo Heavy Industries Ltd., Japan) about 2 g.

In spark plasma sintering technique, the sample after synthesized was clean and remove BN by using sand paper and pin then ground into powder with agate mortar. The powder was loaded to crucible and pressed into pellet, heat to 500°C

under a pressure 60 MPa by Spark Plasma Sintering (SPS).

- Laser flash method (LFA) (NETZSCH LFA457)

The pellet was shape to dimension 10±0.1 mm and thickness 2±0.1 mm (fig 2.5.1) for thermal conductivity measurement, using a laser flash method (NETZSCH LFA457).

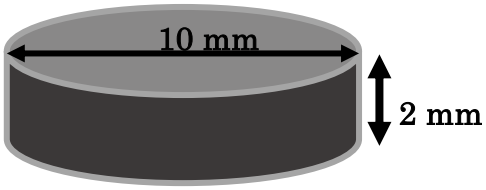

Fig 2.5.1 size of sample for measuring LFA

In Laser flash analysis (LFA) is used to measure thermal diffusivity and calculate . An energy pulse heats one side on the bottom side and detect temperature signal versus time on the top side.

- ZEM-1 (SINKU-RIKO ULVAC ZEM-1)

Electrical transport properties (electrical resistivity and Seebeck coefficient) was measured by ZEM-1 (SINKU-RIKO ULVAC ZEM-1) with sample shape in rectangular with dimension of width (W), height (H) and length 2.0±0.1 mm x 2.0±0.1 mm x 8.0±0.1 mm, respectively. The thermal transport properties and electrical transport properties were measured from 300 K to 723K

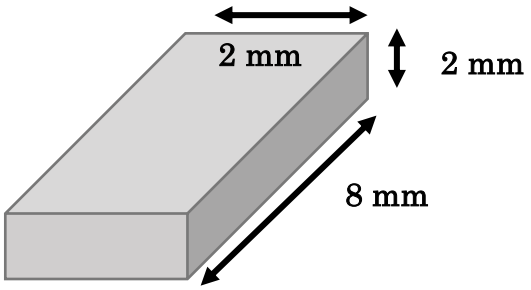

Fig 2.5.2 size of sample for measuring ZEM-1

CHAPTER 3

Results and discussion of $Yb_xRh_4Sb_{12}$ (2GPa)

3.1 Experimental details and Characterization

High-quality polycrystalline sample of skutterudite compounds, $Yb_xRh_4Sb_{12}$ ($0 \leq x \leq 0.9$) were synthesized under high temperature and pressure. At the beginning purified element Ytterbium (Yb), Rhodium (Rh) and Antimony (Sb) were mixed by stoichiometric. Then those element were melted and pressed by a cubic anvil high-pressure apparatus (UHP-500). The element was melted at 750-800^{o}C for 2 minute then decrease to 450-550^{o}C in order to comply with pressure-temperature phase diagram of base $RhSb_3$ (see fig 3.1.1)

The synthesis condition under high pressure is very sensitive in the detection temperature. Thus, the synthesis condition had been controlled by power with temperature. Moreover, the thermocouple position should be good contact with graphite cylinder for reduce error of temperature measuring position. The preparation process, grinding element, has to be avoided, because of possibly oxidation in this process or the oxidation of elementary constituents. Therefore, It is difficult to make good quality sample (purity sample) in every time synthesize. For this reason, a contain of some impurity can determine thermoelectric properties. In fact, the impurity content act as minor carrier, the main influence will be dominated by doping element.

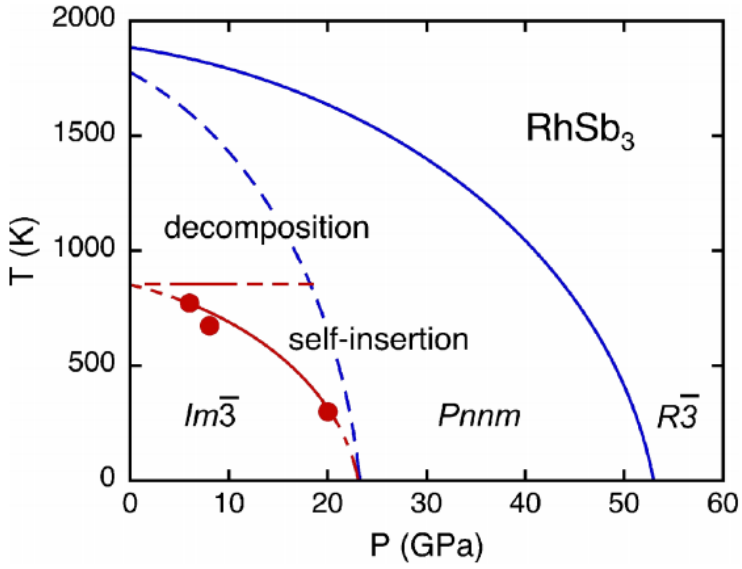

Fig 3.1.1 Pressure-temperature phase diagram of $RhSb_3$ preparation under high pressure technique[12]

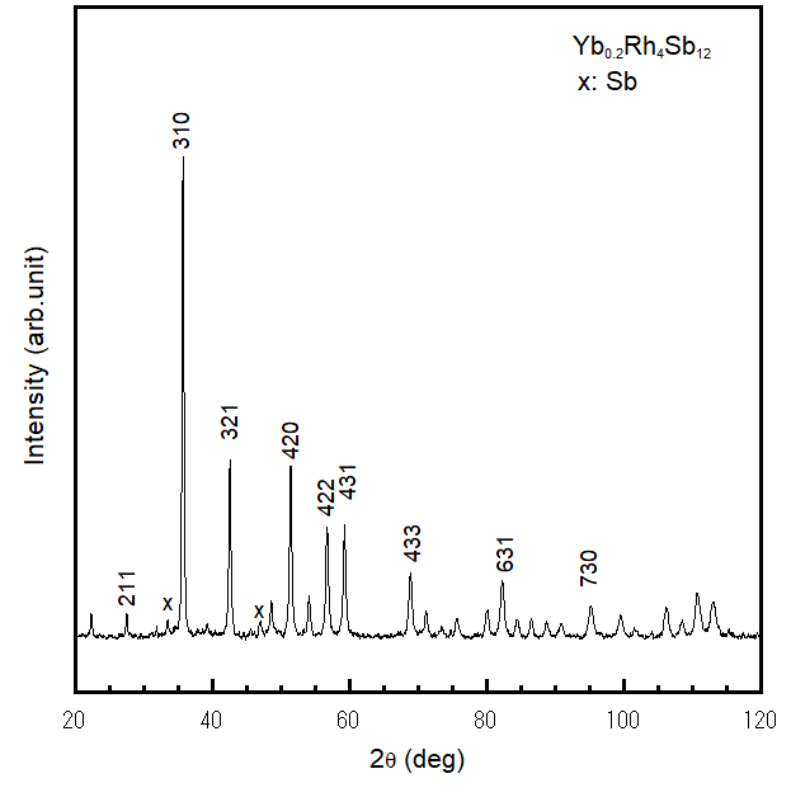

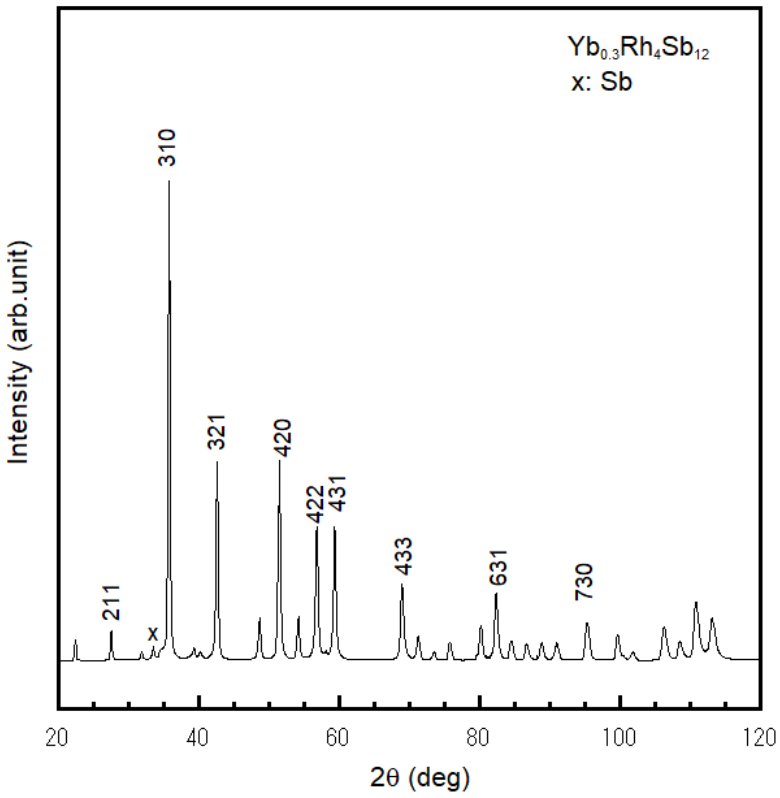
Yb0.3Rh4Sb12
x: Sb
Intensity (arb.unit)
310
321
420
422
431
433
631
730
211
x
20
40
60
80
100
120
2θ (deg)

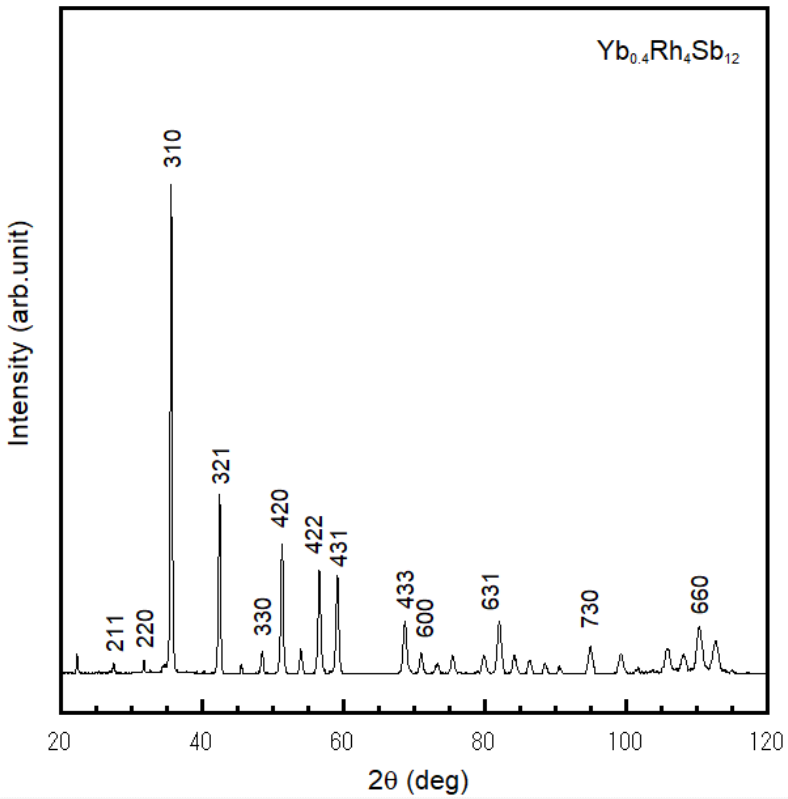
Yb0.4Rh4Sb12
Intensity (arb.unit)
310
321
420
422
431
433
600
631
730
660
211
220
330
20
40
60
80
100
120
2θ (deg)

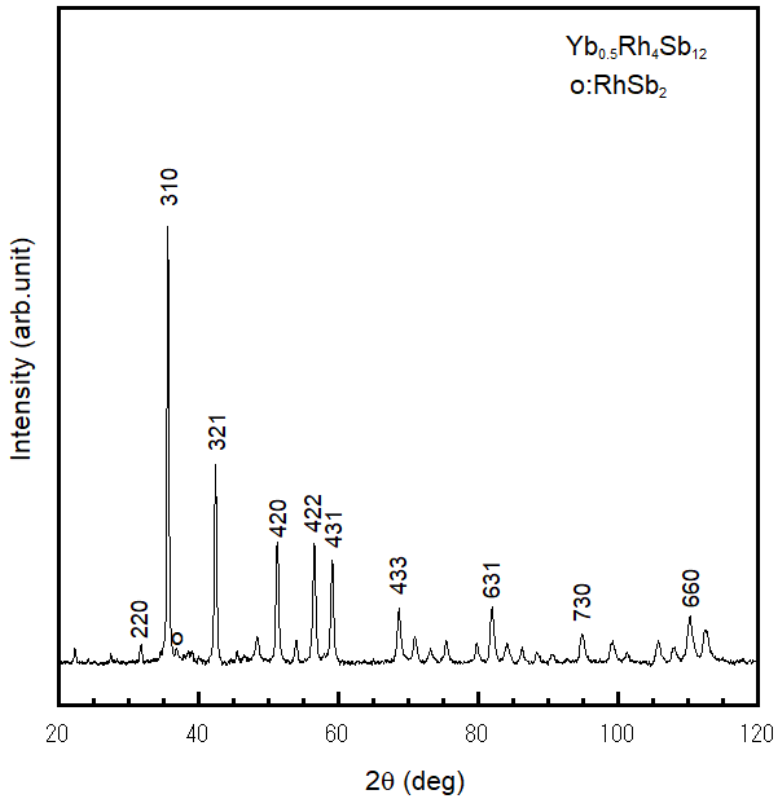
$Yb_{0.5}Rh_4Sb_{12}$
o:$RhSb_2$
Intensity (arb.unit)
310
321
420
422
431
433
631
730
660
220
o
20
40
60
80
100
120
2θ (deg)

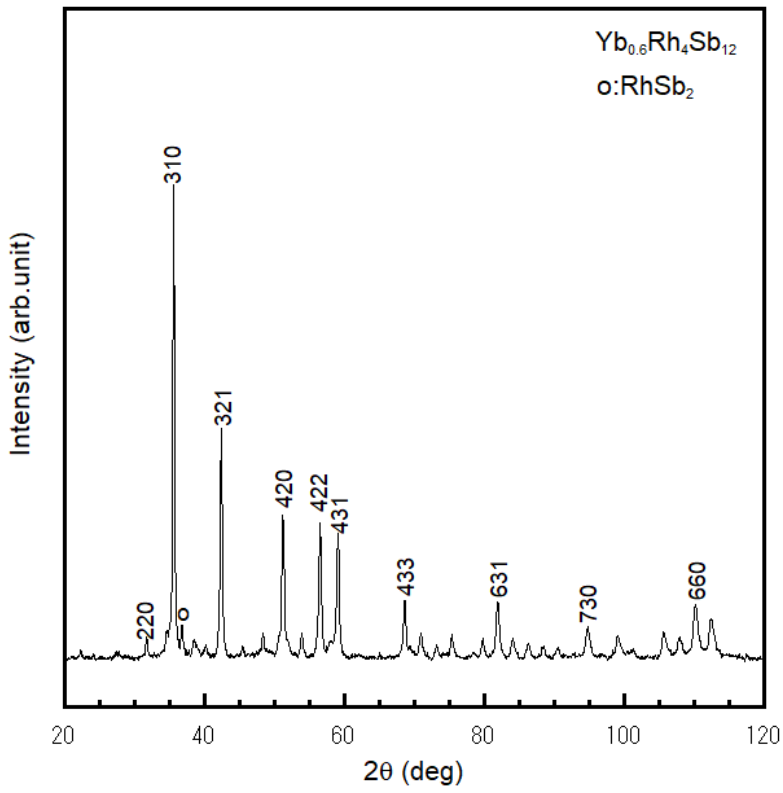
$Yb_{0.6}Rh_4Sb_{12}$
o:$RhSb_2$
Intensity (arb.unit)
310
321
420
422
431
433
631
730
660
220
o
20
40
60
80
100
120
2θ (deg)

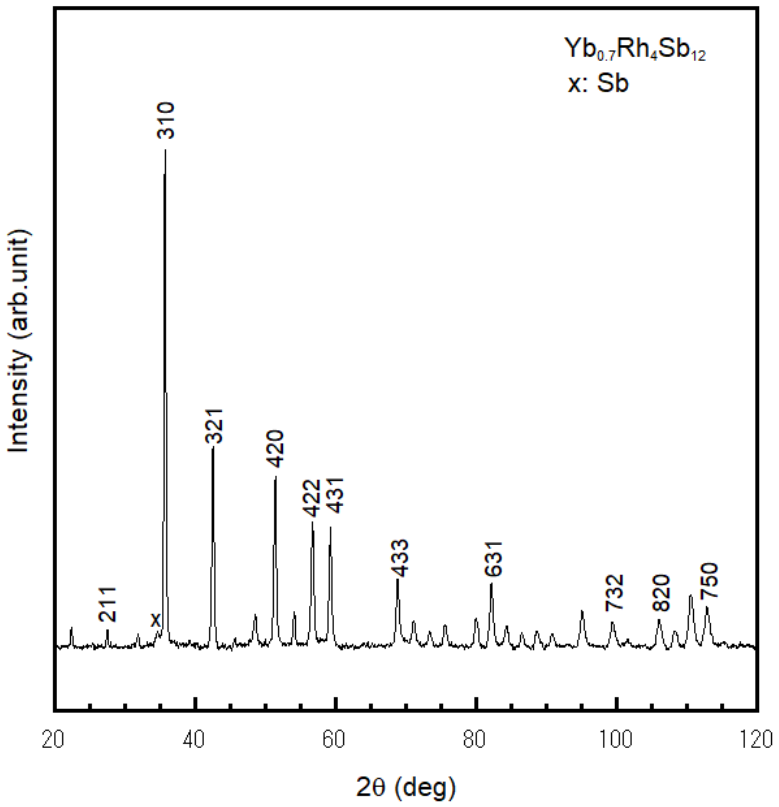
Yb0.7Rh4Sb12
x: Sb
Intensity (arb.unit)
310
321
420
422
431
433
631
732
820
750
211
x
20
40
60
80
100
120
2θ (deg)

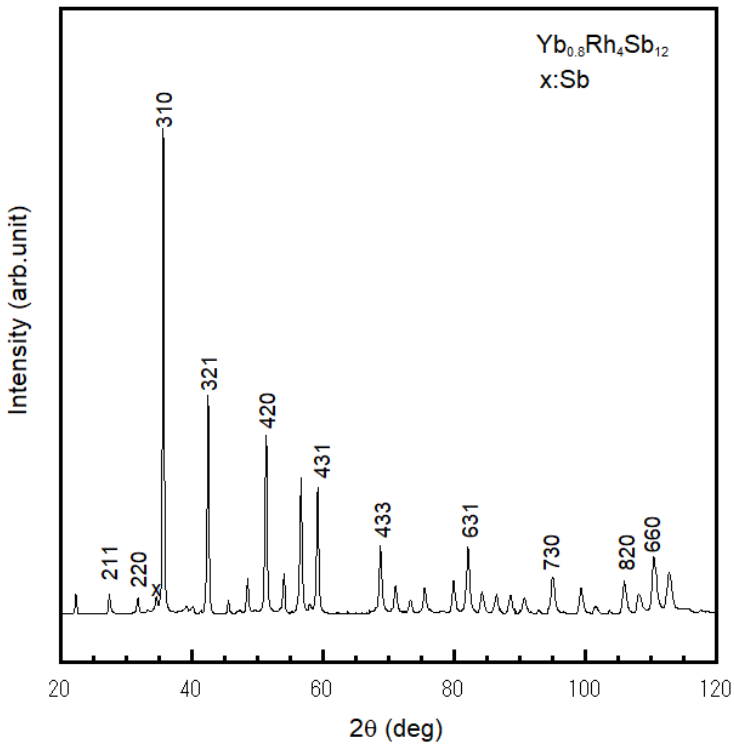
Yb0.8Rh4Sb12
x:Sb
Intensity (arb.unit)
310
321
420
431
433
631
730
820
660
211
220
x
20
40
60
80
100
120
2θ (deg)

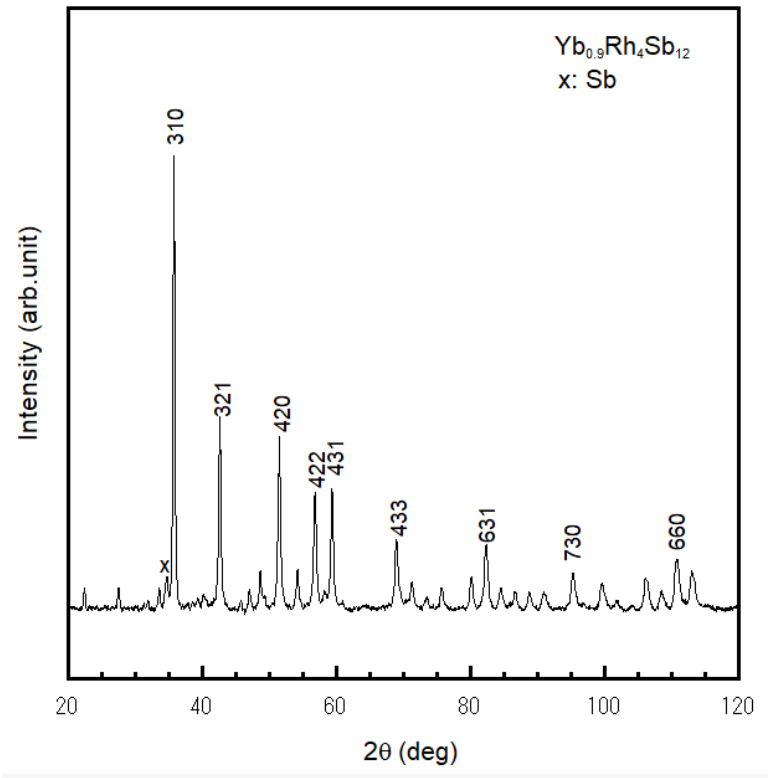

Figure3.1.2 X-ray diffraction pattern of $Yb_xRh_4Sb_{12}$ ($0.2 \leq x \leq 0.9$)

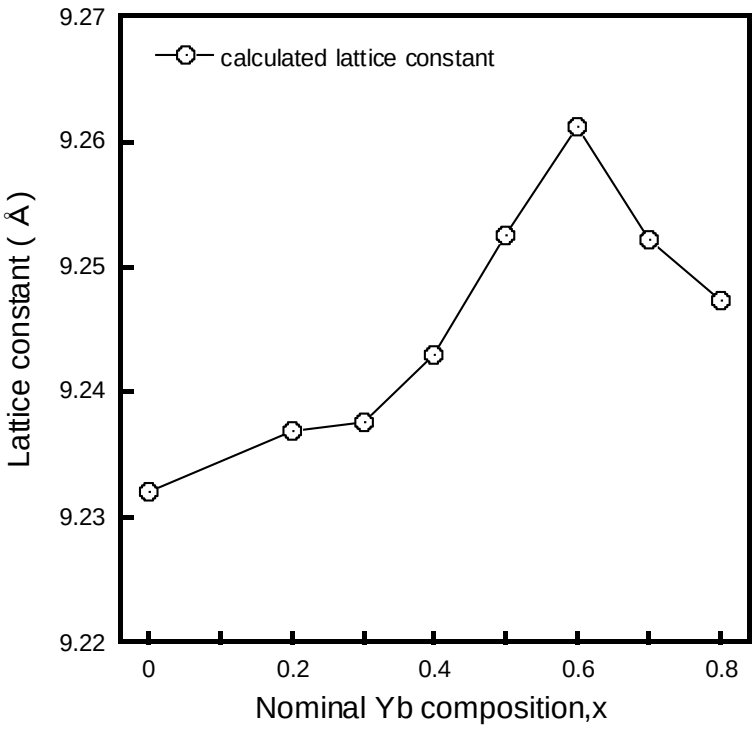

Figure 3.1.3. The relationship between nominal Yb compotion and calculated lattice constant.

Figure 3.1.2 shows the powder X-ray diffraction pattern of polycrystalline $Yb_xRh_4Sb_{12}$ ($0.2 \leq x \leq 0.9$) skutterudite samples with different Ytterbium concentrations. The $Yb_xRh_4Sb_{12}$ skutterudite compounds exhibit in a body-center cubic crystal structure belongs to Im-$\bar{3}$ space group (No. 204). The x-ray diffraction results shows almost a pure skutterudites phase. A negligible peak of secondary phase was observed in X-ray diffraction pattern (see figure 3.1.2). A low insensitivity of secondary phase is corresponding with $RhSb_2$ and Sb. The $RhSb_2$ is a binary compound of antimony and rhodium, exhibit in monoclinic crystal structure in space group P21/c (No. 14). In secondary phase of Sb was observed in R-3m (No. 166) with Trigonal crystal structure. The lattice parameter was calculation from x-ray diffraction pattern by a least-square fitting method. The result of calculation lattice parameter of Yb-filled skutterudites corresponding with nominal composition, as show in figure 3.1.3. From the least-square fitting method the estimated lattice parameter of unfilled Rh_4Sb_{12} is 9.232 Å. the lattice parameter expanded with Yb doping filling fraction up to 9.2612 Å at $Yb_{0.6}Rh_4Sb_{12}$ composition. The lattice parameter of rare-earth filled Rh_4Sb_{12} prepared from ambient pressure, $La_{0.1}Rh_4Sb_{12}$[23] and $Yb_{0.1}Rh_4Sb_{12}$[17] are 9.2213 Å and 9.2289 Å, respectively. Those lattice parameter are smaller than mother compounds, Rh_4Sb_{12} (9.232 Å). This different results from $Yb_xRh_4Sb_{12}$ synthesis under high pressure technique.

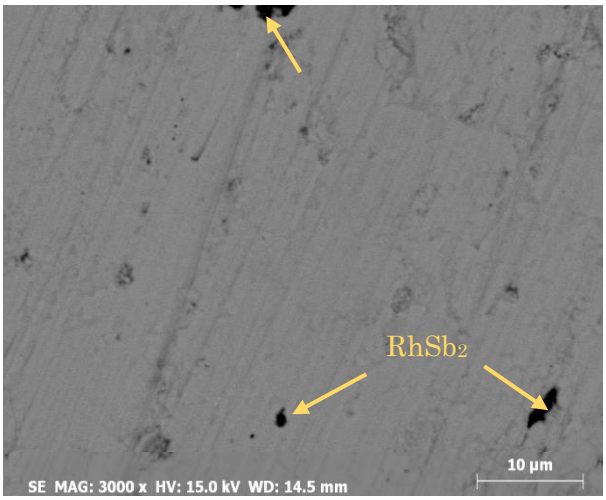

SEM image #1: $Yb_{0.2}Rh_4Sb_{12}$

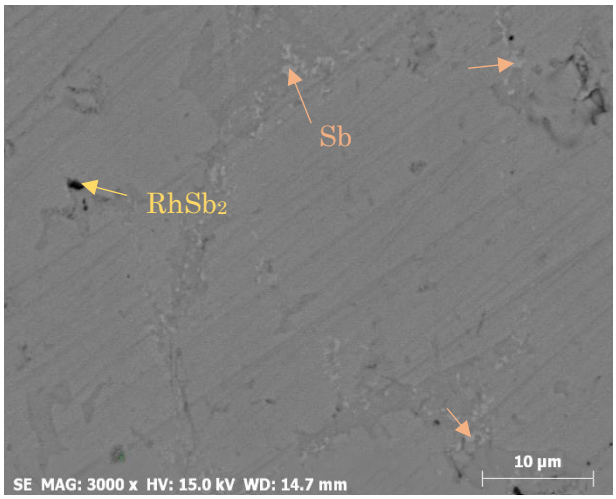

SEM image #2: $Yb_{0.3}Rh_4Sb_{12}$

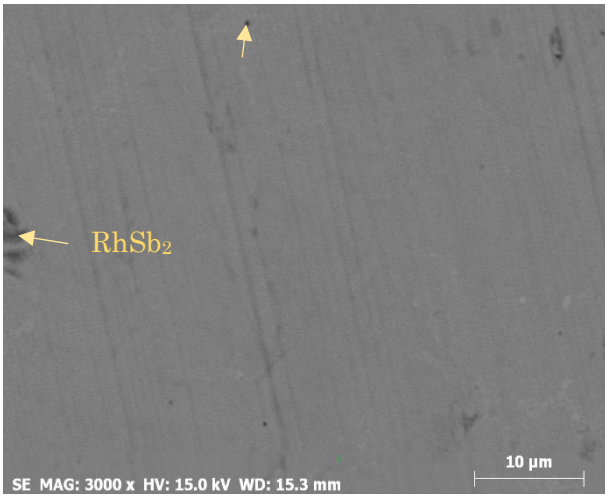

SEM image #3: $Yb_{0.4}Rh_4Sb_{12}$

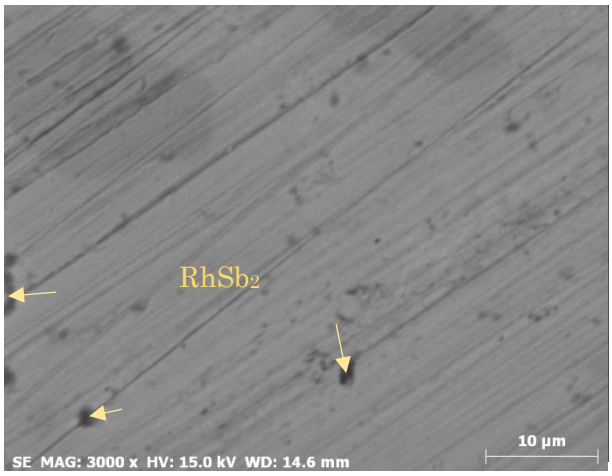

SEM image #4: $Yb_{0.5}Rh_4Sb_{12}$

SEM image #5: $Yb_{0.6}Rh_4Sb_{12}$

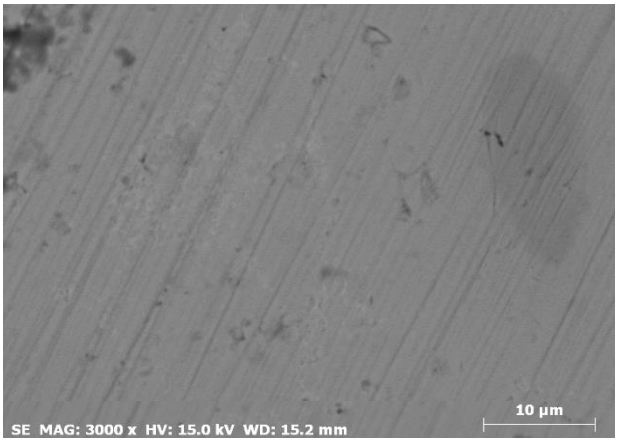

SEM image #7: $Yb_{0.7}Rh_4Sb_{12}$

Figure 3.1.4 BEW-SEM images of polycrystalline $Yb_xRh_4Sb_{12}$ ($0.2 \leq x \leq 0.7$)

A scanning electron microscope (SEM) is produces image of the sample surface and detect the element composition by using energy-dispersive X-ray (EDX). In the

backscattered electron composition, BEC-SEM images the skutterudite material of $Yb_xRh_4Sb_{12}$ ($0.2 \leq x \leq 0.9$) was shown in figure 3.1.4. The surface area of $Yb_xRh_4Sb_{12}$ sample is almost homogeneous with grey colour area. On the other hand, some point areas are inhomogeneous, which are found the secondary phase of $RhSb_2$and Sb in the black point and white point, respectively. The actual filling fraction of homogeneous compound was observed by using EDX as show in table 3.1.1

Table 3.1.1. Nominal composition, actual filling fraction and lattice parameter of $Yb_xRh_4Sb_{12}$ skutterudite compounds.

Nominal composition ($Yb_xRh_4Sb_{12}$)	Actual filling fraction	Lattice parameter (Å)
$Yb_{0.2}Rh_4Sb_{12}$	$Yb_{0.1}Rh_{3.9}Sb_{12}$	9.237
$Yb_{0.3}Rh_4Sb_{12}$	$Yb_{0.28}Rh_{3.64}Sb_{12}$	9.237
$Yb_{0.4}Rh_4Sb_{12}$	$Yb_{0.39}Rh_{3.75}Sb_{12}$	9.243
$Yb_{0.5}Rh_4Sb_{12}$	$Yb_{0.404}Rh_4Sb_{12}$	9.252
$Yb_{0.6}Rh_4Sb_{12}$	$Yb_{0.44}Rh_{3.92}Sb_{12}$	9.261
$Yb_{0.7}Rh_4Sb_{12}$	$Yb_{0.434}Rh_{4.02}Sb_{12}$	9.252
$Yb_{0.8}Rh_4Sb_{12}$	$Yb_{0.39}Rh_{3.95}Sb_{12}$	9.247
$Yb_{0.9}Rh_4Sb_{12}$	$Yb_{0.206}Rh_{3.9}Sb_{12}$	9.238

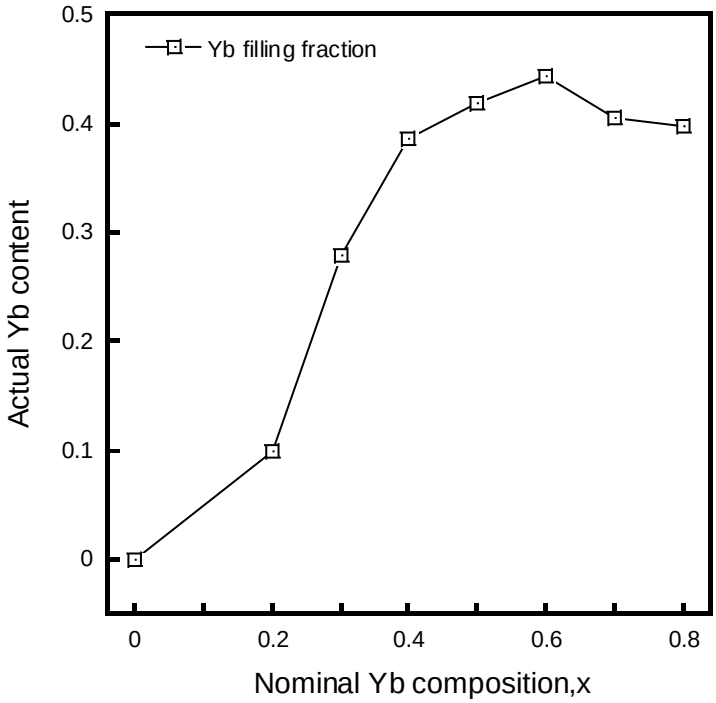

Figure 3.1.5 Dependence of Yb actual content versus nominal Yb composition (x), $Yb_xRh_4Sb_{12}$.

The actual filling fraction is lower than nominal composition, as show in figure 3.1.5. The actual Yb filling fraction was filled to be 0.4 or 40% of filling guest atom in vacancy site of mother compounds (Rh_4Sb_{12}), which is highest than any reported. From the previously study, high pressure synthesis of Yb filled Co_4Sb_{12} was found Yb actual filling fraction at 0.29[8], which is highest than ambient pressure synthesis. Moreover, High pressure synthesis method of $Yb_xCo_4Sb_{12}$ can be insert Yb in Co_4Sb_{12}[8] structure nearly theoretical Yb filling fraction in Co_4Sb_{12}[15]

3.2 Electrical properties

This section descript the result of the Seebeck coefficient, Electrical resistivity and thermal conductivity as a function of temperature. Hall measurement, heat capacity and magnetic properties are presented in the end of this section.

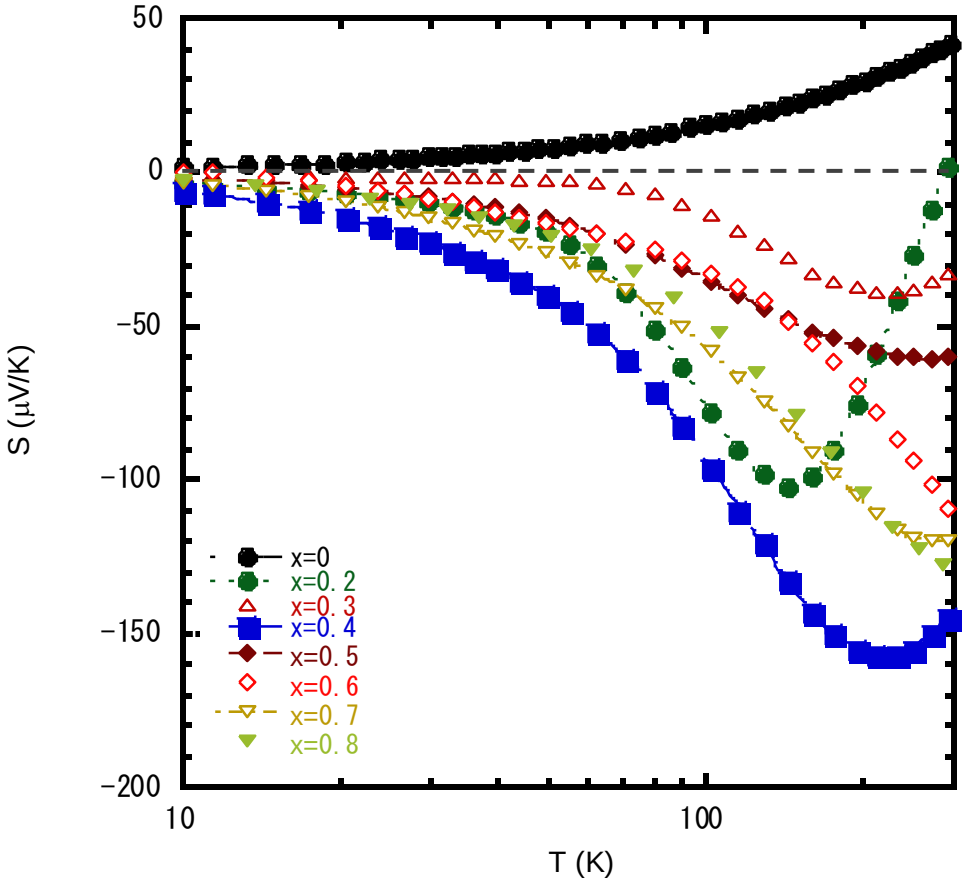

Figure 3.2.1 Temperature dependent Seebeck coefficient of $Yb_xRh_4Sb_{12}$

Figure 3.2.1 Seebeck coefficient (S) of $Yb_xRh_4Sb_{12}$ for $0 \leq x \leq 0.8$. Unfilled skutterudite Rh_4Sb_{12} shows positive (p-type semiconductor) overall temperature range. Whereas all doped sample are negative (n-type), the seebeck coefficient increase with increasing temperature. Temperature dependent of $Yb_{0.2}Rh_4Sb_{12}$, $Yb_{0.3}Rh_4Sb_{12}$ and $Yb_{0.4}Rh_4Sb_{12}$ are decrease fast and then increase nearly room temperature, where the intrinsic conduction behavior is observed. The observed sign and temperature dependence of $Yb_xRh_4Sb_{12}$ change from positive to negative by inserting Yb-content indicating Yb donated electron at elevated temperature. The Seebeck coefficient values up to -150μV/K at 220 K for $Yb_{0.4}Rh_4Sb_{12}$.

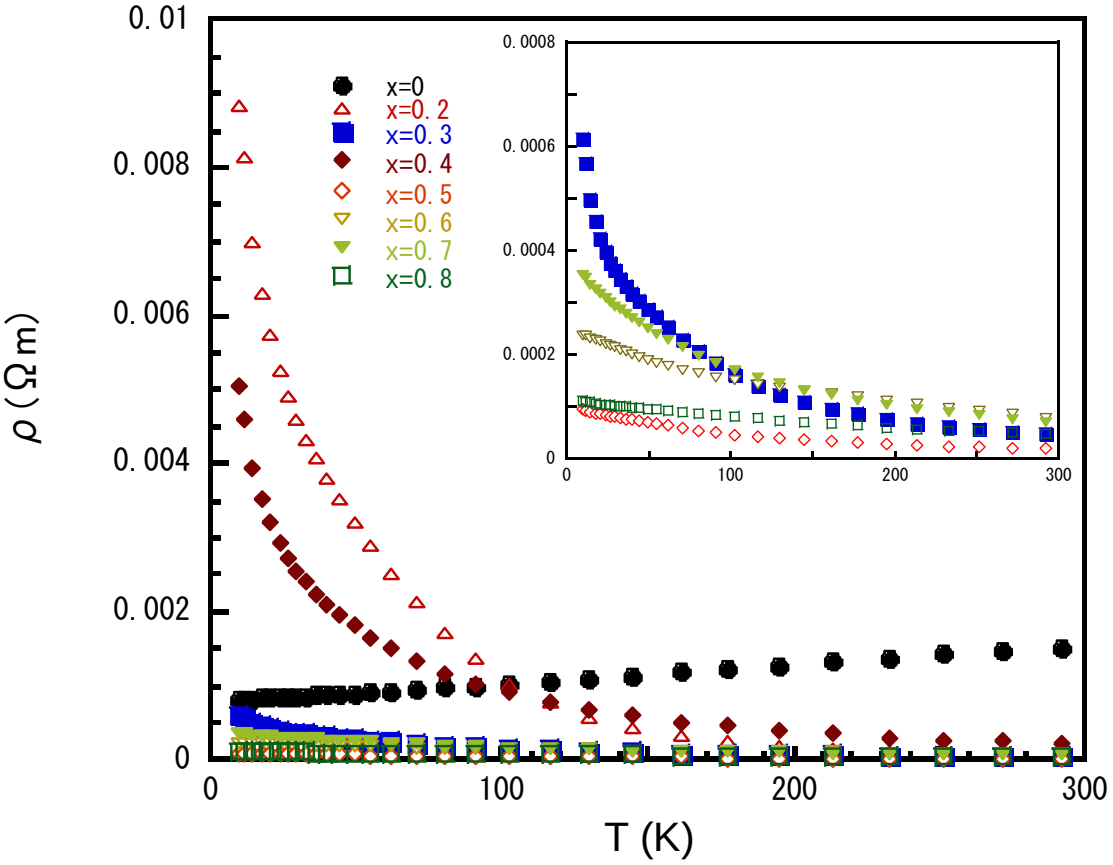

Fig 3.2.2 Temperature dependence of the electrical resistivity for $Yb_xRh_4Sb_{12}$ for $0 \leq x \leq 0.8$.

Fig 3.2.2 shows electrical resistivity as a function of temperature unfilled Rh_4Sb_{12} is metallic behavior as electrical resistivity increase with temperature increase. On the other hand, the decrease of electrical resistivity with increase of Yb content. The Yb filled skutterudite become semiconducting behavior, suggest that this system remain rich of rhodium composition. It seems that contribute of Yb to charge carrier concentration is small compared with the degeneration of Yb-filled, owing to large void-radius Rh_4Sb_{12} system. Those trend are similar in $In_xRh_4Sb_{12}$[7] and $La_xRh_4Sb_{12}$[8]. Despite of the reducing of electrical resistivity of filled Yb is inconsistent with actual Yb but carrier concentration higher than initial sample. At room temperature, electrical resistivity of Yb doping is decrease from 149 mΩ.cm to 1.984 mΩ.cm at Rh_4Sb_{12} and $Yb_{0.5}Rh_4Sb_{12}$, respectively. Room temperature of carrier concentration of nominal Yb composition and carrier mobility shows in Fig 3.2.3 and Fig 3.2.4, respectively.

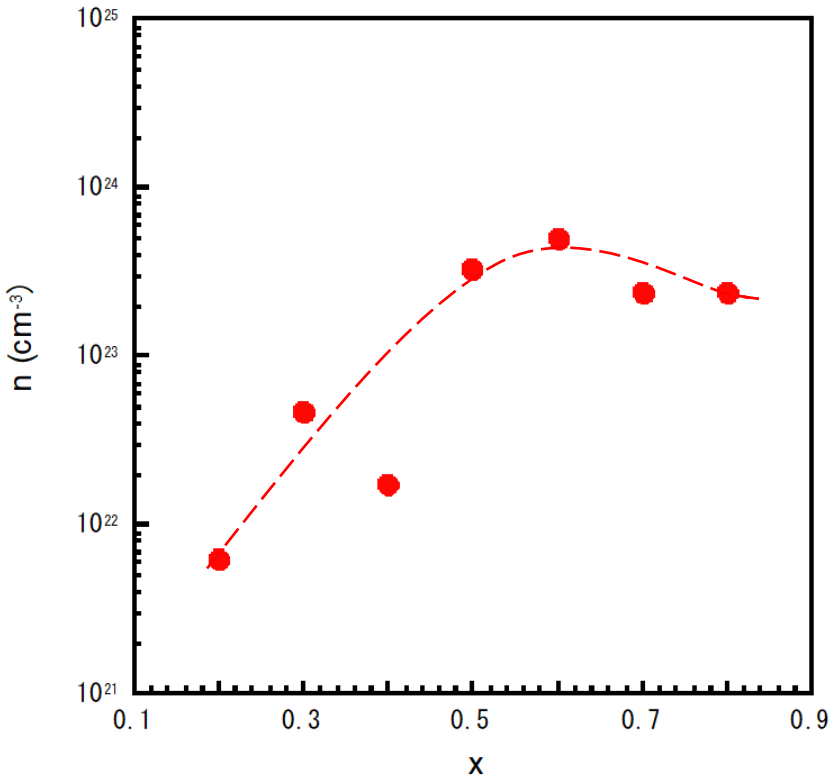

Fig 3.2.3 Room temperature of carrier concentration of nominal Yb composition

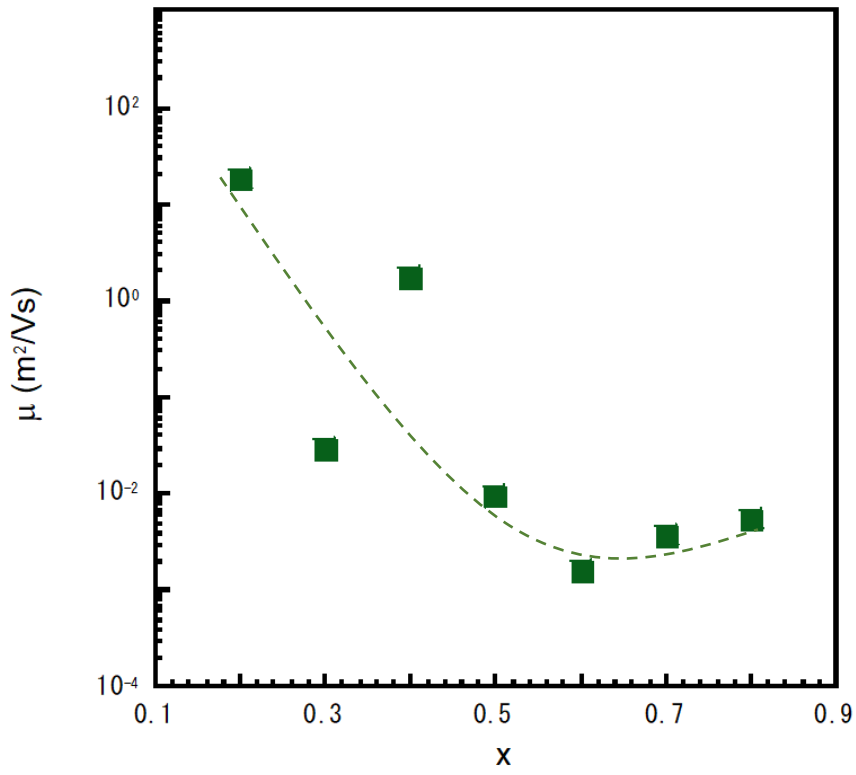

Fig 3.2.4 Room temperature of carrier mobility of nominal Yb composition

From the result of fig 3.2.3 and fig 3.2.4, carrier concentration increase with nominal Yb content increase. On the other hand, mobility in system decrease while increasing of number of Yb. It seem that when increase number of doping atom, the number of scatter also increase. Fig 3.2.5 show temperature dependence of carrier mobility of $Yb_xRh_4Sb_{12}$. While increasing temperature, the mobility of $Yb_xRh_4Sb_{12}$ ($0.2 \leq x \leq 0.5$) increases and the mobility of $Yb_{0.6}Rh_4Sb_{12}$ reduce with temperature decrease. At temperature higher than absolute zero, the donate electron from Yb atom are scattering in structure which tends to decrease carrier mobility. In the part of, the mobility of $Yb_{0.7}Rh_4Sb_{12}$ and $Yb_{0.8}Rh_4Sb_{12}$ are decrease at some range of temperature and then gradually increase, suggesting intrinsic carrier are dominate. These effect can be result of holes minority carrier by temperature excitation. From the result of hall effect measurement obtained that at high filling fraction ratio of $Yb_{0.44}Rh_{3.92}Sb_{12}$ (nominal Yb = 0.6) exhibit high carrier concentration than $Yb_{0.29}Co_4Sb_{11.71}$ ($n=4.96 \times 10^{23}$ cm^{-3}, $n=6.02 \times 10^{20}$ cm^{-3}, respectively.), which correspond to Rh_4Sb_{12} system can insert guest atom to void structure higher than Co_4Sb_{12} system.

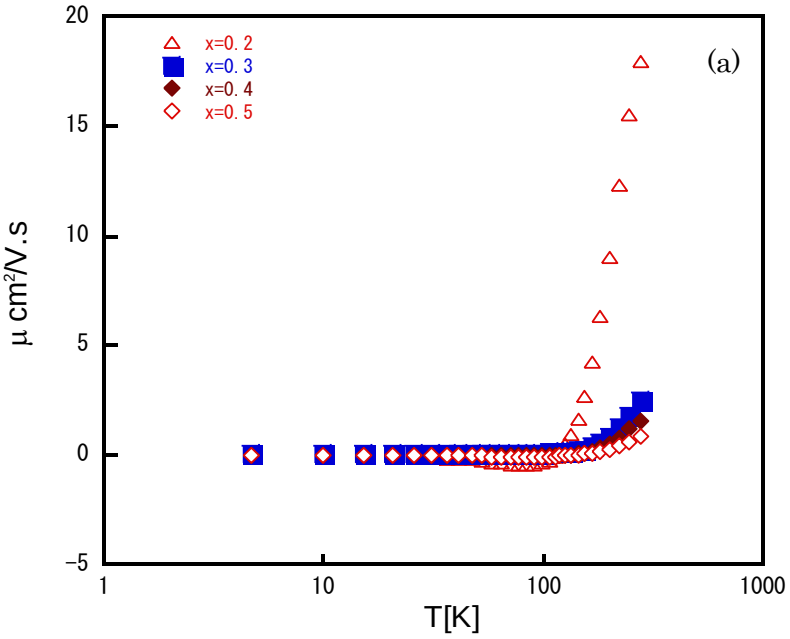
x=0.2
x=0.3
x=0.4
x=0.5
(a)
20
15
10
5
0
−5
μ cm²/V.s
1
10
100
1000
T[K]

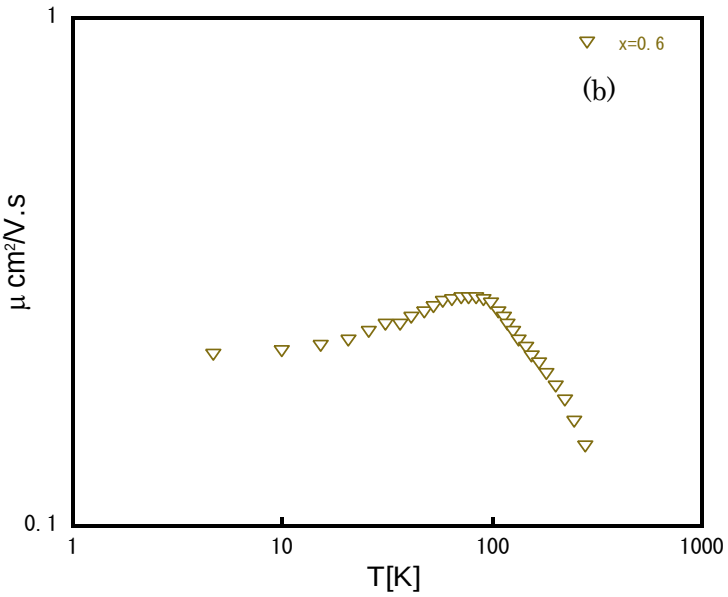
x=0.6
(b)
1
0.1
μ cm²/V.s
1
10
100
1000
T[K]

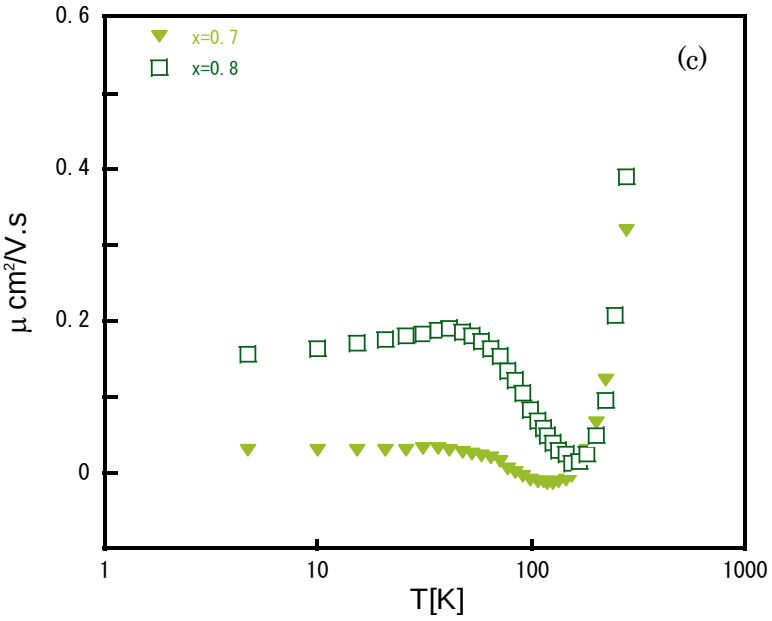

Fig 3.2.5 Temperature dependence of carrier mobility of $Yb_xRh_4Sb_{12}$

3.3 Thermal conductivity

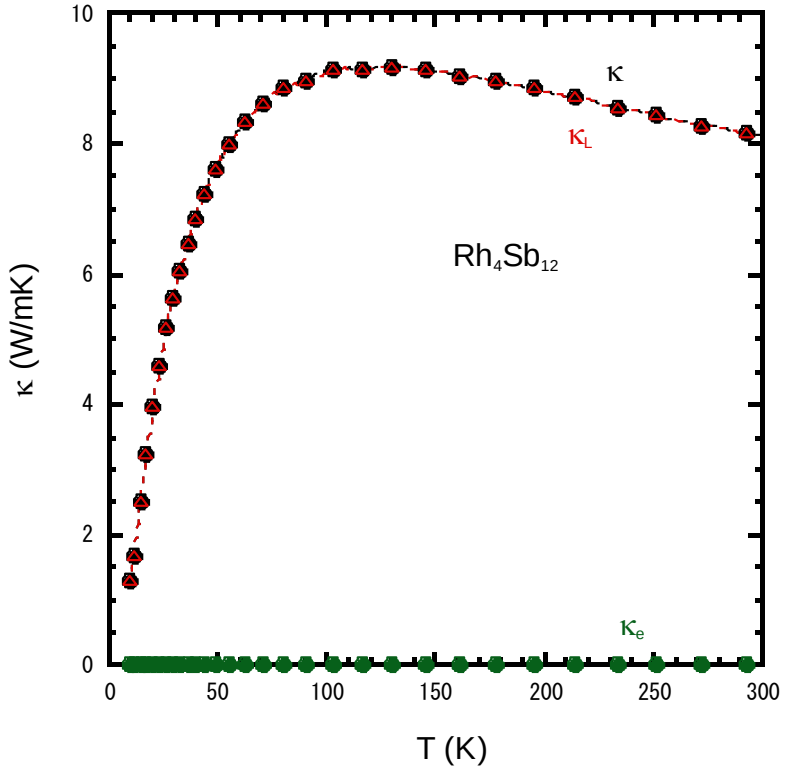

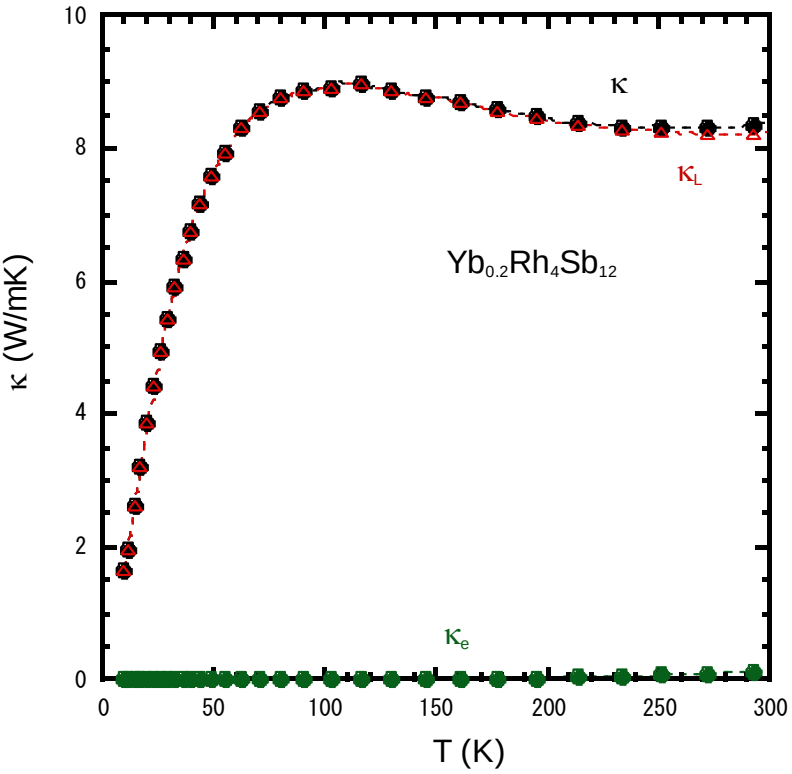

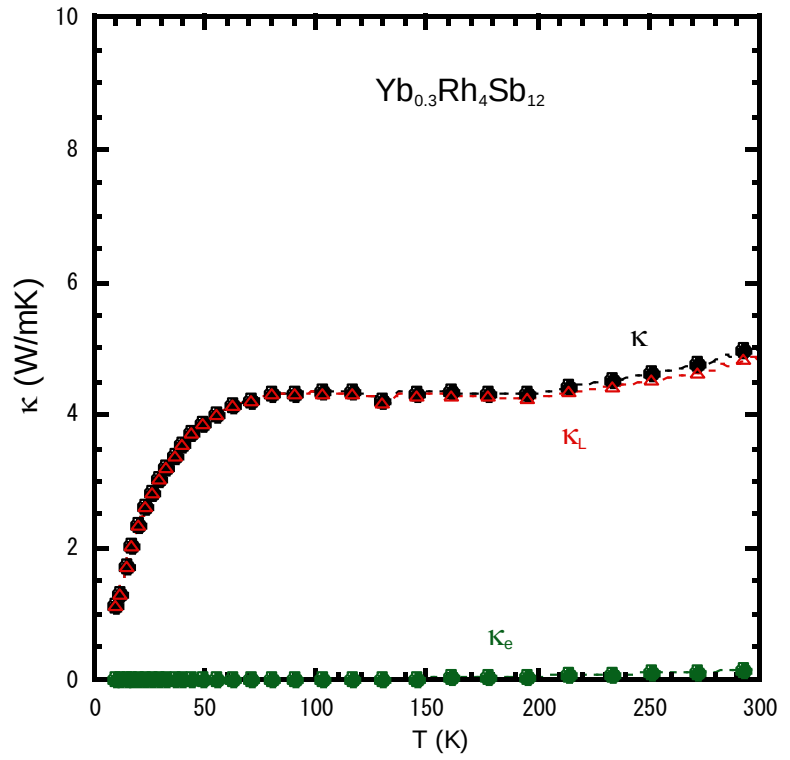
Yb0.3Rh4Sb12
κ (W/mK)
T (K)
κ
κL
κe
0
2
4
6
8
10
0
50
100
150
200
250
300

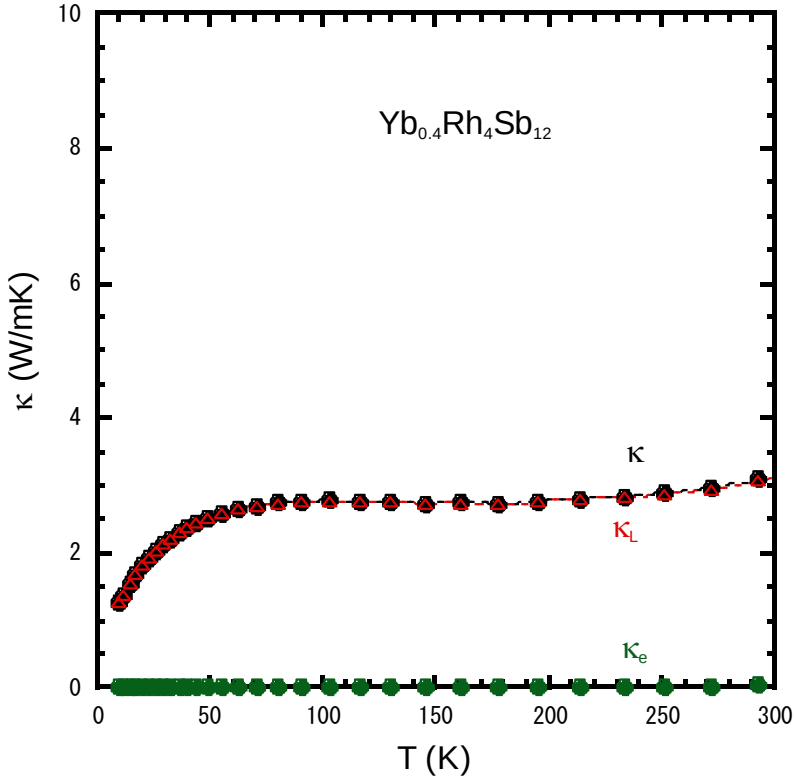
Yb0.4Rh4Sb12
κ (W/mK)
T (K)
κ
κL
κe
0
2
4
6
8
10
0
50
100
150
200
250
300

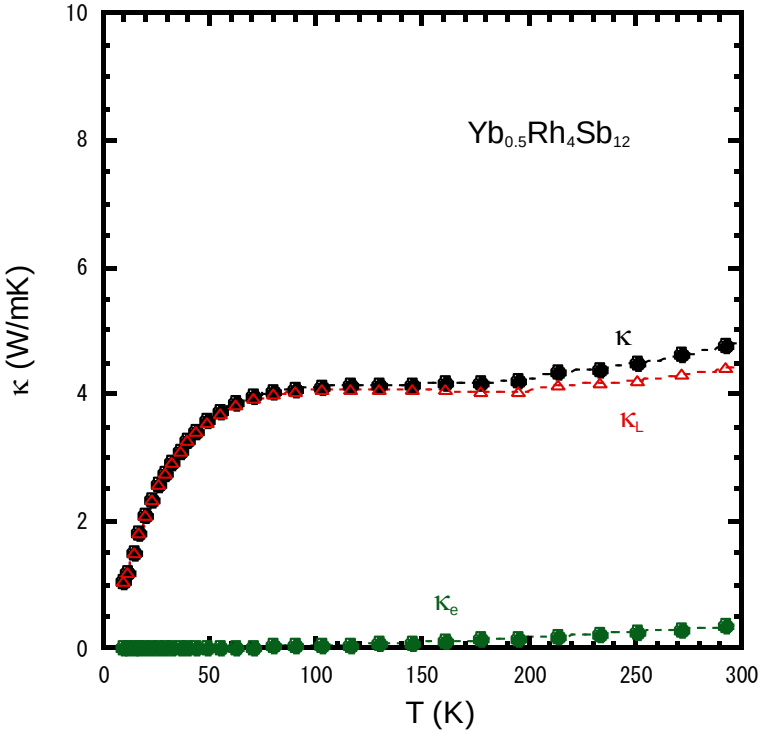
Yb0.5Rh4Sb12
κ (W/mK)
T (K)
κ
κL
κe
0
2
4
6
8
10
0
50
100
150
200
250
300

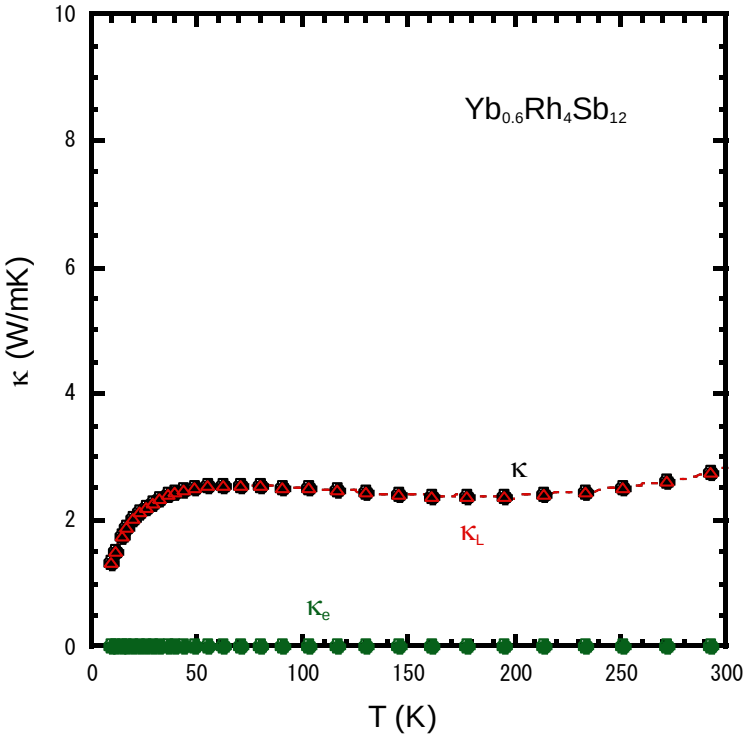
Yb0.6Rh4Sb12
κ (W/mK)
T (K)
κ
κL
κe
0
2
4
6
8
10
0
50
100
150
200
250
300

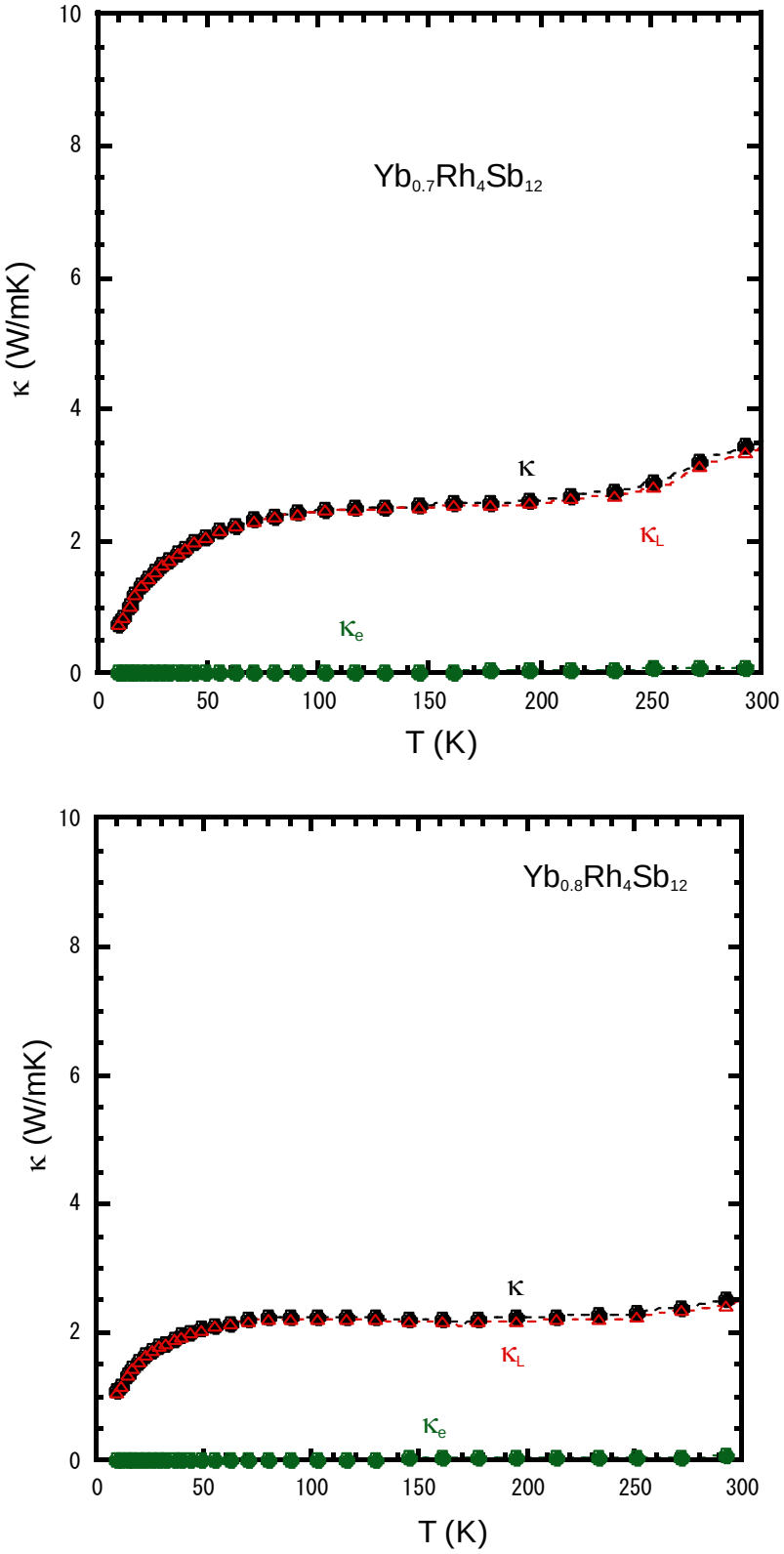

Fig 3.3.1 Temperature dependence of total thermal conductivity (κ), lattice thermal conductivity (κ_L) and electrical thermal conductivity (κ_e) of $Yb_xRh_4Sb_{12}$

Temperature dependence of lattice thermal conductivity (κ_L) and electrical thermal conductivity (κ_e) are presented in fig 3.3.1. The lattice thermal conductivity (κ_L) was calculated from

$$\kappa = \kappa_{L+} \kappa_e$$

All results of $Yb_xRh_4Sb_{12}$ sample, total thermal conductivity (κ), lattice thermal conductivity (κ_L) are decrease with Yb content increase. From this results assumed that the effect of rattling. At room temperature of Rh_4Sb_{12} to $Yb_{0.8}Rh_4Sb_{12}$, lattice thermal conductivity (κ_L) decrease from 8.11 W/mK to 2.43 W/mK for lattice thermal conductivity in Rh_4Sb_{12} to $Yb_{0.8}Rh_4Sb_{12}$.

For whole temperature range, the electrical thermal conductivity (κ_e) increase with temperature increasing, as the effect of electron contribution in void side is corresponding to Wiedemann-Franz law

$$\kappa_e = L\sigma T$$

When $_L = 2x10^{-8}\ V^2.K^{-2}$

σ = electrical conductivity

T = absolute temperature

3.4 Dimensionless figure of merit (ZT)

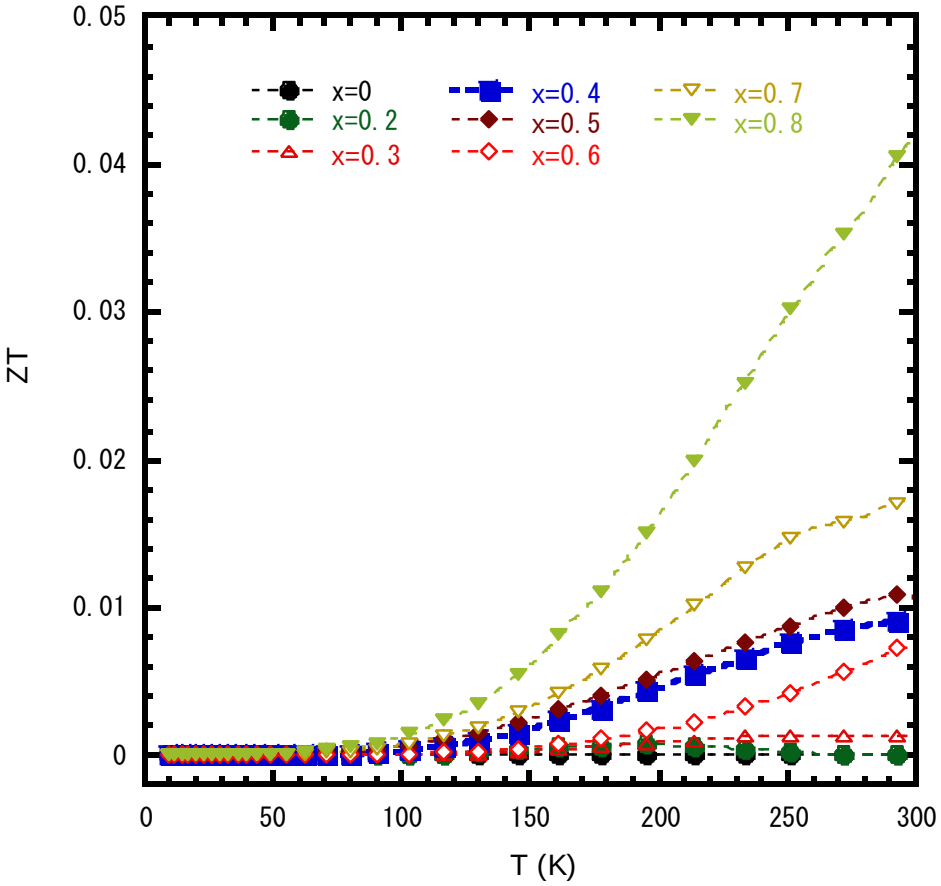

Fig 3.4.1 Temperature dependent dimensionless figure of merit (ZT) of $Yb_xRh_4Sb_{12}$

Temperature dependent dimensionless figure of merit (ZT) of $Yb_xRh_4Sb_{12}$ are present in fig 3.4.1. The figure of merit of YbxRh4Sb12 increase with temperature increase. From these results, it seem that high Yb doping exhibit high figure of merit (ZT) at overall temperature range. We can observe highest figure of merit at $Yb_{0.8}Rh_4Sb_{12}$ with room temperature, value exceeding 0.04. It is evident that we can improve the dimensionless figure of merit (ZT) by control filling fraction ratio of Yb content.

3.5 Specific heat

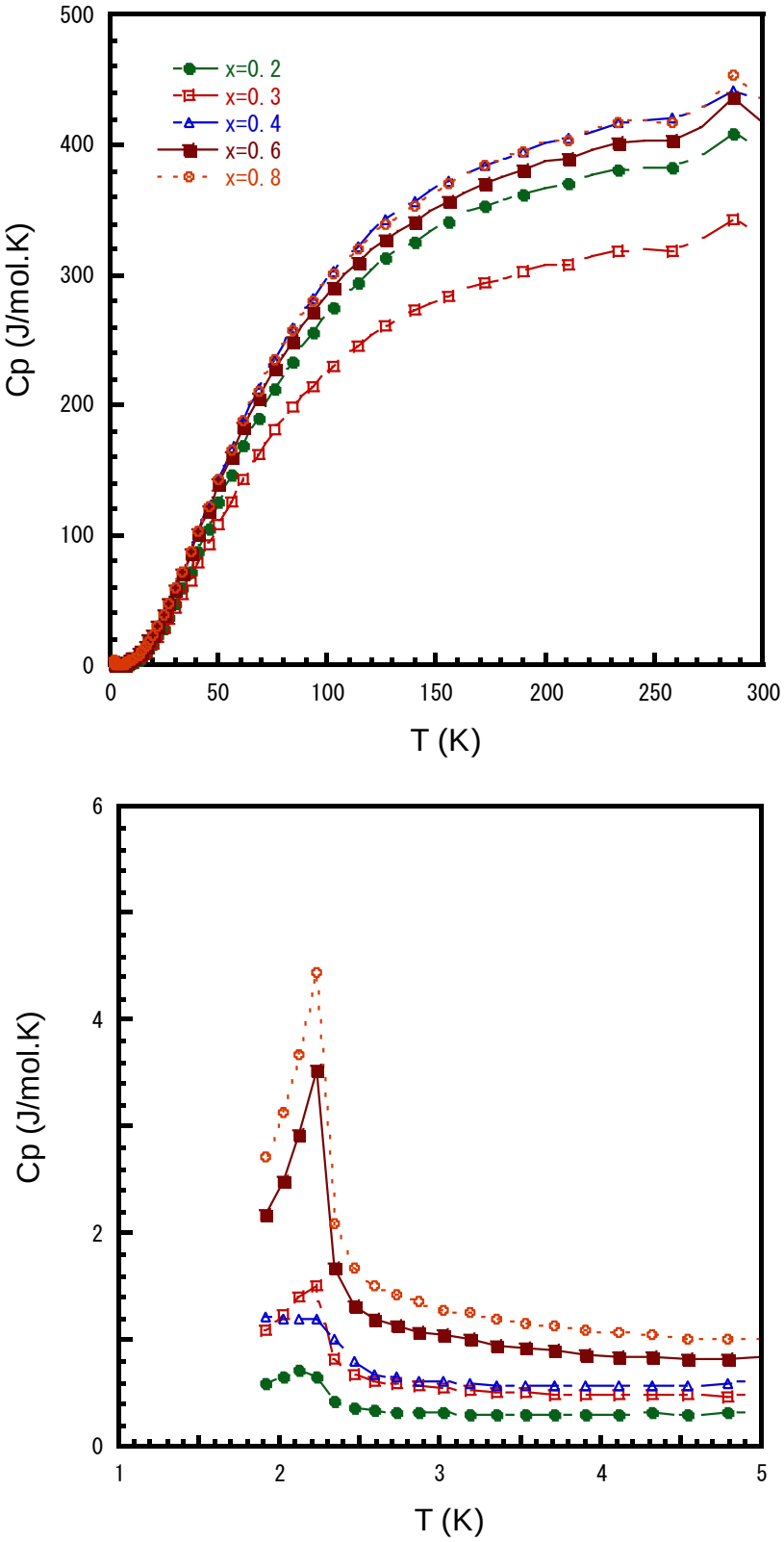

Fig 3.5.1 Specific heat C(T) as a function of temperature (T) for $Yb_xRh_4Sb_{12}$.

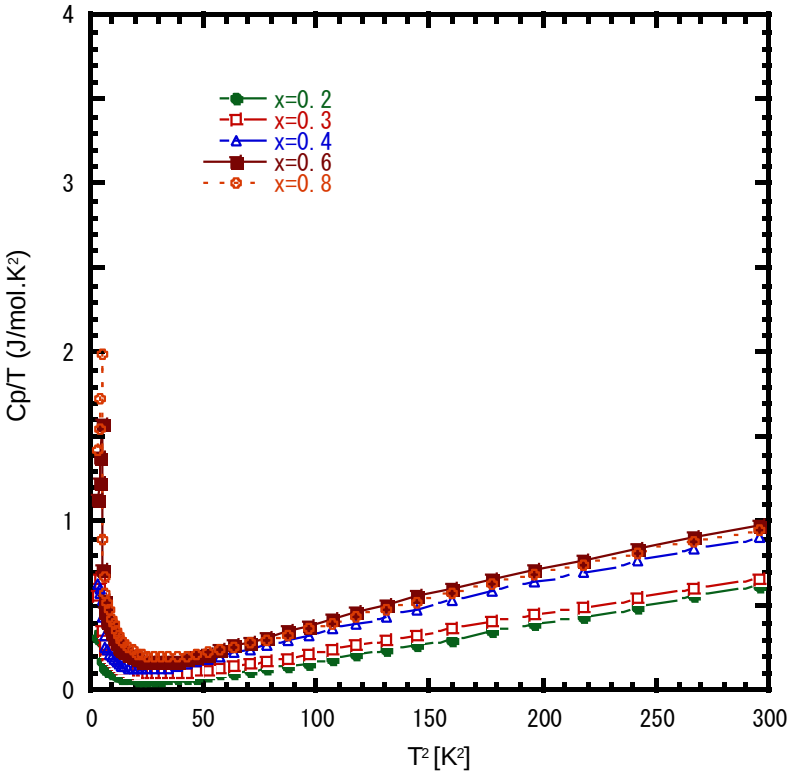

Fig 3.5.2 Specific heat C/T as a function of T^2 for $Yb_xRh_4Sb_{12}$.

Specific heat measurement can observe how energy heat can absorbed into electron or vibrations of the positive charges in lattice at low temperature. A summary of electronic and phonon contribution can fitted by Debye T^3 law

$$C(T)/T = \gamma + \beta T^2$$

Where γ = electronic specific heat coefficient.

βT^3term = lattice term (Debye constant)

From fig 3.5.1 show specific heat C(T) as a function of temperature (T). The overall sample are steep increase at low temperature and lone tail at high temperature. At low temperature show magnetic contribution with a Schottky anomaly at 2.3 K at all sample.

At low temperature of specific heat can be calculated γ function from fig 3.5.2. And Debye temperature (θ_D) can be calculated from

$$\theta_D = \left(\frac{12\pi^4 Rn}{5\beta}\right)^{1/3}$$

Where R = the gas constant

n = the number of atoms/f.u. (17)

From the fitted and calculation above, we can obtainedγ and θ_D are shown in table 3.5.1. From the specific heat measurement results, when the foreign atoms are inserted into the Rh_4Sb_{12} structure, the heat capacity should increase as a result of the increased occupancy of the unit cell. However, the occupancies of the guest atoms are smaller, this structure system cannot calculated Einstein vibration at low temperature.

Table 3.5.1 Electronic specific heat coefficient γandθ_D of $Yb_xRh_4Sb_{12}$.

Nominal Yb (x)	Actual Yb	γ (mJ/mol.K^2)	θ_D (K)
0.2	0.1	65.362	257.8
0.3	0.26	19.663	247.7
0.4	0.39	36.176	220.1
0.6	0.44	70.100	215.4
0.8	0.39	52.215	216.9

3.6 Magnetic properties

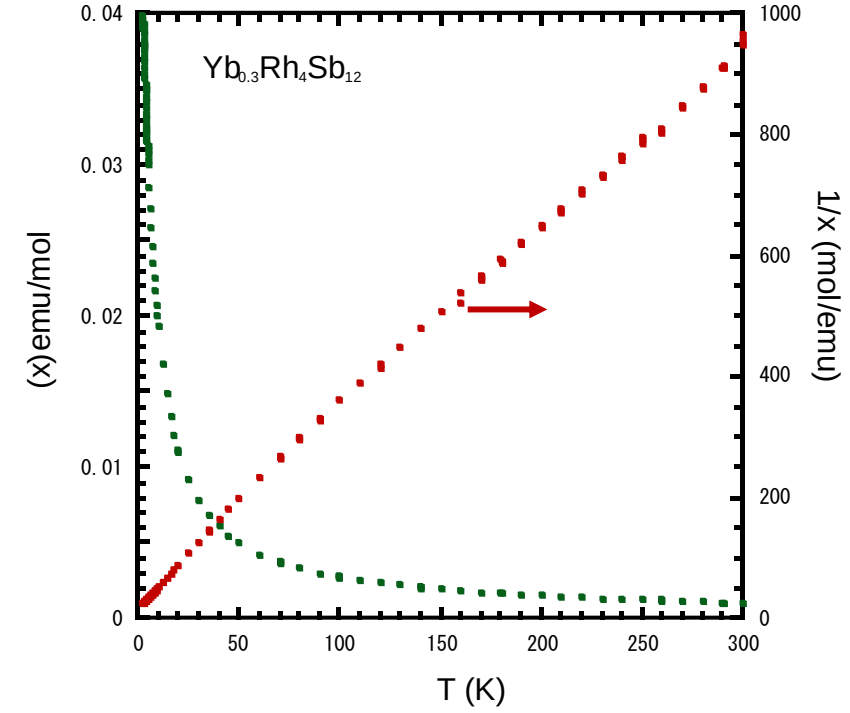

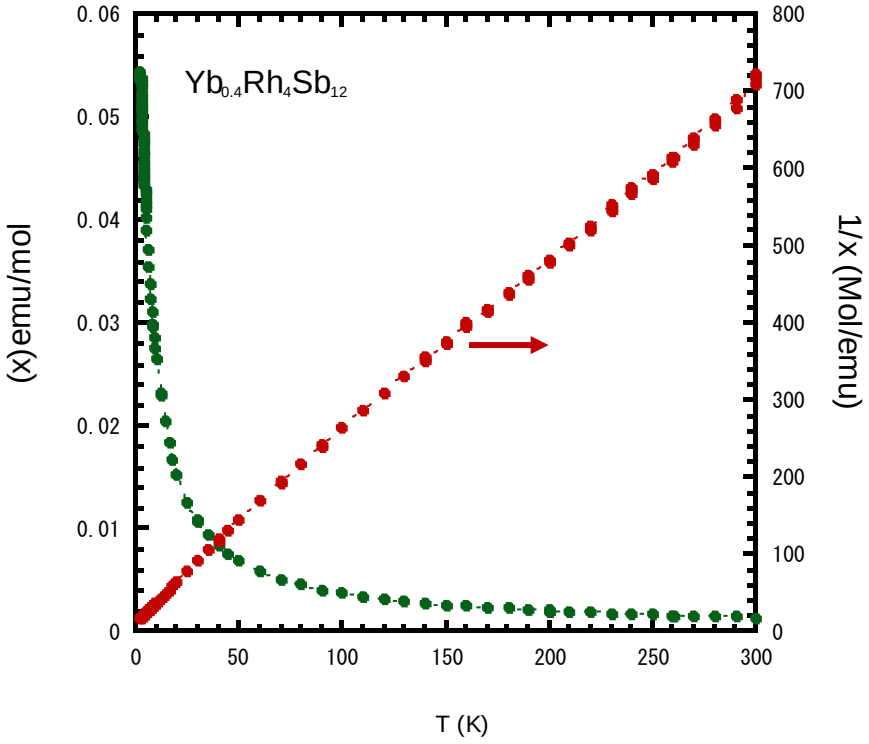

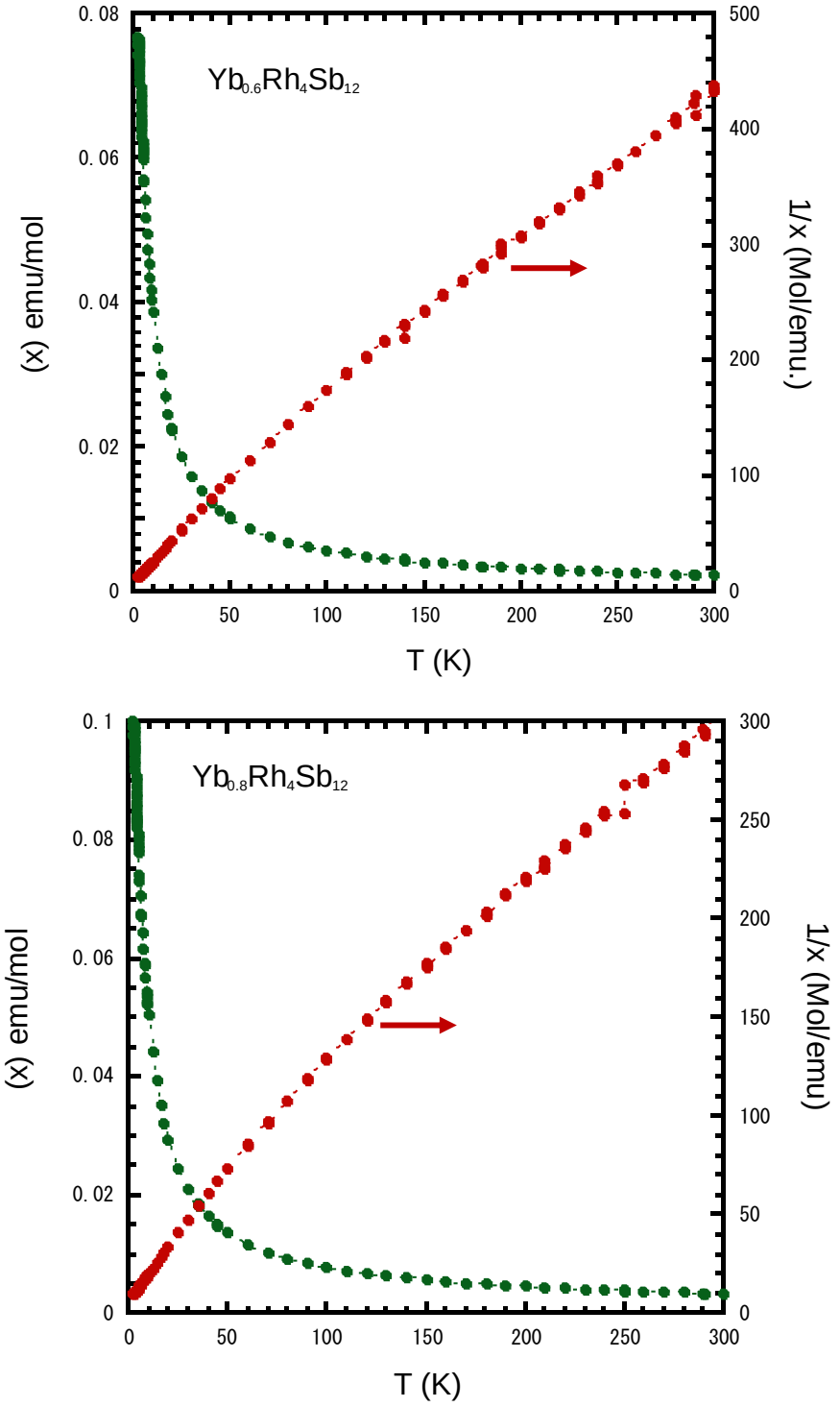

Fig 3.6.1 Temperature dependence of magnetic susceptibility χ and the inverse magnetic susceptibility 1/χ of $Yb_xRh_4Sb_{12}$

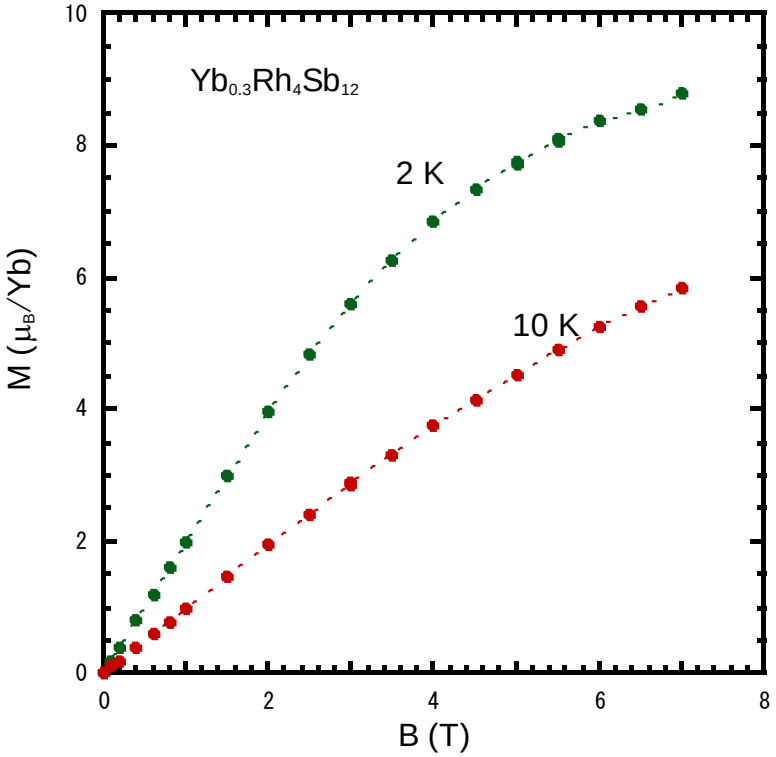
Yb0.3Rh4Sb12
2 K
10 K
M (μB/Yb)
B (T)
0
2
4
6
8
10

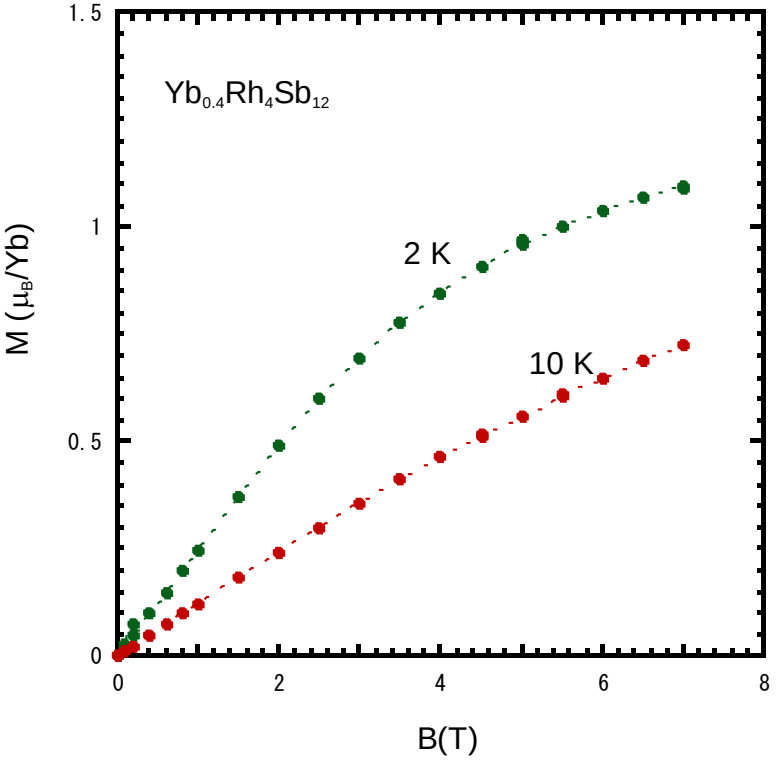
Yb0.4Rh4Sb12
2 K
10 K
M (μB/Yb)
B(T)
0
0.5
1
1.5
2
4
6
8

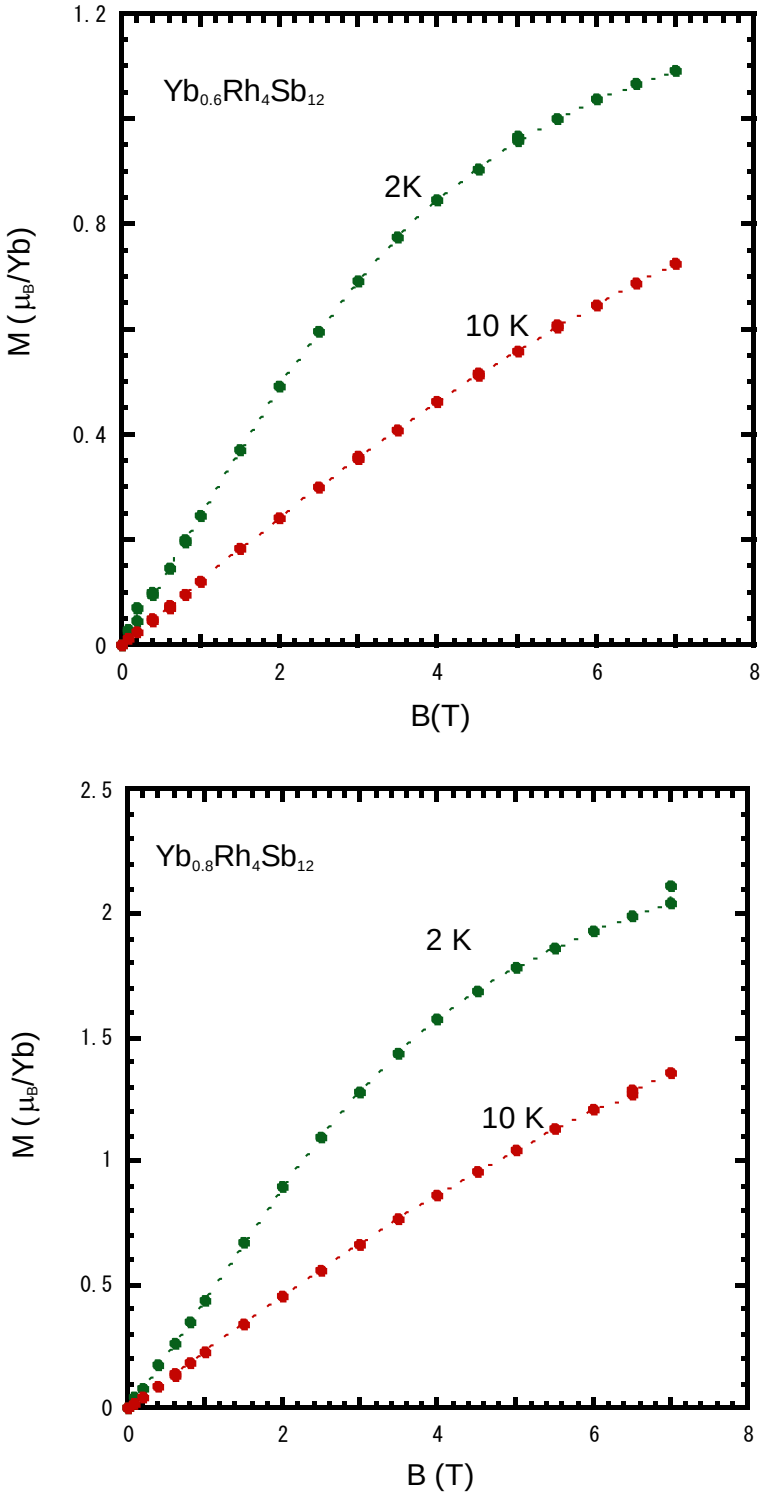

Fig 3.6.2 Magnetization curve of $Yb_xRh_4Sb_{12}$ at 2 K and 10 K

Table 3.6.1 Curie constant C, effective magnetic moment μ_{eff} and Weiss temperature θ_p of $Yb_xRh_4Sb_{12}$

Nominal Yb (x)	Curie constant,C	μ_{eff}	θ_p (K)
0.3	0.35	1.68	23.37
0.4	0.45	1.90	16.03
0.6	0.79	2.52	37.90
0.8	1.21	3.10	53.94

Fig 3.6.1 shows temperature dependence of magnetic susceptibility χ at 1 Tesla and the inverse magnetic susceptibility $1/\chi$ of $Yb_xRh_4Sb_{12}$. The temperature dependence ofχ follows the Curie-Weiss. From the fitting linear slope of $1/\chi$versus temperature. When nominal Yb content increase, the effective magnetic moment is also increase, as show in table 3.6.1. It seem that the effective magnetic momentμ_{eff} are lower than Yb^{3+} ion ($\mu_{eff} = 4.54\mu_B$), suggesting Yb exhibits an intermediate valence. From the magnetization curve, no anomaly sign at 2 K and 10 K, as show in fig 3.6.2. Magnetization cure at 2 K exhibit paramagnetic behaviour.

CHAPTER 4

Results and discussion of $Yb_xRh_4Sb_{12}$ (SPS)

4.1 Experimental details and Characterization

The high filling fraction ratio of $Yb_xRh_4Sb_{12}$ (x=0.7) were prepared by combination of a high-pressure apparatus (UHP-500, Sumitomo Heavy Industries Ltd., Japan) and spark plasma sintering. high-pressure method, the purity of starting material (Yb, 99.9%, Rh 99.9% and Sb, 99.9999%) powder were mixed well and load into boron nitrate (BN) container and assemble to pyrophyllite.[3],[4] The sample was prepared under pressure 2 GPa, overshoot temperature up to 750°C for 2 min, kept temperature 450-550°C for 120 min (heating rate at 50°C/min). The purity of specimen was investigated by X-ray diffraction with Si powder standard (Rigaku RINT-RAPID-II). In spark plasma sintering technique, the sample after synthesized was clean and remove BN by using sand paper and pin then ground into powder with agate mortar. The powder was loaded to crucible and pressed into pellet, heat to 500°C under a pressure 60 MPa by Spark Plasma Sintering (SPS). The pellet was shape to dimension 10±0.1 mm and thickness 2±0.1 mm for thermal conductivity measurement, using a laser flash method (NETZSCH LFA457). Electrical transport properties (electrical resistivity and Seebeck coefficient) was measured by ZEM-1 (SINKU-RIKO ULVAC ZEM-1) with sample shape in rectangular with dimension of width (W), height (H) and length 2.0±0.1 mm, 2.0±0.1 mm, 8.0±0.1 mm, respectively. The thermal transport properties and electrical transport properties were measured from room temperature to 723K

Figure 4.1.1 shows the powder X-ray diffraction pattern of polycrystalline $Yb_xRh_4Sb_{12}$ (x=0.7). This pattern shows skutterudite structure in a body-center cubic crystal structure belongs to Im-$\bar{3}$ space group (No. 204). $RhSb_2$, RhSb and Sb were found in this sample as a secondary phase. From the least square fitting method, lattice parameter shows 9.225 Å

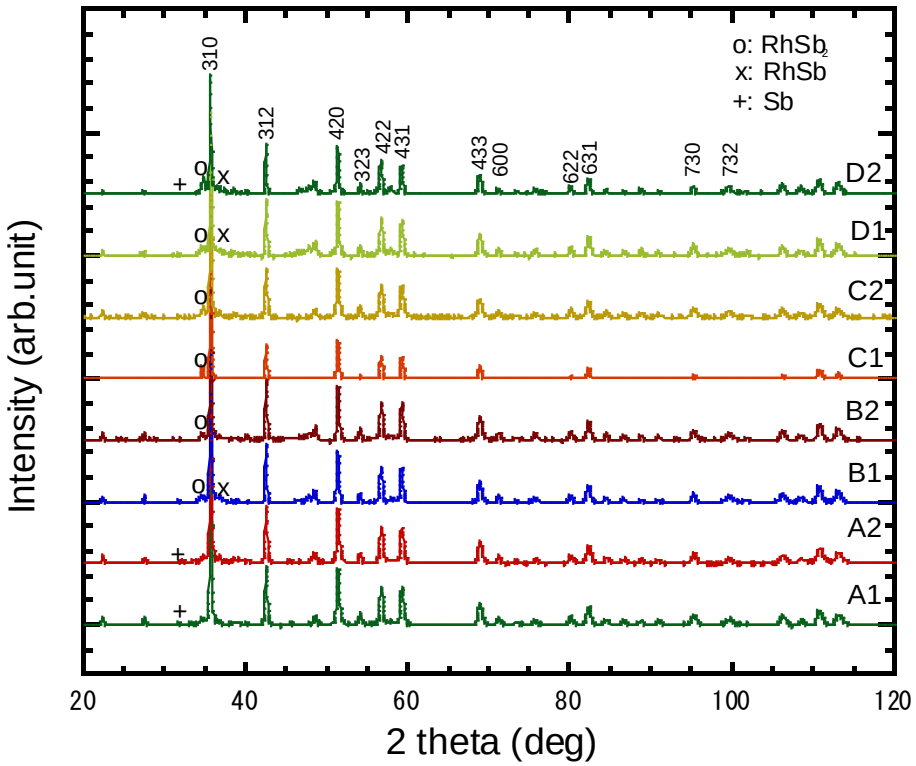

Fig 4.1.1 X-ray diffraction pattern from SPS method.

A scanning electron microscope (SEM) and using energy-dispersive X-ray (EDX), as show result in fig 4.1.2 and table 4.1.1. The backscattering image of SPS sample is almost homogeneous with grey color area. In black area is the roughness or cracking in sample. Before sintering method by SPS, this stating sample have actual Yb filling fraction about 40%. After sintering method, the actual filling ratio is found to be $Yb_{0.25}Rh_4Sb_{12.51}$. The lower filling ratio might be the effect of lower pressure in SPS method.

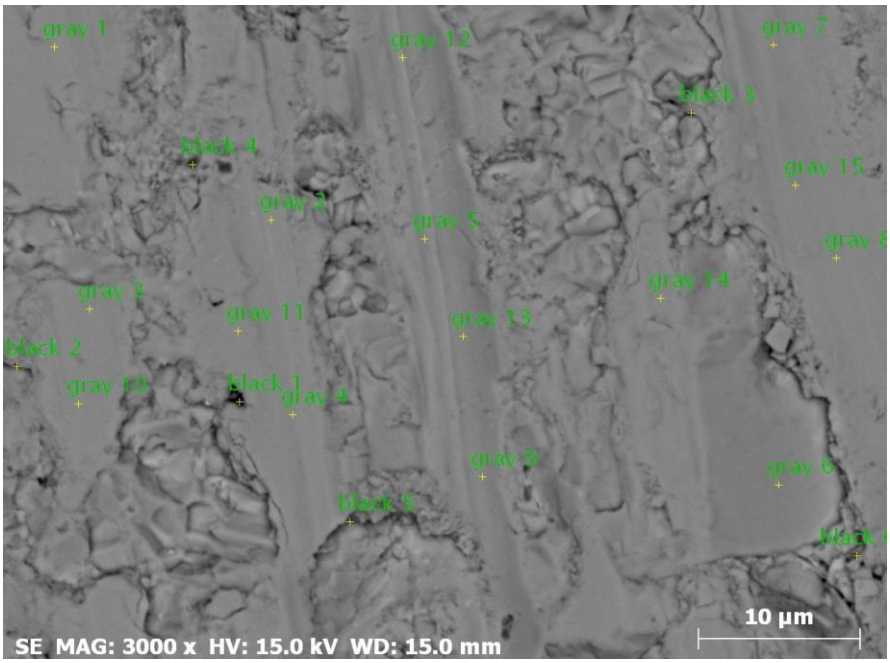

Fig 4.1.2 backscattering image

Table 4.1.1 Actual filling faction of $Yb_xRh_4Sb_{12}$ composition analysis by SEM-EDS

	Rh	Sb	Yb
gray 1	4	12.23	0.27
gray 2	4	12.01	0.29
gray 3	4	12.83	0.32
gray 4	4	12.30	0.18
gray 5	4	11.45	0.19
gray 8	4	12.66	0.21
gray 9	4	13.39	0.40
gray 10	4	12.65	0.07
gray 11	4	13.14	0.22
gray 13	4	12.47	0.32
Average	4	12.51	0.25

4.2 Electrical properties

Fig 4.2.1 shows the temperature dependence of electrical resistivity ρ and Fig 4.2.2 shows temperature dependence of seebeck coefficient. Electrical resistivity exhibit semiconductor behavior, electrical resistivity decrease with temperature increase through temperature range. Seebeck coefficient exhibit negative and increase roughly linearly with temperature. When temperature range enters, both carrier of electron and hole are excited from valence band to conduction band, It can be explained in equation (4.2.1),(4.2.2) as following

$$\sigma = \sigma_e + \sigma_h = e(n_e\mu_e + n_h\mu_h) \quad 4.2.1$$

$$S = \frac{S_e\sigma_e + S_h\sigma_h}{\sigma_e + \sigma_h} \quad 4.2.2$$

Where both symbol n, μ are present carrier concentration and carrier mobility, respectively. At low temperature, carrier mobility of SPS sample decrease and carrier concentration increase, suggesting below 300K filling atom (Yb-atom) is donated electron in this structure. That results according to seebeck coefficient at low temperature range. The carrier mobility and carrier concentration were measurement from 2-300 K, as shows in fig 4.4.3, fig 4.4.4, respectively. The fact that, Yb element is heavy element and small in ionic radii. While high Yb-filled was inserted in large void site of Sb in Rh_4Sb_{12} system as a result of lattice expansion and small energy band gap (Eg = 0.11 eV.). When temperature increase, the carrier contribution (electron and hole) are easier to excited indication of Seebeck coefficient become positive and electrical resistivity become small at high temperature.

At higher temperature indicates the onset of intrinsic semiconductor behavior. The results of seebeck coefficient measurements which implies that the bipolar conduction is at play at temperatures above 300 K. this can be a consequence of the fine grain structure of SPS sintering samples which enhances the charge carrier scattering.

the energy band gap can be fitting from electrical conductivity or electrical resistivity and calculated from Arrhenius law,

$$\sigma = A\exp(\frac{-Ea}{kT}) \quad 4.2.3$$

where, E_a = the activation energy

k = Boltzmann`s constant (1.3806×10^{-22} J/K)

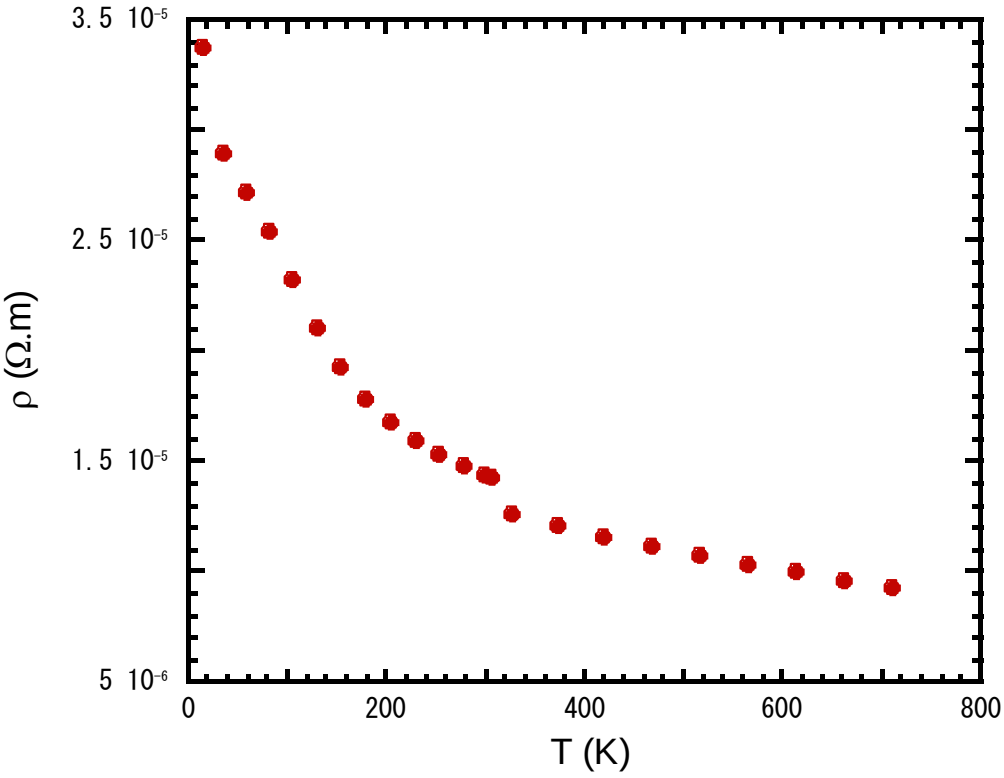

Fig 4.2.1 Temperature dependence of electrical resistivity

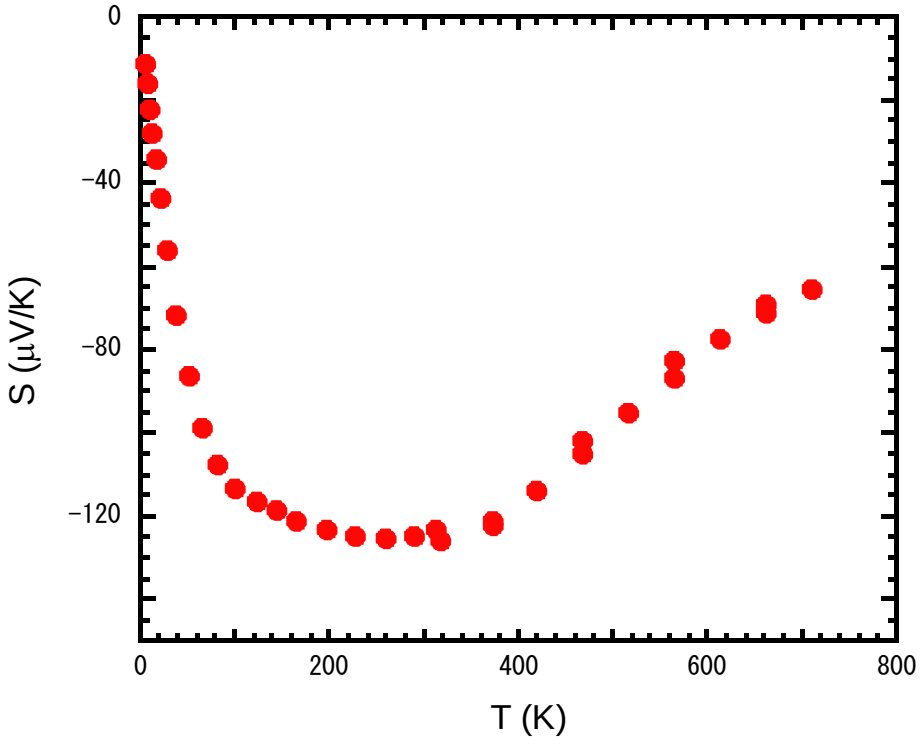

Fig 4.2.2 Temperature dependence of seebeck coefficient.

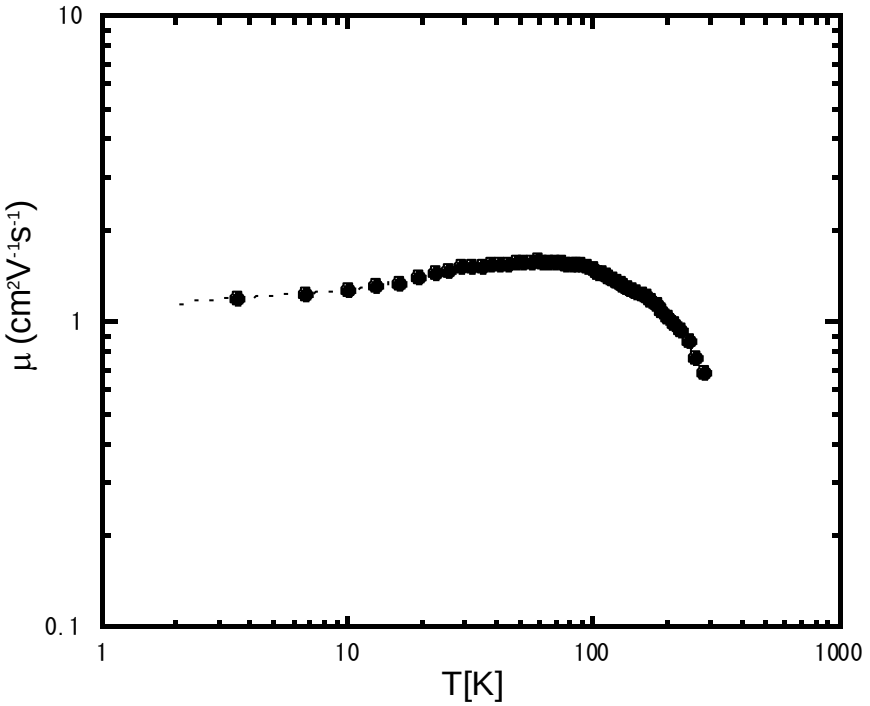

Fig 4.2.3 Temperature dependence of carrier mobility

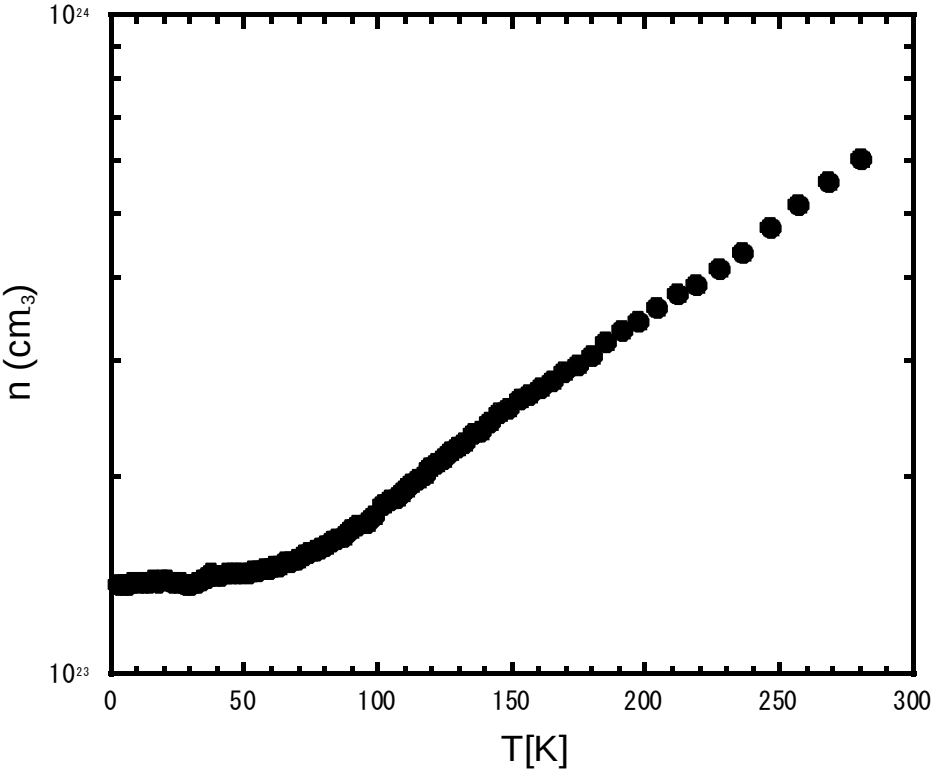

Fig 4.2.4 Temperature dependence of carrier concentration

4.3 Thermal property

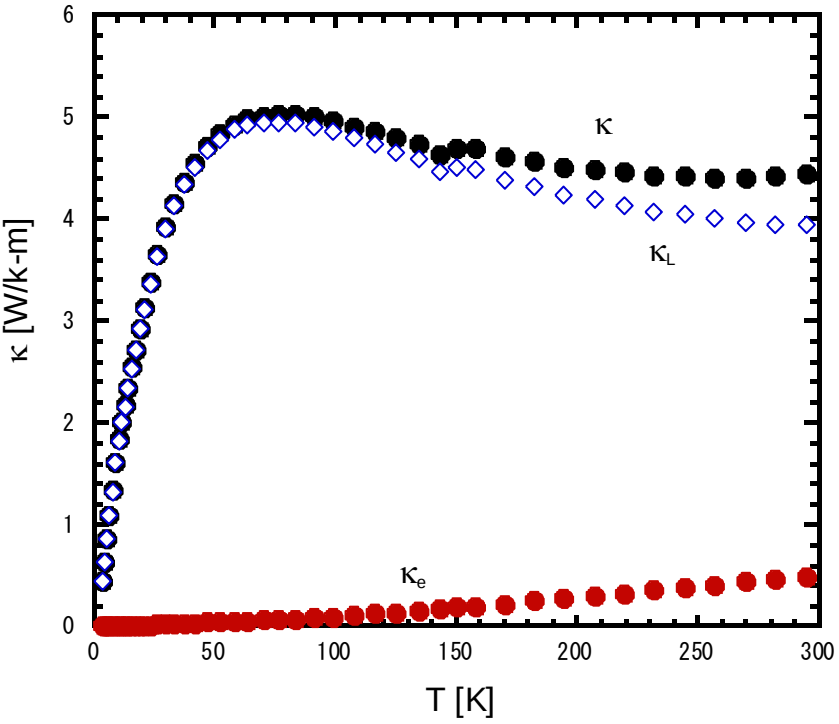

Fig 4.3.1 Temperature dependence of thermal conductivity (κ), lattice thermal conductivity (κ_L) and electrical thermal conductivity (κ_e) below 300 K

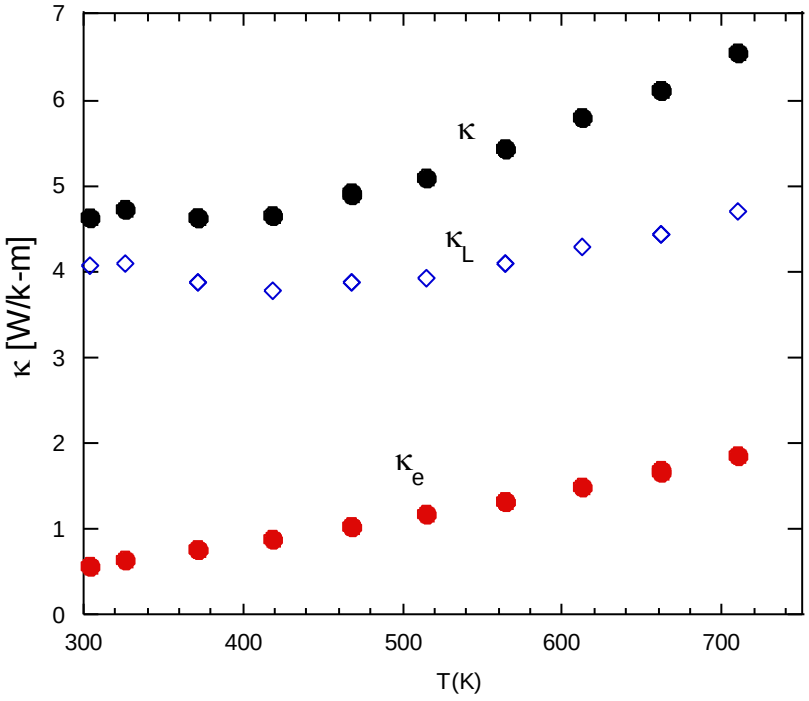

Fig 4.3.2 Temperature dependence of thermal conductivity (κ), lattice thermal conductivity (κ_L) and electrical thermal conductivity (κ_e) higher 300 K

Fig 4.3.1 show temperature dependence of thermal conductivity (κ), lattice thermal conductivity (κ_L) and electrical thermal conductivity (κ_e) below 300 K and Fig 4.3.2 show temperature dependence of thermal conductivity (κ), lattice thermal conductivity (κ_L) and electrical thermal conductivity (κ_e) higher than 300 K. At below 300 K, lattice thermal conductivity gradually decrease from 150 K.

At high temperature, heat flow is carried by carrier, lattice and bipolar diffusion. The total thermal conductivity increases due to the intrinsic excitation as observed in the electrical properties (bipolar diffusion). In bipolar thermal diffusion (κ_b) is an appreciable by both charge carriers in electrical conductivity and Seebeck coefficient, can estimated by

$$\kappa_b = \frac{\sigma_e \sigma_h}{\sigma_e + \sigma_h}(S_e - S_h)^2 . T \qquad 4.3.1$$

Where symbol of $e\ and\ h$ are present electron and hole, respectively and T is absolute temperature. The total thermal conductivity increases over the entire temperature range, which mean that bipolar diffusion had occurred. This result suggests that, both carrier in intrinsic and extrinsic were activated and vibrated with lattice vibration inside void site in Sb atom as a result of reduction lattice thermal conductivity by heat transfer dependent temperature. Bipolar thermal diffusion has been reported in alkaline earth and rare earth doped small band-gap skutterudite structures.

4.4 Figure of merit

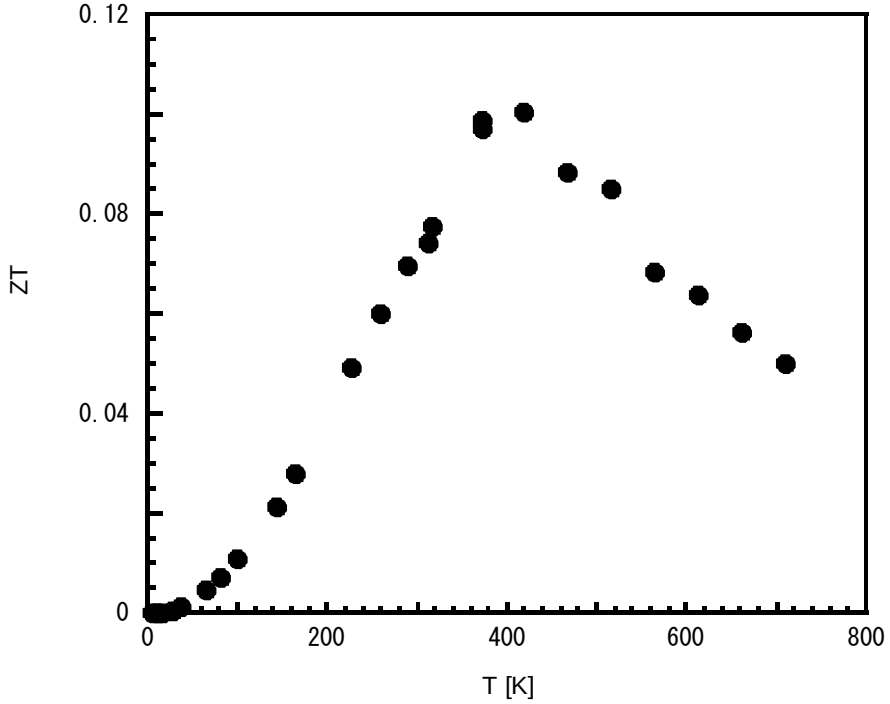

Figure 4.4.1 temperature dependence of figure of merit

Figure 4.4.1 shows the temperature dependence of dimensionless figure of merit ZT. The maximum ZT value of $Yb_xRh_4Sb_{12}$ (x=0.7) reaches 0.1 at 420K. The ZT exhibit low value might be the effect of transport carrier of electron and hole. It is expected that double fill, triple fill or substitution should be insert in Yb-doped Rh_4Sb_{12} structure for improve higher thermoelectric performance.

CHAPTER 5

SUMMARY

5.1 Summary

Skutterudite structure of $Yb_xRh_4Sb_{12}$ were synthesis under high pressure and high temperature method. Because of skutterudite structure have high performance of thermoelectric properties. Filled - into $CoSb_3$ based skutterudite have been best for candidate especially heavy rare earth element. From previous report, $Yb_xCo_4Sb_{12}$ are successfully to filling with maximum of Yb nearly theoretical by using high pressure method. So, Yb-atom was tried to filling in Rh_4Sb_{12} system because this structure have large void site than Co_4Sb_{12}. Moreover, Yb-atom have small and heavy atoms that should be more effective in reduce lattice thermal conductivity and improve performance of thermoelectric properties.

In this experiment, the maximum Yb-filled in Rh_4Sb_{12} system was found to be 0.4 or the filing fraction ratio up to 40%. As a matter of fact, Thermal transport properties have effect on efficiency of thermoelectric properties, is clearly seen in Yb-content (x=0.8), When consider only electronic transport properties, the PF value reach up to 3.6 $\mu W/cmK^2$ at 300 K. While thermal conductivity reducing with temperature increase, the ZT value increase to 0.042 at 300K for $Yb_xRh_4Sb_{12}$ (x=0.8). This obviously seen that the reduction of thermal conductivity because phonon interact between carrier and lattice structure in compounds attributed to the rattling motion of the heavy rare earth element in its Sb atom. At maximum filling fraction ratio of $Yb_xRh_4Sb_{12}$ (x=0.6) exhibit show small ZT because large electrical resistivity, indicate that small energy band gap in this compound. It is expected that further on substitution effect and combination method would result in even higher performance n-type skutterudite material.

To enhancement efficiency of thermoelectric of $Yb_xRh_4Sb_{12}$. The maximum of actual filling fraction was sintering by using spark plasma sintering (SPS). Yb-atom insertion into void-site of Rh_4Sb_{12} had effect on Seebeck coefficient and thermal conductivity, especially in lattice thermal conductivity at elevated temperature. This result exhibit low ZT due to high thermal conductivity that results from excitation in intrinsic.

Reference

1 Nolas, G. S., Morelli, D. T. & Tritt, T. M. SKUTTERUDITES: A Phonon-Glass-Electron Crystal Approach to Advanced Thermoelectric Energy Conversion Applications. *Annu. Rev. Mater. Sci.* **29,** 89–116 (1999).

2. Nicholas Brown, "GMZ TEG Module Successfully Generates 200W From Engine Heat",Website :http://cleantechnica.com/2014/06/13/gmz-teg-module-successfully-generates-200w-engine-heat/, 2019.04.10

3. Chen, Shuo, Ren, Zhifeng, Recent progress of half-Heusler for moderate temperature thermoelectric applications. Materials Today. 16, 387-395 (2010)

4 Ibuka, S., Imai, M., Miyakawa, M. & Taniguchi, T. Electrical and magnetic properties of La<inf>0.5</inf>Rh<inf>4</inf>Sb<inf>12</inf> filled skutterudite synthesized at high pressure. *J. Alloys Compd.* **646,** 912–915 (2015).

5. Liu, R., Qiu, P., Chen, X., Huang, X. & Chen, L. Composition optimization of p-type skutterudites CeyFexCo4-xSb12and YbyFexCo4-xSb12. *J. Mater. Res.* **26,** 1813–1819 (2011).

6. Tang, Y., Chen, S. wen & Snyder, G. J. Temperature dependent solubility of Yb in Yb–CoSb3skutterudite and its effect on preparation, optimization and lifetime of thermoelectrics. *J. Mater.* **1,** 75–84 (2015).

7. Bauer, E. *et al.* Physical properties of skutteruditesYb x M 4 Sb 12 , M = Fe , Co , Rh , Ir. *Eur. Phys. J. B* **14,** 483–493 (2000).

8 Chen, Y., Kawamura, Y., Hayashi, J. & Sekine, C. Thermoelectric properties of YbxCo4Sb12prepared under high pressure. *Jpn. J. Appl. Phys.* (2015). doi:10.7567/JJAP.54.055501

9 Shi, X., Zhang, W., Chen, L. D., Yang, J. & Uher, C. Thermodynamic analysis of the filling fraction limits for impurities in CoSb3based on ab initio calculations. *Acta Mater.* **56,** 1733–1740 (2008).

10 Mori, Hiroshi Anno, Hiroaki Matsubara, Kakuei, Effect of Yb Filling on Thermoelectric Properties of Ge-Substituted Mater. Trans. **46**, 1476-1480 (2005).

11. JIANG, Y. *et al.* HPHT synthesis and electrical transport properties of SmxCo4Sb12. *J. Rare Earths* **28,** 407–410 (2010).

12 Sekine, C. & Mori, Y. Development of thermoelectric materials using high-pressure synthesis technique. *Jpn. J. Appl. Phys.* **56,** 0–6 (2017).

13 Matsui, K. *et al.* Structural instability of unfilled skutterudite Compounds MX3(M = Co, Rh, and Ir; X = As and Sb) under high pressure. *J. Phys. Soc. Japan* **81,** 1–7 (2012).

14 Ibuka, S., Imai, M., Miyakawa, M. & Taniguchi, T. Electrical and magnetic properties of La<inf>0.5</inf>Rh<inf>4</inf>Sb<inf>12</inf> filled skutterudite synthesized at high pressure. *J. Alloys Compd.* **646,** 912–915 (2015).

15 Mei, Z. G., Zhang, W., Chen, L. D. & Yang, J. Filling fraction limits for rare-earth atoms in Co Sb3: An ab initio approach. *Phys. Rev. B - Condens. Matter Mater. Phys.* **74,** 1–4 (2006).

16 Wojciechowski KT. Study of transport properties of the Co1-xRhxSb3. *J Alloys Compd*. 2007;439(1-2):18-24

17 Guo JQ, Geng HY, Ochi S, Kim HK, Hyodo H, Kimura K. Thermoelectric Properties of (Yb , Ca) x (Co , Fe) 4 Sb 12 Skutterudites. *Adv Mater*. 2008:2008-2011. Guo JQ, Geng HY, Ochi S, Kim HK, Hyodo H, Kimura K. Thermoelectric Properties of (Yb , Ca) x (Co , Fe) 4 Sb 12 Skutterudites. *Adv Mater*. 2008:2008-2011.

18 Matsui K, Hayashi J, Akahira K, Ito K, Takeda K, Sekine C. Pressure-induced irreversible isosymmetric transition of TSb3(T=Co, Rh and Ir). *J Phys Conf Ser*. 2010;215.

19 Kim SW, Kimura Y, Mishima Y. Effects of doping on the high-temperature thermoelectric properties of IrSb3 skutterudite compounds. *J Electron Mater*. 2003;32(11):1141-1147

ACKNOWLENDGEMENT

Firstly, I would like to express my sincere gratitude to my advisor Prof. Chihiro SEKINE for the continuous support of my Ph.D study and related research, for his patience, motivation, and immense knowledge. His guidance helped me in all the time of research and writing of this thesis. I could not have imagined having a better advisor and mentor for my Ph.D study. Besides my advisor, I would like to thank Assis. Prof. Yukihiro KAWAMURA and technical staff Junichi HAYASHI who kindly supporting in experiment detail and analysis.

My thanks also goes to Dr. Chul-Ho LEE, Dr. Kunihiro KIHOU, Hirotaka NISHIATE, who provided me an opportunity to join their team as intern, and who gave access to the laboratory and research facilities. Without they precious support it would not be possible to conduct this research.

A special thanks to all student in Sekine lab member, who help me in experiment, living life support, all happy day.